VOLUME 34 APRIL 1956 NUMBER 4

Canadian Journal of Physics

Published by THE NATIONAL RESEARCH COUNCIL

OTTAWA CANADA

CANADIAN JOURNAL OF PHYSICS

(Formerly Section A, Canadian Journal of Research)

Under the authority of the Chairman of the Committee of the Privy Council on Scientific and Industrial Research, the National Research Council issues THE CANADIAN JOURNAL OF PHYSICS and six other journals devoted to the publication, in English or French, of the results of original scientific research. Matters of general policy concerning these journals are the responsibility of a joint Editorial Board consisting of: members representing the National Research Council of Canada; the Editors of the Journals; and members representing the Royal Society of Canada and four other scientific societies.

Manuscripts for publication should be submitted to Dr. Léo Marion, Editor-in-Chief, Canadian Journal of Physics, National Research Council, Ottawa 2, Canada.
(For instructions on preparation of copy, see **Notes to Contributors** (inside back cover).)

Proof, correspondence concerning proof, and orders for reprints should be sent to the Manager, Editorial Office (Research Journals), Division of Administration, National Research Council, Ottawa 2, Canada.

Subscriptions, renewals, requests for single or back numbers, and all remittances should be sent to Division of Administration, National Research Council, Ottawa 2, Canada. Remittances should be made payable to the Receiver General of Canada, credit National Research Council.

The journals published, frequency of publication, and prices are:

Canadian Journal of Biochemistry and Physiology	Bimonthly	$3.00 a year
Canadian Journal of Botany	Bimonthly	$4.00 a year
Canadian Journal of Chemistry	Monthly	$5.00 a year
Canadian Journal of Microbiology	Bimonthly	$3.00 a year
Canadian Journal of Physics	Monthly	$4.00 a year
Canadian Journal of Technology	Bimonthly	$3.00 a year
Canadian Journal of Zoology	Bimonthly	$3.00 a year

The price of single numbers of all journals is 75 cents.

Reprinted in entirety by photo-offset.

Canadian Journal of Physics

Issued by The National Research Council of Canada

VOLUME 34 APRIL 1956 NUMBER 4

INFELD FACTORIZATION AND ANGULAR MOMENTUM[1]

By H. R. Coish

ABSTRACT

The connection between Infeld factorization operators and angular momentum operators, well known for spherical harmonics, is extended to other factorization problems by explicitly recognizing them as angular momentum problems. These other problems are: the symmetric top, electron-magnetic pole system, Weyl's spherical harmonics with spin, free particle on a hypersphere. The Kepler problem is also included for it may be thrown into the form of a four-dimensional angular momentum problem. The transformation to momentum space for this problem is very much simplified by the connection between Infeld factorization and angular momentum.

1. INTRODUCTION

There are two main papers on the Infeld factorization method (Infeld 1941; Infeld and Hull 1951). The present paper partially answers the question raised by the suggestion made by Infeld (1941) that the factorization method is something more than merely a mathematical trick.

In the problem of the spherical harmonics,* it is clear that the Infeld factorization operators are closely related to the angular momentum ladder operators,†

$$L_x \pm iL_y \equiv e^{\pm i\phi}\left\{i\cot\theta\frac{\partial}{\partial\phi} \pm \frac{\partial}{\partial\theta}\right\}. \tag{1}$$

With $P_l^m(\cos\theta)e^{im\phi}$ written for the operand this ladder property yields

$$\left\{m\cot\theta \mp \frac{d}{d\theta}\right\} P_l^m \sim P_l^{m\pm1} \tag{2}$$

in agreement with the recurrence relations obtained by the Infeld method.

Similarly, by elimination of the co-ordinate ϕ from the angular momentum identities

$$\begin{aligned}(L_x+iL_y)(L_x-iL_y) &= L^2-L_z(L_z+1),\\ (L_x-iL_y)(L_x+iL_y) &= L^2-L_z(L_z-1),\end{aligned} \tag{3}$$

the doubled factoring characteristic of the factorization method is obtained.

[1]Manuscript received October 7, 1955.
Contribution from the Department of Mathematical Physics, University of Manitoba, Winnipeg, Manitoba, and the Canadian Mathematics Congress Summer Research Institute, Queen's University, Kingston, Ontario.

*Infeld and Hull (1951) Sec. 4.1.

†Infeld and Hull (1951) page 30, footnote 6.

2. THE SYMMETRIC TOP,* THE ELECTRON-MAGNETIC POLE,† WEYL'S SPHERICAL HARMONICS WITH SPIN‡

These are problems for which the components of the total angular momentum are constants of the motion. Although the connection has not before been pointed out explicitly, one might expect that again the angular momentum ladder operators would lead directly to Infeld factorization operators.

In the symmetric top problem we use Euler angles such that θ, ϕ are the polar co-ordinates of the axis of symmetry about which the spin ψ takes place. We find for the total angular momentum

$$\mathbf{J} = \mathbf{L}+\mathbf{a} \tag{4}$$

where

$$\begin{aligned} a_x &= p_\psi \csc\theta\cos\phi, \\ a_y &= p_\psi \csc\theta \sin\phi, \\ a_z &= 0, \end{aligned} \tag{5}$$

p_ψ being the momentum canonically conjugate to ψ, while the components of $\mathbf{L}$ have exactly the form of the components of orbital angular momentum of a particle and hence as operators will have the usual orbital angular momentum operator form.

The ladder operators are

$$J_x \pm iJ_y \equiv L_x \pm iL_y + a_x \pm ia_y.$$

Operating on an eigenfunction of $L_z \equiv -i\,\partial/\partial\phi$ for the eigenvalue m these take the forms

$$J_x \pm iJ_y = -e^{\pm i\phi}\left\{m\cot\theta - \frac{p_\psi}{\sin\theta} \mp \frac{\partial}{\partial\theta}\right\} \tag{6}$$

which give the Infeld factorization operators for this problem.

From the identities corresponding to (3) one could get the Infeld double factoring.

The energy eigenvalues in terms of the moments of inertia A, C

$$E = \frac{J(J+1)}{2A} + \frac{1}{2}\left(\frac{1}{C}-\frac{1}{A}\right)K^2 \tag{7}$$

follow immediately from the eigenvalues $J(J+1)$ for total angular momentum and K for p_ψ.

Similarly the Infeld factorization may be derived from angular momentum properties and the ladder operators related to angular momentum operators in the electron-magnetic pole problem and in the case of Weyl's spherical harmonics with spin, if in the former the electromagnetic angular momentum and in the latter the Pauli spin are taken into account.

3. FREE PARTICLE ON A HYPERSPHERE§

The problem of the motion of a free particle on a hypersphere leads to Infeld's first example of the factorization method. It is an angular momentum

*Infeld and Hull (1951) Sec. 4.5.
†Infeld and Hull (1951) Sec. 4.7 and Dirac (1931).
‡Infeld and Hull (1951) Sec. 4.6 and Weyl (1931).
§Infeld (1941) Sec. 1 and Sec. 7.

problem but in four dimensions, and this occasions a change in the style of argument. There are now *two* angular momentum vector operators, namely

$$\mathbf{L} \equiv -i\,\mathbf{r} \times \nabla, \tag{8}$$

$$\mathbf{D} \equiv -i\left[x_4\nabla - \mathbf{r}\frac{\partial}{\partial x_4}\right], \tag{9}$$

where the vector notation denotes vectors under rotations of the x_1, x_2, x_3 space.

L is just the usual three-dimensional angular momentum vector operator satisfying the relation

$$\mathbf{L} \times \mathbf{L} = i\,\mathbf{L}. \tag{10}$$

Other angular momentum relations which may be verified by using (8) and (9) are

$$\mathbf{D} \times \mathbf{D} = i\,\mathbf{L}, \tag{11}$$

$$\mathbf{D} \times \mathbf{L} + \mathbf{L} \times \mathbf{D} = 2\,i\,\mathbf{D}. \tag{12}$$

These relations hold for a system of particles as well as for a single particle, but a fourth relation exists for a particle which does not hold generally for a system of particles

$$\mathbf{D}\cdot\mathbf{L} = \mathbf{L}\cdot\mathbf{D} = 0. \tag{13}$$

In terms of these operators the Schrödinger equation on the hypersphere of radius R

$$\Delta\psi + 2mE\psi = 0 \tag{14}$$

becomes

$$(\mathbf{D}^2 + \mathbf{L}^2)\,\psi = \lambda\psi \tag{15}$$

where

$$\lambda = 2\,m\,E\,R^2. \tag{16}$$

Since $\mathbf{L}^2$ commutes with $\mathbf{D}^2$ we may impose

$$\mathbf{L}^2\psi = l(l+1)\psi \tag{17}$$

and our problem becomes one of finding four-dimensional angular momentum ladder operators which raise and lower l.

To find these and relate them to Infeld factorization operators we introduce the Pauli spin matrices σ_1, σ_2, σ_3, and the vector

$$\boldsymbol{\sigma} \equiv \mathbf{i}\,\sigma_1 + \mathbf{j}\,\sigma_2 + \mathbf{k}\,\sigma_3 \tag{18}$$

with the properties

$$\boldsymbol{\sigma} \times \boldsymbol{\sigma} = 2\,i\,\boldsymbol{\sigma}, \tag{19}$$

$$(\boldsymbol{\sigma}\cdot\mathbf{a})(\boldsymbol{\sigma}\cdot\mathbf{b}) = \mathbf{a}\cdot\mathbf{b} + i\,\boldsymbol{\sigma}\cdot\mathbf{a} \times \mathbf{b}, \tag{20}$$

where **a**, **b** are two vector operators which need not commute with each other but must commute with $\boldsymbol{\sigma}$.

The operator

$$K \equiv \boldsymbol{\sigma}\cdot\mathbf{L} + 1 \tag{21}$$

has the property that

$$(K-1)\,K \equiv \mathbf{L}^2 \tag{22}$$

which follows from (10) and (20), so that an eigenfunction of K for the eigenvalue k is an eigenfunction of $\mathbf{L}^2$ for the eigenvalue $l(l+1)$ with $l = k-1$ if k is positive and $l = -k$ if k is negative. We take ψ to be a two-component column matrix which is an eigenfunction of K so that both its components are eigenfunctions of $\mathbf{L}^2$ for the same value of l.

Any operator which anticommutes with K changes ψ into another eigenfunction of K for the eigenvalue $K = -k$ and hence into another eigenfunction of $\mathbf{L}^2$ for the eigenvalue $(l+1)(l+2)$ if k is positive and for the eigenvalue $(l-1)l$ if k is negative. That is, it raises or lowers l by one depending on whether k is positive or negative. It is a ladder operator.

Just this property of anticommuting with K is held by the operator $\boldsymbol{\sigma}\cdot\mathbf{D}$ as follows from (12), (13), (20). Furthermore as a consequence of (11), (20), (22) we have

$$\mathbf{D}^2+\mathbf{L}^2 \equiv (\boldsymbol{\sigma}\cdot\mathbf{D})^2+K^2-1 \tag{23}$$

so that $\boldsymbol{\sigma}\cdot\mathbf{D}$ commutes with $\mathbf{D}^2+\mathbf{L}^2$. Hence it is exactly the ladder operator we seek.

In terms of polar co-ordinates α, θ, ϕ, given by

$$\begin{aligned} x_1 &= R\sin\alpha\sin\theta\cos\phi, \\ x_2 &= R\sin\alpha\sin\theta\sin\phi, \\ x_3 &= R\sin\alpha\cos\theta, \\ x_4 &= R\cos\alpha, \end{aligned} \tag{24}$$

the ladder operator $\boldsymbol{\sigma}\cdot\mathbf{D}$ becomes

$$\boldsymbol{\sigma}\cdot\mathbf{D} \equiv -i\sigma_r\left[\frac{\partial}{\partial\alpha}-(K-1)\cot\alpha\right] \tag{25}$$

where

$$\sigma_r \equiv (\boldsymbol{\sigma}\cdot\mathbf{r})/r. \tag{26}$$

Applying this to a ψ taken to be of the form

$$\psi_l = \mathbf{Y}_l(\theta,\phi)\,u_l(\alpha) \tag{27}$$

where $\mathbf{Y}_l$ is a (matrix) eigenfunction of K for $k = l+1$ whereas u_l is an ordinary function, we obtain

$$-i\sigma_r\mathbf{Y}_l\left[\frac{d}{d\alpha}-l\cot\alpha\right]u_l \sim \mathbf{Y}_{l+1}\,u_{l+1}. \tag{28}$$

Cancelling off the factors depending on θ, ϕ only we have

$$\left[\frac{d}{d\alpha}-l\cot\alpha\right]u_l \sim u_{l+1}. \tag{29}$$

Similarly by taking $\mathbf{Y}_l$ to be an eigenfunction of K for $k = -l$ we get

$$\left[\frac{d}{d\alpha}+(l+1)\cot\alpha\right]u_l \sim u_{l-1}. \tag{30}$$

These are just the recursion relations which would be obtained by the Infeld factorization method.

We can derive the doubled factoring of the Infeld method by considering:

(31) $$(\boldsymbol{\sigma}\cdot\mathbf{D})^2 \equiv \mathbf{D}^2+\mathbf{L}^2-K^2+1$$

or

(32) $$-\sigma_r\left[\frac{\partial}{\partial\alpha}-(K-1)\cot\alpha\right]\sigma_r\left[\frac{\partial}{\partial\alpha}-(K-1)\cot\alpha\right]\psi = \left[\lambda-K^2+1\right]\psi.$$

Now we permute the σ_r in the middle through to the left to combine it with the σ_r already there. Making use of the facts that σ_r commutes with $\partial/\partial\alpha$ and anticommutes with K, and that its square is unity, we obtain:

(33) $$\left[(K+1)\cot\alpha+\frac{\partial}{\partial\alpha}\right]\left[(K-1)\cot\alpha-\frac{\partial}{\partial\alpha}\right]\psi = \left[\lambda-K^2+1\right]\psi.$$

On substituting an eigenfunction of K for $k = l+1$ and cancelling off the θ, ϕ dependent factors the result is

(34) $$\left[(l+2)\cot\alpha+\frac{d}{d\alpha}\right]\left[l\cot\alpha-\frac{d}{d\alpha}\right]u_l = \left[\lambda-l(l+2)\right]u_l.$$

On the other hand the use of an eigenfunction of K for $k = -l$ yields

(35) $$\left[(l-1)\cot\alpha-\frac{d}{d\alpha}\right]\left[(l+1)\cot\alpha+\frac{d}{d\alpha}\right]u_l = \left[\lambda-(l-1)(l+1)\right]u_l.$$

These last two equations form just the factorings of the factorization method and here have been obtained by angular momentum arguments. The factorization operators have been related to four-dimensional angular momentum ladder operators.

Similarly the Infeld factorization for the problem of the particle in a space of constant negative curvature could be related to angular momentum properties.

The factorization of the Bessel equation may be obtained from the above by taking the limit of zero curvature.

It must be noted that the argument in this four-dimensional case depends essentially on a relation (13) which holds for a single particle but not in general for a system of particles. Hence it would not be possible to extend this treatment as can be done in the three-dimensional case for the symmetric top.

4. THE KEPLER PROBLEM

Jackson (1953) has pointed out that the Kepler problem can be thrown into the form of a four-dimensional angular momentum problem with

(36) $$\mathbf{D} = (-2mE)^{-\frac{1}{2}}[\tfrac{1}{2}(\mathbf{p}\times\mathbf{L}-\mathbf{L}\times\mathbf{p})-me^2\mathbf{r}/r],$$

(37) $$2E(\mathbf{D}^2+\mathbf{L}^2+1) = -me^4,$$

where $\mathbf{D}$ and $\mathbf{L}$ have the four-dimensional angular momentum properties (10), (11), (12), (13).

Now the ladder operator from the angular momentum point of view is

$$\boldsymbol{\sigma}\cdot\mathbf{D} = -(-2mE)^{-\frac{1}{2}}[(\boldsymbol{\sigma}\cdot\nabla)K+me^2\sigma_r], \tag{38}$$

where we have made use of

$$(\boldsymbol{\sigma}\cdot\nabla)K-K(\boldsymbol{\sigma}\cdot\nabla) \equiv i\boldsymbol{\sigma}\cdot(\nabla\times\mathbf{L}-\mathbf{L}\times\nabla) \tag{39}$$

from (20) and (21), and also of the fact that $\boldsymbol{\sigma}\cdot\nabla$ and K anticommute. Putting our ladder operator in terms of polar co-ordinates we finally obtain the result

$$\boldsymbol{\sigma}\cdot\mathbf{D} = -(-2mE)^{-\frac{1}{2}}\sigma_r\left[\left(\frac{\partial}{\partial r}-\frac{K-1}{r}\right)K+me^2\right]. \tag{40}$$

We next apply this to an eigenfunction of K for the eigenvalue $k = l+1$, that is to an operand of the form (27) but with $u_l(\alpha)$ replaced by a function of the radial co-ordinate,

$$\boldsymbol{\sigma}\cdot\mathbf{D} = -(-2mE)^{-\frac{1}{2}}\sigma_r\left[\left(\frac{\partial}{\partial r}-\frac{l}{r}\right)(l+1)+me^2\right]. \tag{41}$$

From this we can pick out the operator on the radial function which is clearly just of the Infeld type for raising l

$$\frac{d}{dr}-\frac{l}{r}+\frac{me^2}{l+1}. \tag{42}$$

Similarly we may pick out the Infeld ladder operator for lowering l by choosing $k = -l$

$$\frac{d}{dr}+\frac{l+1}{r}-\frac{me^2}{l}. \tag{43}$$

Thus the Infeld factorization of the Kepler problem is also a consequence of angular momentum properties.

5. KEPLER PROBLEM IN MOMENTUM SPACE

A problem to which considerable effort was devoted in the thirties is that of finding the momentum space wave functions for the Kepler problem (Podolsky and Pauling 1929; Hylleraas 1932; Elsasser 1933; Fock 1935). With the ladder operators as we now have them in terms of physical operators it is possible to obtain the result in a few lines with elementary operations.

The hamiltonian for this problem is

$$(p^2/2m)-e^2/r = E \tag{44}$$

so that in momentum space the operator e^2/r may be represented by

$$e^2/r = (p^2/2m)-E. \tag{45}$$

If we write

$$e^2\sigma_r \equiv e^2\boldsymbol{\sigma}\cdot\mathbf{r}/r = i(\boldsymbol{\sigma}\cdot\nabla_p)(p^2-2mE)/2m, \tag{46}$$

where ∇_p is the gradient operator in momentum space, we may transform $\boldsymbol{\sigma}\cdot\mathbf{D}$ (38) into a momentum space operator,

$$\boldsymbol{\sigma}\cdot\mathbf{D} = -i(-2mE)^{-\frac{1}{2}}[(\boldsymbol{\sigma}\cdot\mathbf{p})K+(\boldsymbol{\sigma}\cdot\nabla_p)(p^2-2mE)/2]. \tag{47}$$

Introducing polar co-ordinates p, θ_p, ϕ_p, in momentum space we may write

$$\boldsymbol{\sigma}\cdot\nabla_p \equiv \sigma_p\left[\frac{\partial}{\partial p}-\frac{K-1}{p}\right], \tag{48}$$

where

$$\sigma_p \equiv (\boldsymbol{\sigma}\cdot\mathbf{p})/p. \tag{49}$$

We now substitute this into (47) and pick out the recursion relations for the 'radial' function $P(p)$ in momentum space,

$$\left[\frac{d}{dp}-\frac{l}{p}+\frac{2p(l+1)}{p^2-2mE}\right](p^2-2mE)\,P_l \sim P_{l+1}, \tag{50a}$$

$$\left[\frac{d}{dp}+\frac{l+1}{p}-\frac{2pl}{p^2-2mE}\right](p^2-2mE)\,P_l \sim P_{l-1}. \tag{50b}$$

The case $l = n-1$ is the 'top of the ladder' and for this case the operator of (50a) annihilates the corresponding P,

$$\left[\frac{d}{dp}-\frac{n-1}{p}+\frac{2np}{p^2-2mE}\right](p^2-2mE)\,P_{n-1} = 0. \tag{51}$$

This is a first-order differential equation for P_{n-1} whose solution is

$$P_{n-1} \sim \frac{p^{n-1}}{(p^2-2mE)^{n+1}}. \tag{52}$$

The solutions for other values of l may be obtained simply by applying the operator of (50b) for lowering l.

ACKNOWLEDGMENTS

I wish to acknowledge the assistance of a Summer Research Institute Fellowship granted by the Canadian Mathematical Congress. Discussions with Dr. S. M. Neamtan of the Mathematical Physics Department have been invaluable. The idea of applying the factorization method to the momentum space Kepler problem was suggested to me some years ago by Dr. L. Infeld, then at Toronto.

REFERENCES

DIRAC, P. A. M. 1931. Proc. Roy. Soc. (London), A, **133**: 60.
ELSASSER, W. 1933. Z. Physik, **81**: 332.
FOCK, V. 1935. Z. Physik, **98**: 145.
HYLLERAAS, E. 1932. Z. Physik, **74**: 216.
INFELD, L. 1941. Phys. Rev. **59**: 737.
INFELD, L. and HULL, T. E. 1951. Revs. Mod. Phys. **23**: 21.
JACKSON, T. A. S. 1953. Proc. Phys. Soc. (London), A, **66**: 958.
PODOLSKY, B. and PAULING, L. 1929. Phys. Rev. **34**: 109.
WEYL, H. 1931. The theory of groups and quantum mechanics. E. P. Dutton & Co., Inc., New York.

HIGH RESOLUTION RAMAN SPECTROSCOPY OF GASES

VI. ROTATIONAL SPECTRUM OF SYMMETRIC BENZENE-d_3[1]

BY A. LANGSETH[2] AND B. P. STOICHEFF

ABSTRACT

The pure rotational Raman spectrum of $C_6H_3D_3$ vapor at a pressure of 15 cm. Hg was photographed in the second order of a 21 ft. grating. The value of the rotational constant was found to be $B_0 = 0.1716_5 \pm 0.0001$ cm^{-1}. This result confirms the earlier spectroscopic values of the internuclear distances in the benzene molecule.

A. INTRODUCTION

Recently the carbon–carbon distance in the benzene molecule was evaluated by two methods, each capable of high precision, but the resulting values were significantly different. From the rotational Raman spectra of gaseous C_6H_6 and C_6D_6, Stoicheff (1954*b*) obtained the value of $1.397_3 \pm 0.001$ Å for the carbon–carbon distance in benzene while from the X-ray diffraction analysis of crystalline benzene at $-3°$ C., Cox and Smith (1954) obtained the value of 1.378 ± 0.0033 Å for this distance. These values differ by 0.02 Å, that is, by approximately ten times the quoted errors. More recently, Cox, Cruickshank, and Smith (1955) have been able to ascribe most of this difference to a systematic error in the X-ray analysis arising from the anisotropy of the thermal oscillations of the benzene molecule as a whole. The corrected X-ray value of the carbon–carbon bond length is 1.39_2 Å which is now in satisfactory agreement with the spectroscopic value.

Even though there is agreement at present between the X-ray and spectroscopic values, it seemed worth while to continue with an experiment conceived prior to the explanation of the original discrepancy, in order to check the spectroscopic value. The present investigation of the rotational Raman spectrum of symmetric benzene-d_3 confirms the earlier spectroscopic results obtained with C_6H_6 and C_6D_6, namely that the internuclear distances in the benzene molecule are

$$r_0(\text{C–C}) = 1.397_3 \text{ Å and } r_0(\text{C–H}) = 1.084 \text{ Å}.$$

B. OBSERVED SPECTRUM

The apparatus has already been described (Stoicheff 1954*a*). A cylindrical lens was mounted in front of the photographic plate resulting in a 10-fold reduction in exposure time with no noticeable loss in resolving power. The sample of $C_6H_3D_3$ had a purity of about 90 mol. %, the remainder being mainly 1,3-$C_6H_4D_2$ with a trace of C_6H_5D. The pressure of benzene was 15 cm. Hg and the exposure time one to two hours.

The rotational Raman spectrum of $C_6H_3D_3$ similar to that of C_6H_6 consists of a series of sharp lines extending to about 50 cm^{-1} on both sides of the

[1]Manuscript received December 14, 1955.
Contribution from the Division of Pure Physics, National Research Council, Ottawa, Canada. Issued as N.R.C. No. 3874.

[2]Chemistry Department, University of Copenhagen; visiting Professor at N.R.C. in 1954.

exciting line. These are the lines of the S branches for which $\Delta J = 2$. The line spacing is therefore $4B_0$ and is observed to be about 0.68 cm^{-1}. The lines of the R branches ($\Delta J = 1$) have half the spacing of the main series of lines and are unresolved, thus producing a continuum which extends about 20 cm^{-1} from the exciting line.

Two plates of the $C_6H_3D_3$ spectrum were evaluated. About 120 Stokes and anti-Stokes lines were measured on each plate and the agreement between the line measurements on the two plates was within ± 0.02 cm^{-1}. The average values of the wave number shifts are given in Table I.

TABLE I

OBSERVED WAVE NUMBER SHIFTS OF THE ROTATIONAL RAMAN LINES OF $C_6H_3D_3$

J	$\mid\Delta\nu\mid$,[a] cm^{-1}	c − o, cm^{-1}	J	$\mid\Delta\nu\mid$,[a] cm^{-1}	c − o, cm^{-1}
21	15.44_4[b]	+.003	51	36.03_5	−.003
22	16.11_4[b]	+.019	52	36.72_4	−.007
23	16.81_2	+.008	53	37.43_5*	−.032
24	17.50_4	+.003	54	38.07_1*	+.017
25	18.20_1*	−.008	55	38.75_1	+.023
26	18.87_6*[b]	+.003	56	39.45_8	+.002
27	19.54_7*[b]	+.019	57	40.13_2	+.013
28	20.24_7	+.005	58	40.83_5	−.004
29	20.93_7	+.001	59	41.51_2	+.004
30	21.63_1	−.006	60	42.19_6	+.006
31	22.30_5	+.006	61	42.87_9	+.009
32	23.00_0	−.003	62	43.57_8	−.006
33	23.68_8	−.005	63	44.26_7	−.010
34	24.39_4	−.024	64	44.94_2	+.001
35	25.06_2	−.006	65	45.63_6	−.007
36	25.74_7	−.005	66	46.33_5	−.021
37	26.44_0	−.012	67	47.02_1	−.023
38	27.12_5	−.011	68	47.67_9*	+.004
39	27.80_5	−.004	69	48.35_7*	+.012
40	28.47_3*	+.014	70	49.06_0	−.006
41	29.12_2*	+.050	71	49.74_0	−.001
42	29.84_0	+.018	72	50.44_0	−.016
43	30.54_3	+.002	73	51.12_6	−.017
44	31.21_5	+.016	74	51.79_7	−.003
45	31.90_5	+.011	75	52.48_2	−.004
46	32.59_2	+.010	76	53.13_8	+.025
47	33.27_7	+.012	77	53.83_3	+.015
48	33.97_2	+.002	78	54.51_6[b]	+.016
49	34.66_4	−.005	79	55.22_7[b]	−.010
50	35.35_2	−.006	80	55.90_3[b]	−.001

[a]All values are averages of Stokes and anti-Stokes lines measured on two plates, except the values marked [b].
[b]Measurement on one plate only.
*Lines blended with grating ghosts.

C. ROTATIONAL ANALYSIS

The method of analysis used to determine the rotational constants is described in section D of paper II (Stoicheff 1954*b*). Once the rotational numbering was established, a graph of the values $\mid\Delta\nu\mid/(J+3/2)$ was plotted against $(J+3/2)^2$. The intercept on the ordinate axis yielded a value of $4B_0$ and the

slope a value of $8D_J$. From these values, the rotational constants

$$B_0 = 0.1716_5 \pm 0.0001 \text{ cm}^{-1} \quad \text{and} \quad D_J = 1.3 \times 10^{-8} \text{ cm}^{-1}$$

were obtained for the $C_6H_3D_3$ molecule. As a check, these values were used to calculate the wave number shifts of the Raman lines which were then compared with the observed shifts. The agreement between the calculated and observed values is within ± 0.03 cm^{-1} for all the lines, as shown in Table I. The effective moment of inertia about any axis in the plane of the molecule passing through its center was calculated from the above value of B_0 and the atomic constants of DuMond and Cohen (1953), giving

$$I_B{}^0 = (163.06 \pm 0.10) \times 10^{-40} \text{ gm. cm.}^2$$

Within the experimental error, this value is equal to the mean of the moments of inertia of C_6H_6 and C_6D_6, 147.59×10^{-40} and 178.45×10^{-40} gm. cm.^{2}, respectively, thus confirming the earlier results obtained from the Raman spectra of C_6H_6 and C_6D_6.

The agreement between the results of the present investigation and the earlier one can also be seen from a graphical determination of the internuclear distances. In Fig. 1 are shown the graphs of the C–H distances and C–C dis-

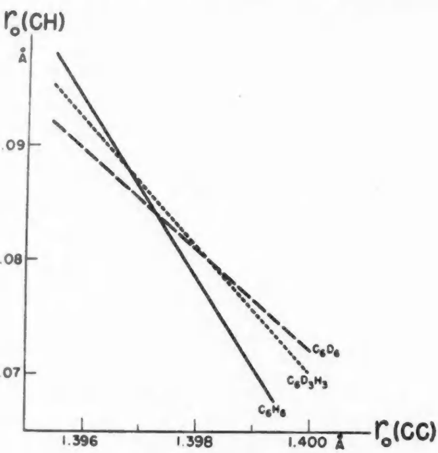

FIG. 1. Graphical determination of the internuclear distances in the benzene molecule. The graphs represent the values of the C–H and C–C distances that are consistent with the measured values of B_0 for the molecules C_6H_6, C_6D_6, and $C_6H_3D_3$.

tances consistent with the B_0 values of C_6H_6, C_6D_6, and $C_6H_3D_3$, assuming a planar hexagonal structure. The values of the internuclear distances are given by the intersections of any two of the curves. All three sets of values are in close agreement.

A least squares calculation using the three moments of inertia to determine the two internuclear distances of the benzene molecule gives the values

$$r_0(\text{C–C}) = 1.397_4 \pm 0.001 \text{ Å} \quad \text{and} \quad r_0(\text{C–H}) = 1.084 \pm 0.005 \text{ Å}.$$

Although it is fortuitous that these values agree exactly with the earlier values, it seems safe to conclude that the spectroscopic values are correct to within the quoted errors.

REFERENCES

Cox, E. G., Cruickshank, D. W. J., and Smith, J. A. S. 1955. Nature, **175**: 766.
Cox, E. G. and Smith, J. A. S. 1954. Nature, **173**: 75.
DuMond, J. M. W. and Cohen, E. R. 1953. Revs. Mod. Phys. **25**: 691.
Stoicheff, B. P. 1954*a*. Can. J. Phys. **32**: 330.
——— 1954*b*. Can. J. Phys. **32**: 339.

ON THE THEORY OF A COAXIAL TRANSMISSION LINE CONSISTING OF ELLIPTIC CONDUCTORS[1]

By J. Y. Wong

ABSTRACT

A coaxial transmission line consisting of conductors of elliptic cross-section is treated as a boundary-value problem. Using elliptic-cylinder wave functions, a formula is derived for the propagation constant of the allowed symmetric modes of propagation. A condition for the generation of the higher-order modes is established in terms of the physical parameters. The analysis is restricted to the case where both the inner and outer conductors are confocal. A configuration of practical interest follows for the limiting case of the inner conductor consisting of a flat strip. The resulting structure can be regarded as constituting a form of shielded "strip" transmission line. The analysis may be used to provide an approximate theory for the "rectangular" coaxial line.

INTRODUCTION

In this paper, a coaxial transmission line consisting of conductors of elliptic cross-section is treated as a boundary-value problem. Using elliptic-cylinder wave functions, a formula is derived for the propagation constant of the allowed symmetric modes in the direction of propagation. The analysis is restricted to the case where the inner conductor and the outer conductor are confocal. An expression for the critical frequencies of the higher-order modes is found to be expressed in terms of a simple function of the physical parameters of the line. An obvious extension of the present analysis is the determination of the characteristic impedance.

A configuration which may be of practical interest results for the limiting case of the inner conductor consisting of a flat strip. For large ellipticities of the outer conductor, the structure may be regarded as constituting a form of shielded "strip" transmission line. A common type of strip line encountered in practice consists of a flat conductor placed between two parallel conducting ground planes in the form of a sandwich. Papers describing this type of line have appeared extensively in the literature (Begovich and Margolin 1950; Cohn 1954; Trans. I.R.E. 1955). It is apparent that such a configuration cannot be analyzed rigorously from the electromagnetic point of view and the determination of some of the electrical parameters must be restricted necessarily to a study of the electrostatic model. In the present case the electric field is confined entirely within the region between the conductors; consequently loss due to radiation and a reduction in the characteristic impedance due to a fringing field do not exist, as in the case of the conventional shielded strip line. Finally, the present analysis may be used to provide an approximate theory for the rectangular coaxial line.

WAVE EQUATION IN ELLIPTIC CYLINDER COORDINATES

In problems dealing with cylinders of elliptic cross-section, it is necessary to introduce an elliptic cylinder coordinate system. Elliptic cylinder coor-

[1]Manuscript received October 31, 1955.
Contribution from the Radio and Electrical Engineering Division, National Research Council, Ottawa, Canada. Issued as N.R.C. No. 3878.

dinates (u, v, z) are related to cartesian coordinates (x, y, z) through the following transformation equations:

$$x = c_0 \cosh u \cos v, \quad y = c_0 \sinh u \sin v. \tag{1}$$

The coordinate surfaces are confocal elliptic and hyperbolic cylinders,

$$\frac{x^2}{c_0^2\cosh^2 u}+\frac{y^2}{c_0^2\sinh^2 u} = 1, \quad \frac{x^2}{c_0^2\cos^2 v}-\frac{y^2}{c_0^2\sin^2 v} = 1, \tag{2}$$

and planes z = constant. From eq. (2) it is apparent that c_0 is the semifocal distance of the ellipse.

Fig. 1 illustrates a family of confocal elliptic and hyperbolic cylinders.

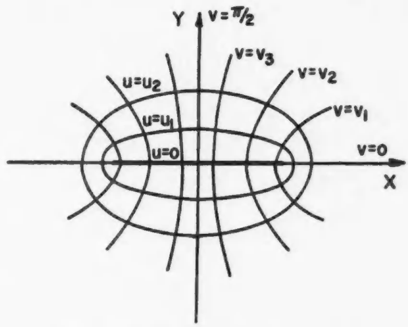

FIG. 1. Elliptic cylinder coordinate system.

In a cylindrical coordinate system, the electromagnetic field can be resolved into two partial fields, each derivable from a purely scalar function Π_z and Π_z^* respectively. Let ψ represent either function, then ψ must satisfy the wave equation

$$(\nabla^2+k^2)\psi = 0, \tag{3}$$

where ∇^2 is the Laplacian operator, and

$$k^2 = -i\omega\mu(\sigma+i\omega\epsilon). \tag{4}$$

Here the rationalized m.k.s. system of units is employed and the time function $e^{i\omega t}$ is understood. In eq. (4), μ is the permeability, σ is the conductivity, and ϵ is the dielectric constant of the medium.

In elliptic cylinder coordinates, elementary solutions of eq. (3) can be represented by the form

$$\psi = f(u, v)\, e^{\pm ihz},$$

where $f(u, v)$ is a solution of

$$\frac{\partial^2 f}{\partial u^2}+\frac{\partial^2 f}{\partial v^2}+c_0^2\Gamma^2(\cosh^2 u-\cos^2 v)f = 0; \tag{5}$$

in eq. (5)

$$\Gamma^2 = k^2 - h^2. \tag{6}$$

Using the method of separation of variables, eq. (5) yields the two well-known radial and angular Mathieu equations. Thus, within a homogeneous isotropic domain, every electromagnetic field can be represented by a linear combination of the elementary wave functions

$$\psi e, o_m = Je,o_m(s, u) Se,o_m(s, v)\, e^{\pm ihz}, \tag{7}$$

$$\psi e, o_m = He^{(2)}_{,}o_m(s, u) Se,o_m(s, v)\, e^{\pm ihz}. \tag{8}$$

In eqs. (7) and (8), $s = c_0^2\Gamma^2$. The wave functions consist of both even and odd cylinder functions and, of these two equations, (7) applies to the finite domain. At great distances from the source eq. (8) must be employed, since it reduces asymptotically to a wave travelling radially outward.

Definitions of the various radial and angular wave functions can be found in numerous sources in the literature (Morse and Feshbach 1953; Sinclair 1951; Stratton, Morse, Chu, and Hutner 1941), and will not be repeated here.

Consider an elliptic cylinder $u = u_0$ of infinite length, immersed in an infinite homogeneous medium. Utilizing the results of eq. (7), the field components at all interior points, $u < u_0$, can be written down as follows:

$$\begin{aligned}
E_u &= \sum_{m=0}^{\infty} \{-(ih/\Gamma_1^2 h_u) Je',o_m(s_1, u) Se,o_m(s_1, v) ae,o_m \\
&\qquad - (i\omega\mu_1/\Gamma_1^2 h_v) Je,o_m(s_1, u) Se',o_m(s_1, v) be,o_m\}\, e^{-ihz}, \\
E_v &= \sum_{m=0}^{\infty} \{-(ih/\Gamma_1^2 h_v) Je,o_m(s_1, u) Se',o_m(s_1, v) ae,o_m \\
&\qquad + (i\omega\mu_1/\Gamma_1^2 h_u) Je',o_m(s_1, u) Se,o_m(s_1, v) be,o_m\}\, e^{-ihz}, \\
E_z &= \sum_{m=0}^{\infty} \{Je,o_m(s_1, u) Se,o_m(s_1, v) ae,o_m\}\, e^{-ihz}, \\
H_u &= \sum_{m=0}^{\infty} \{(ik_1^2/\Gamma_1^2 \mu_1\omega h_v) Je,o_m(s_1, u) Se',o_m(s_1, v) ae,o_m \\
&\qquad - (ih/\Gamma_1^2 h_u) Je',o_m(s_1, u) Se,o_m(s_1, v) be,o_m\}\, e^{-ihz}, \\
H_v &= \sum_{m=0}^{\infty} \{-(ik_1^2/\Gamma_1^2 \mu_1\omega h_u) Je',o_m(s_1, u) Se,o_m(s_1, v) ae,o_m \\
&\qquad - (ih/\Gamma_1^2 h_v) Je,o_m(s_1, u) Se',o_m(s_1, v) be,o_m\}\, e^{-ihz}, \\
H_z &= \sum_{m=0}^{\infty} \{Je,o_m(s_1, u) Se,o_m(s_1, v) be,o_m\}\, e^{-ihz}.
\end{aligned} \tag{9}$$

The fields are represented as a set of even and odd transverse magnetic and transverse electric waves whose amplitudes are given by the coefficients ae,o_m and be,o_m respectively. h_u and h_v are the metrical coefficients whose values are given by $h_u = h_v = c_0\sqrt{(\cosh^2 u - \cos^2 v)}$. The primes above a cylinder function denote differentiation with respect to either the variable u or the variable v.

By employing eq. (8) a similar set of field equations can be written for the external region $u > u_0$.

PROPAGATION MODES ALONG A COAXIAL LINE

The problem investigated in this paper can be considered as constituting an extension of the general problem of wave propagation along an elliptic cylinder (Karbowiak 1954). The method of analysis follows essentially the excellent treatment given by Stratton (1941, Chap. 9, Sec. 9.19) to the problem of a coaxial cable of circular conductors. Consider two confocal elliptic cylinders (1) and (3) whose surfaces are denoted by u_0 and u_1 respectively. A cross section of the coaxial line is illustrated in Fig. 2. The central conductor

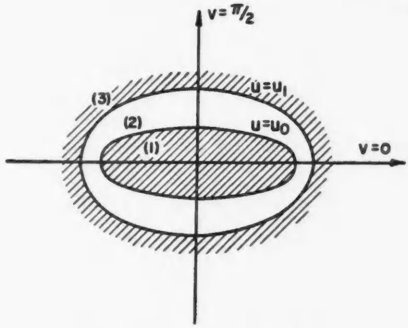

FIG. 2. Cross section of coaxial line.

is assumed to be carrying an axial current. It is required to investigate the nature of the propagation modes and to determine the propagation constant of these modes.

The set of expressions in eq. (9) implies that an infinite number of modes of propagation are possible along a solid conducting cylinder. However, for the case of a conductor carrying an axial current, it can be demonstrated that only the transverse magnetic mode corresponding to $m = 0$ possesses a relatively low attenuation. The asymmetric modes corresponding to $m > 0$ are highly attenuated, consequently they never play a part in the propagation of current along a conductor.

In practice the outer conductor of any coaxial transmission line is of finite thickness. However, for the purposes of this analysis it is necessary to assume an outer conductor of infinite thickness. This assumption is justified if we assume that the skin depth is very much less than the thickness of the outer conducting cylinder. In effect, this means that the analysis is restricted to frequencies whereby this condition is valid. It will be seen that in order to obtain a solution for the propagation constant, it will be necessary to assume that the conductors possess infinite conductivity.

The analysis requires the determination of the radial impedance function at each of the boundary surfaces. The impedance Z_u can be found by applying the definition

$$E_z = -Z_u H_v. \tag{10}$$

Utilizing the results of eq. (9), one obtains the following expression for region (1),

$$^{(1)}Z_u = \frac{\Gamma_1^2 \mu_1 \omega h_u Je_0(s_1, u)}{ik_1^2 Je_0'(s_1, u)}. \tag{11}$$

To construct a solution appropriate to region (2) which will satisfy the internal and external boundary conditions, two independent Mathieu functions must be used. Consequently for region (2), $u_0 < u < u_1$, let us write

$$^{(2)}H_v = \frac{ik_2^2}{\Gamma_2^2 \mu_2 \omega h_u}\left\{A\,Je_0'(s_2, u)Se_0(s_2, v) + BNe_0'(s_2, u)Se_0(s_2, v)\right\} e^{-ihz}, \tag{12}$$

where $Ne_0(s_2, u)$ is an even radial Mathieu function of the second kind, and A and B are undetermined coefficients.

The radial impedance for region (2) becomes

$$^{(2)}Z_u = \frac{-\Gamma_2^2 \mu_2 \omega h_u A\,Je_0(s_2, u) + BNe_0(s_2, u)}{ik_2^2 A\,Je_0'(s_2, u) + BNe_0'(s_2, u)}. \tag{13}$$

In the outer conductor, the proper behavior of the field at infinity is ensured by choosing a Mathieu function of the fourth kind. Hence for $u > u_1$, let

$$^{(3)}H_v = \frac{ik_3^2}{\Gamma_3^2 \mu_3 \omega h_u}\left\{CHe_0^{(2)\prime}(s_3, u)Se_0(s_3, v)\right\} e^{-ihz}, \tag{14}$$

where C is likewise an undetermined coefficient.

The radial impedance in region (3) becomes

$$^{(3)}Z_u = \frac{-\Gamma_3^2 \mu_3 \omega h_u He_0^{(2)}(s_3, u)}{ik_3^2 He_0^{(2)\prime}(s_3, u)}. \tag{15}$$

The coefficients A, B, and C are determined by applying the continuity condition of the radial impedance functions, namely:

$$\begin{aligned} ^{(1)}Z_u &= {}^{(2)}Z_u \text{ at } u = u_0, \\ ^{(2)}Z_u &= {}^{(3)}Z_u \text{ at } u = u_1. \end{aligned} \tag{16}$$

The substitution of eqs. (11), (13), and (15) in the above relations yields the following set of equations:

$$\begin{aligned} \frac{\Gamma_1^2 \mu_1 \omega h_u Je_0(s_1, u_0)}{ik_1^2 Je_0'(s_1, u_0)} &= \frac{\Gamma_2^2 \mu_2 \omega h_u A\,Je_0(s_2, u_0) + BNe_0(s_2, u_0)}{ik_2^2 A\,Je_0'(s_2, u_0) + BNe_0'(s_2, u_0)}, \\ \frac{\Gamma_3^2 \mu_3 \omega h_u He_0^{(2)}(s_3, u_1)}{ik_3^2 He_0^{(2)\prime}(s_3, u_1)} &= \frac{\Gamma_2^2 \mu_2 \omega h_u A\,Je_0(s_2, u_1) + BNe_0(s_2, u_1)}{ik_2^2 A\,Je_0'(s_2, u_1) + BNe_0'(s_2, u_1)}. \end{aligned} \tag{17}$$

Rearranging the terms in eq. (17) and solving for the ratio A/B, one obtains finally

$$(18)\qquad -\frac{A}{B}\left\{\begin{aligned} &= \frac{Ne_0(s_2,u_0)-\dfrac{\Gamma_1^{\,2}\mu_1 k_2^{\,2} Je_0(s_1,u_0)}{\Gamma_2^{\,2}\mu_2 k_1^{\,2} Je_0'(s_1,u_0)}\,Ne_0'(s_2,u_0)}{Je_0(s_2,u_0)-\dfrac{\Gamma_1^{\,2}\mu_1 k_2^{\,2} Je_0(s_1,u_0)}{\Gamma_2^{\,2}\mu_2 k_1^{\,2} Je_0'(s_1,u_0)}\,Je_0'(s_2,u_0)},\\[2ex] &= \frac{Ne_0(s_2,u_1)-\dfrac{\Gamma_3^{\,2}\mu_3 k_2^{\,2} He_0^{(2)}(s_3,u_1)}{\Gamma_2^{\,2}\mu_2 k_3^{\,2} He_0^{(2)\prime}(s_3,u_1)}\,Ne_0'(s_2,u_1)}{Je_0(s_2,u_1)-\dfrac{\Gamma_3^{\,2}\mu_3 k_2^{\,2} He_0^{(2)}(s_3,u_1)}{\Gamma_2^{\,2}\mu_2 k_3^{\,2} He_0^{(2)\prime}(s_3,u_1)}\,Je_0'(s_2,u_1)}.\end{aligned}\right.$$

The roots of this determinantal equation are the characteristic values h_{0p} $(p = 1, 2, 3, \ldots)$ which establish the allowed symmetric modes of propagation.

However, it is necessary to resort to an approximate method for determining the roots of eq. (18), by assuming that the inner and outer conductors have infinite conductivity. From eq. (6), it is recalled that $\Gamma_1^2 = k_1^2 - h^2$ and $\Gamma_3^2 = k_3^2 - h^2$. The imaginary part of h must remain finite if a wave is to be propagated. Hence as the conductivity approaches infinity, $\Gamma_1 \to k_1$ and $\Gamma_3 \to k_3$, and at the same time the absolute values of both k_1 and k_3 approach infinity. Under these conditions eq. (18) reduces to

$$(19)\qquad -\frac{A}{B} = \frac{Ne_0(s_2,u_0)}{Je_0(s_2,u_0)} = \frac{Ne_0(s_2,u_1)}{Je_0(s_2,u_1)}.$$

Eq. (19) is satisfied when $s_2 = 0$. By definition, $s_2 = c_0^2\Gamma_2^2$ and since c_0 is always finite for all practical cases, it follows that the principal root of eq. (19) corresponds to $\Gamma_2 = 0$, or

$$(20)\qquad h = k_2.$$

In addition to the principal wave, higher-order modes may also exist. If Γ_2 is large, then the following asymptotic expressions can be employed (Stratton 1941, Chap. 6, Sec. 6.12),

$$(21)\qquad \begin{aligned} Je_0(s_2,u_0) &\to \frac{1}{\sqrt{(c_0\,\Gamma_2\cosh u_0)}}\cos(c_0\,\Gamma_2\cosh u_0-(\pi/4)),\\ Ne_0(s_2,u_0) &\to \frac{1}{\sqrt{(c_0\,\Gamma_2\cosh u_0)}}\sin(c_0\,\Gamma_2\cosh u_0-(\pi/4)).\end{aligned}$$

Hence eq. (19) simplifies to

$$(22)\qquad \frac{\sin(c_0\,\Gamma_2\cosh u_0-(\pi/4))}{\cos(c_0\,\Gamma_2\cosh u_0-(\pi/4))} = \frac{\sin(c_0\,\Gamma_2\cosh u_1-(\pi/4))}{\cos(c_0\,\Gamma_2\cosh u_1-(\pi/4))}.$$

Simplification of eq. (22) yields

$$(23)\qquad \sin c_0\,\Gamma_2(\cosh u_1-\cosh u_0) = 0.$$

Recalling that $\Gamma_2^2 = k_2^2 - h^2$, eq. (23) yields an expression for the propagation constant of the higher-order symmetric modes. There results

$$(24)\qquad h_{0p} = \sqrt{k_2^{\,2}-\left[\frac{p\pi}{c_0(\cosh u_1-\cosh u_0)}\right]^2}\qquad (p = 1, 2, 3, \ldots).$$

In eq. (24) note that $c_0 \cosh u_1 = a_1$, the semimajor axis of the outer conductor, and $c_0 \cosh u_0 = a_0$, the semimajor axis of the inner conductor. It is apparent that the condition for the propagation of the higher-order modes is a function of the relative sizes of the two conductors. Further, by equating the two terms under the radical sign of eq. (24), one obtains a simple expression for the critical frequencies of the higher-order modes.

Consider again the condition for the propagation of the principal wave. For $\Gamma_2 \rightarrow 0$, and utilizing the equivalent series expansions for the functions $Je_0'(s_2, u)$ and $Ne_0'(s_2, u)$, it can be shown that in the limiting case $Je_0'(s_2, u) \rightarrow 0$ and $Ne_0'(s_2, u) \rightarrow \sqrt{(2/\pi)} \tanh u$. Consequently in eq. (12), $A = 0$ and the expression for the magnetic field in region (2) becomes

$$(25) \qquad {}^{(2)}H_v = \frac{-ik_2^2}{\Gamma_2^2 \mu_2 \omega h_u} \{B\sqrt{(2/\pi)} \tanh u \; Se_0(s_2, v)\} \, e^{-ik_2 z}.$$

The longitudinal current can be obtained from Ampere's law

$$(26) \qquad I = \oint {}^{(2)}H_v \, h_v \, dv$$

where the current is of the form $I = I_0 e^{-ik_2 z}$. Hence,

$$(27) \qquad B = \frac{\Gamma_2^2 \mu_2 \omega I_0}{2\sqrt{2\pi} \, . \, i \, k_2^2 \tanh u}.$$

Inserting B in eq. (25) yields

$$(28) \qquad {}^{(2)}H_v = 1/2\pi \, h_u.$$

The transverse voltage along the line can be found by integrating the radial component of the electric field from u_0 to u_1,

$$(29) \qquad V = \int_{u_1}^{u_0} E_u \, h_u \, du = \frac{\omega \mu_2 I}{2\pi k_2} (u_1 - u_0).$$

Finally, the characteristic impedance Z_0, which is defined as the ratio of the transverse voltage to the longitudinal current, is given by:

$$(30) \qquad Z_0 = \frac{\omega \mu_2}{2\pi \, k_2} (u_1 - u_0).$$

For the special case of the inner conductor consisting of a flat strip, $u_0 = 0$; hence the characteristic impedance becomes simply

$$(31) \qquad Z_0 = \frac{\omega \mu_2}{2\pi k_2} \cosh^{-1}(a_1/c_0).$$

In passing it should be mentioned that the characteristic impedance can also be determined from electrostatic considerations. A solution using a conformal transformation method is given as an example in Smythe (1939).

CONCLUDING REMARKS

A formula has been derived for the propagation constant of the allowed symmetric modes of propagation. It was discovered that a principal wave exists whose propagation constant is that of the medium bounded by the two conducting cylinders. Higher-order modes may also exist, but in a practical

line they are characterized by high attenuation and therefore belong to the class of evanescent modes. The preceding analysis may be useful in providing an approximate theory for a coaxial line consisting of a strip inner conductor surrounded by an outer sheath of rectangular cross section.

ACKNOWLEDGMENT

The author is indebted to Dr. G. C. McCormick for his helpful comments and suggestions in the preparation of this paper.

REFERENCES

BEGOVICH, N. A. and MARGOLIN, A. R. 1950. Hughes Aircraft Company Rept. No. **234**. May.

COHN, S. B. 1954. Trans. I.R.E. MTT-**2**: 52.

KARBOWIAK, A. E. 1954. Brit. J. Appl. Phys. **5**: 328.

MORSE, P. M. and FESHBACH, H. 1953. Methods of theoretical physics. Part II. McGraw-Hill Book Company, Inc., New York. Chap. 11.

SINCLAIR, G. 1951. Proc. I.R.E. **39**: 660.

SMYTHE, W. R. 1939. Static and dynamic electricity. McGraw-Hill Book Company, Inc., New York. Chap. 4.

STRATTON, J. A. 1941. Electromagnetic theory. McGraw-Hill Book Company, Inc., New York.

STRATTON, J. A., MORSE, P. M., CHU, L. J., and HUTNER, R. A. 1941. Elliptic cylinder wave functions. John Wiley & Sons, Inc., New York.

Trans. I.R.E. 1955. MTT-**3**. Mar.

ON THE EFFECT OF SPEED ON THE KINETIC FRICTION OF SOME PLASTIC MATERIALS ON ICE[1]

BY C. D. NIVEN

ABSTRACT

Curves are shown illustrating the effect of speed on the friction of teflon, bakelite, nylon, terylene, plexiglas (perspex), cellulose acetate, polystyrene, and polyethylene, sliding on ice at $-5°$ C. and $-15°$ C. Bakelite and teflon had the lowest kinetic friction of the materials examined. Terylene also slid easily but polyethylene had rather high friction. Departure from Amontons' Law was very evident at high speed.

INTRODUCTION

Very little is known about the friction of plastic materials on ice and the work described below was originally started with a view to tabulating friction constants on ice like the other physical constants of plastics. The investigation soon revealed that friction on ice depends on several factors besides temperature. While the work was in progress a paper was published by Bowden (1953) in which it was concluded that teflon (polytetrafluoroethylene) had a much lower static friction than perspex (methyl methacrylate), nylon, or terylene (ethylene terephthalate) on packed snow, and that Amontons' Law was obeyed for static friction values.

The writer's results had, however, shown up to that date that kinetic friction on solid ice violated Amontons' Law and was definitely dependent on loading. Bowden gave an order of magnitude for the kinetic friction values of some of the plastics but did not show drag vs. load curves for moderate or higher speeds. The work described in the present communication concerns the effect of speed on the drag values of samples 10 cm.^{2} loaded heavily.

METHODS

The work was done on the turntable described already (Niven 1954); the method of loading has also been described and accounts for the non-integral load values of 14.9, 39.1, 63.3, and 87.6 kgm. being used in the measurements. The drag was measured as before by direct weighing. The table was driven by means of a d-c. motor, the speed of which could be varied by a resistance. It was found that when the speed was cut down the motor had insufficient power to drive the table owing to the "stick-slip" phenomenon so well known in friction measurements. This trouble of course entirely disappeared at high speeds, but at very low speed the table had to be turned by hand or the motor helped by hand. The exact speed of revolution was thus not known accurately and is simply designated as under 12 r.p.m. Another set of measurements was made at about 20 r.p.m. and a third set at around 80 r.p.m. These speeds correspond to "less than 1.1 m.p.h.", 1.8 m.p.h., and 7.1 m.p.h. However in view of the fact that the slider was sliding in the same track at each revolution,

[1]Manuscript received November 10, 1955.
Contribution from the Division of Applied Physics, National Research Council, Ottawa, Canada. Issued as N.R.C. No. 3881.

the drag values are probably too low—particularly at high speeds—and in order to avoid the possibility that the casual reader might take too much out of the graphs, r.p.m. values and not m.p.h. values have been assigned to the various curves.

The results must be considered approximate; in most cases at least two points are given for drag values, but in many instances more points were available for plotting. Getting exact repetition in friction measurements is a constant source of disappointment to the experimentalist and when conditions are such that the slider starts the stick-slip motion it becomes almost guesswork to assign a drag value at all. Poor repetition at slow speeds and low temperatures was therefore to be expected. At high speed repetition was, however, good enough to permit of a satisfactory estimate being made of the position of the drag vs. load curve. To indicate how often the same value for a drag measurement was obtained arabic numerals have been attached to repeated points, and so in tracing the curves points with a high numeral attached have been favored. These curves are approximate and have been drawn mainly to show at a glance the important effect of speed.

The samples consisted of pieces of material $2\frac{1}{2}$ cm. wide and $4\frac{1}{2}$ cm. long, which gave an area of 10 $cm.^2$ after the front edge had been rounded off. Since perspex, lucite, and plexiglas are trade names for the same material, the chemical name, methyl methacrylate, has been used to avoid ambiguity. The material called terylene was, according to the supplier, "essentially polyethylene terephthalate with an admixture of titanium oxide as a delustrant. It is made by the addition reaction of ethylene glycol with terephthalic acid or an equivalent compound." Pliofilm is a rubber hydrochloride and was received from the manufacturer as a thin sheet 0.0025 in. thick. The vinylite sample was cut from a flexible sheet 0.036 in. thick. These two samples had to be specially clamped to small blocks of smooth flat brass for the tests. Since Bowers, Clinton, and Zisman (1954) have found that a thin film of a polymer on a metal surface has lower friction than the bulk polymer, it is unsafe to compare the curves for these two samples, particularly that for the thin pliofilm, with those for the other samples. They are shown in Fig. 5 but will not be referred to further in this article.

RESULTS AND DISCUSSION

The results are shown in Figs. 1–5. Fig. 1 refers entirely to teflon; so many observations were made on this important material that clarity demanded a separate diagram for each speed. Figs. 2, 3, and 4 refer to bakelite, terylene, methyl methacrylate, polystyrene, cellulose acetate, nylon, and polyethylene. They have been grouped roughly according to sliding qualities. Fig. 5 was mentioned above.

The figures show graphically what Bowden mentioned in the text, namely, that when sliding speed is increased there is a very marked drop in friction—in other words speed is another variable which has to be taken into account in evaluating an ice friction constant. The graphs also show that the drag vs. load relation curves toward the load axis at high speed more markedly than

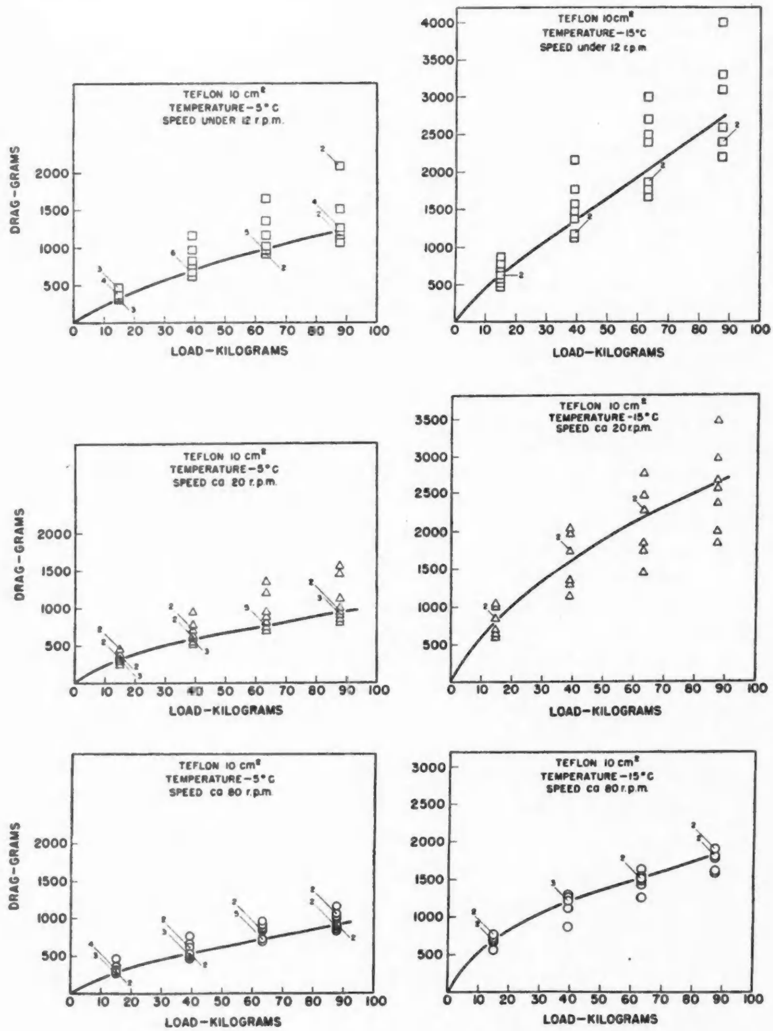

FIG. 1. Drag vs. load curves for teflon at −5° C. and −15° C.

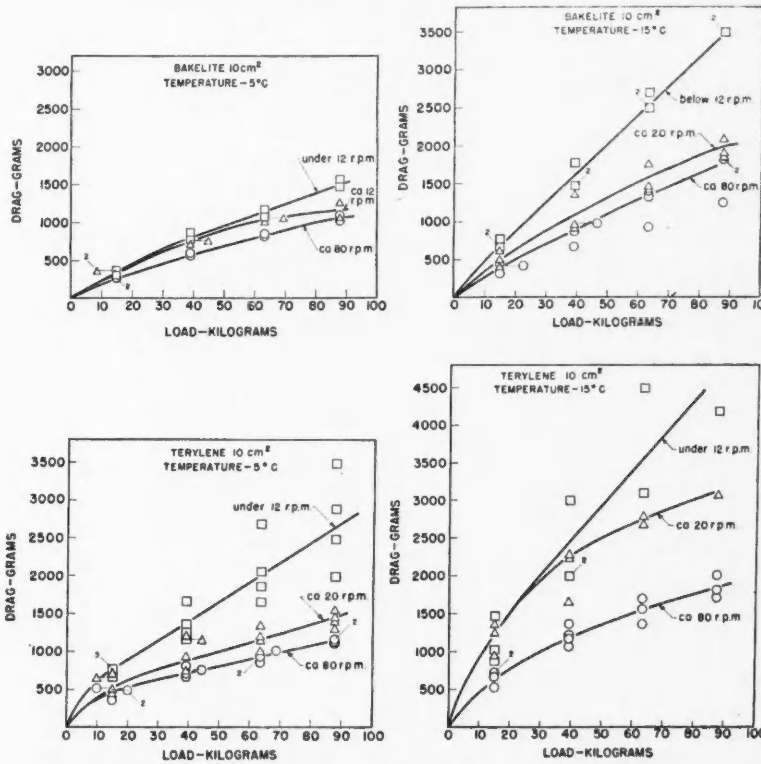

FIG. 2. Drag vs. load curves for bakelite and terylene at −5° C. and −15° C.

at low speed. Thus there is a suggestion that as speed is lowered to zero the curvature may disappear altogether and the relation become linear. Bowden working with loadings of less than 6 kgm. on 75.4 cm.[2] found a linear relation for velocities close to zero; such loadings correspond to about 1.2 kgm. on the writer's graphs. Over such a small range departure from the linear relation might be quite difficult to detect; nonetheless the points for perspex and nylon given in Fig. 7 of Bowden's paper would permit of a slight curvature for the relation which has been drawn in that diagram as a straight line.

The finding that ice friction decreases with increase of speed fits in quite well with the conception that the tips of the asperities melt by "frictional heat". This being so, the usefulness of the turntable in making precise measurements of friction may be limited because the frictional heating effect must be cumulative, when the slider passes over the same track again and again. On the other hand the fact that the friction drops immediately as soon as the turntable is speeded up shows that the cumulative effect is secondary and not the main cause of the reduction in friction with speed.

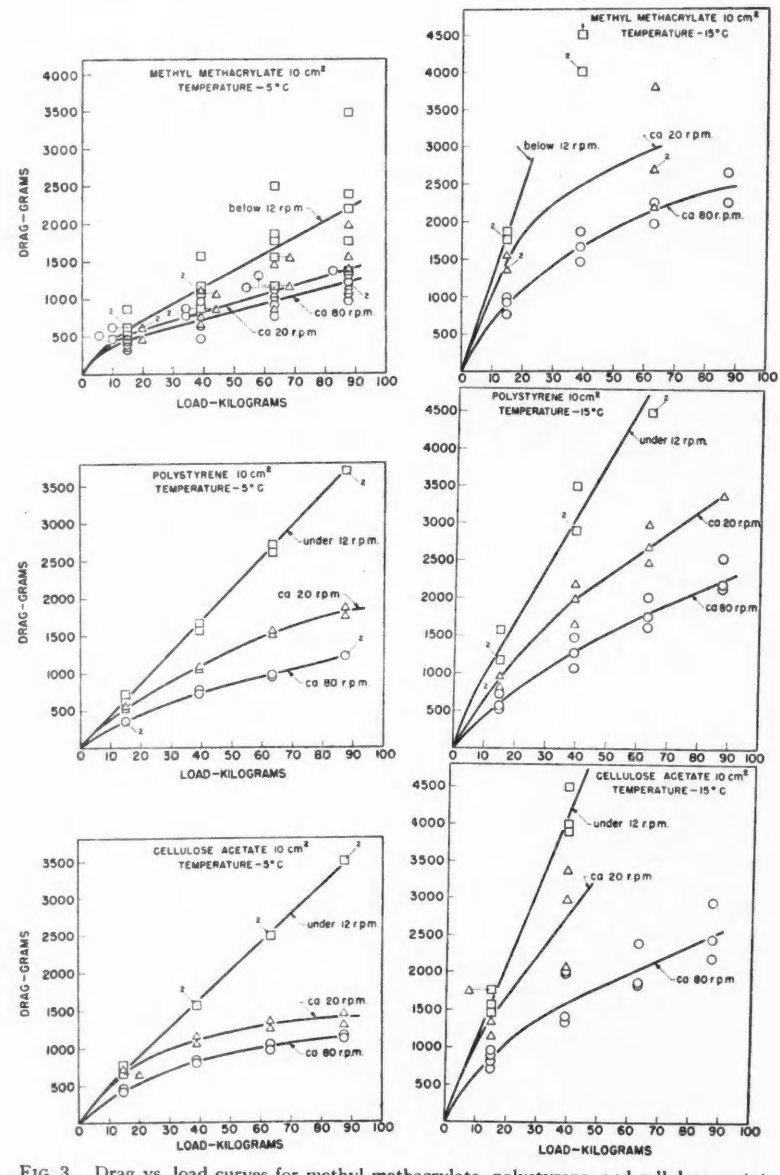

FIG. 3. Drag vs. load curves for methyl methacrylate, polystyrene, and cellulose acetate at −5° C. and −15° C.

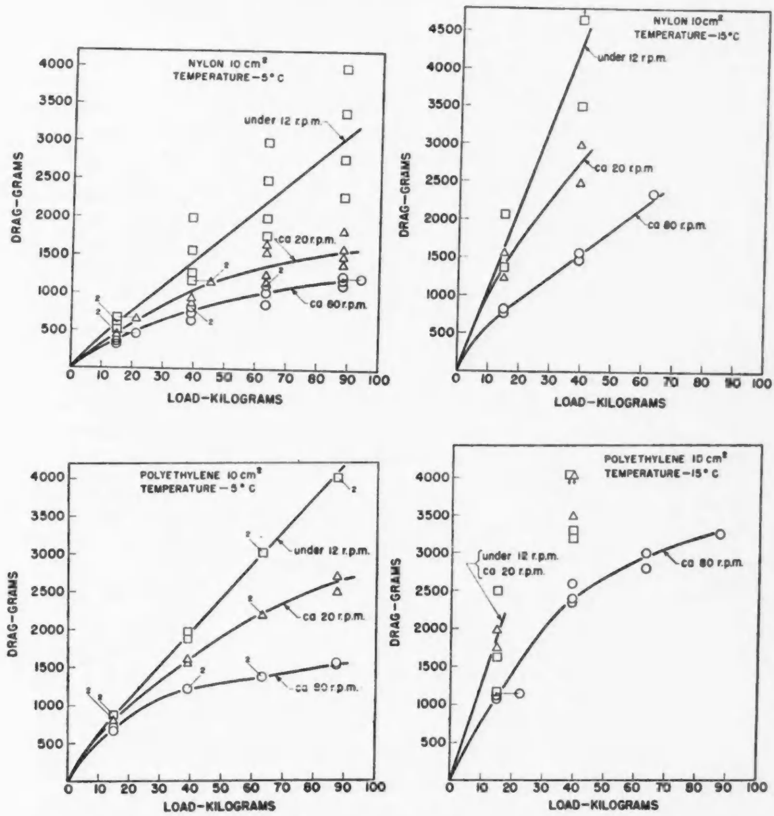

FIG. 4. Drag vs. load curves for nylon and polyethylene at −5° C. and −15° C.

The graphs for the various plastics do not entirely endorse such an outstanding superiority for teflon as Bowden implies nor do they permit of grouping nylon, terylene, and methyl methacrylate together. Since the curvature on the writer's graphs below 1.5 kgm. is not accurately known, it is hard to make a comparison with Bowden's values. Table I must therefore be considered as giving merely a rough estimate of the kinetic friction of teflon, nylon, terylene, and methyl methacrylate—at −5° C. and −15° C.—loaded with less than 1 kgm. on a 10 cm.² area and moving over the ice very slowly.

Bowden gives a value for "real ski" of 0.045 at −5° C. and 0.05 at −11° C. for teflon on packed snow. The writer's estimate is not too far out of line with these values. However Bowden's values of 0.34 for perspex and 0.30 for nylon on packed snow at −10° C. do not fit in with the writer's results. Small changes in r.p.m. at low speeds do undoubtedly make large changes in friction so there

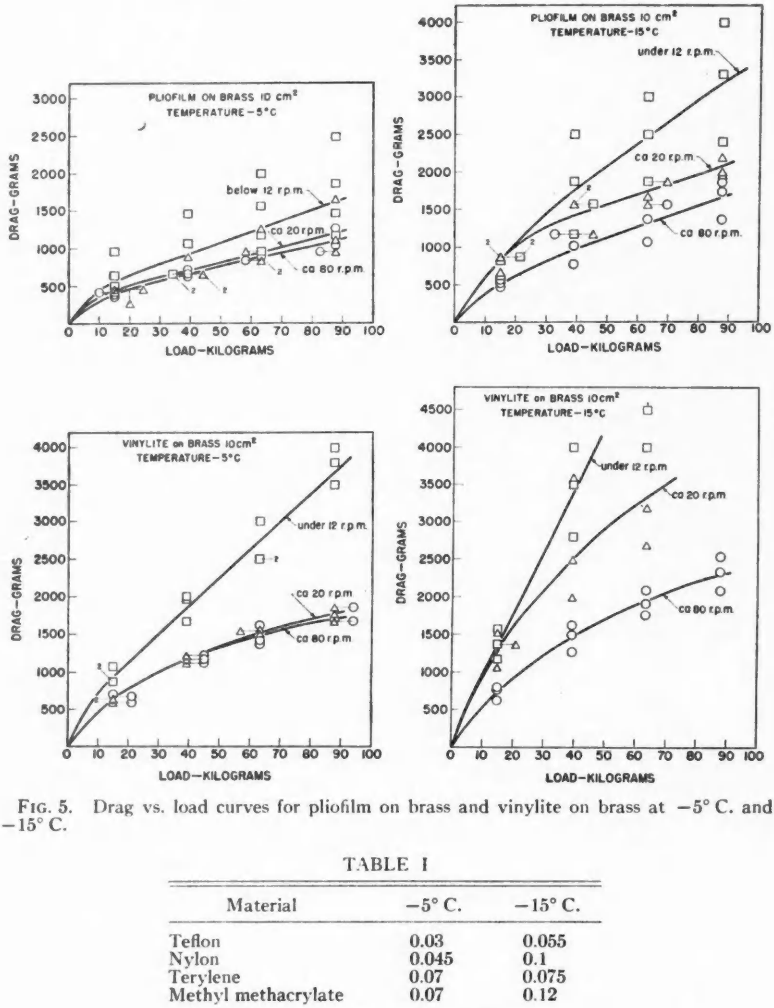

FIG. 5. Drag vs. load curves for pliofilm on brass and vinylite on brass at −5° C. and −15° C.

TABLE I

Material	−5° C.	−15° C.
Teflon	0.03	0.055
Nylon	0.045	0.1
Terylene	0.07	0.075
Methyl methacrylate	0.07	0.12

is the possibility that the writer's lowest speed was still too high to simulate static friction.

Bowden's instrumentation did not permit of precise values being given for the kinetic friction but his estimate of 0.02 for a kinetic friction value at −10° C. fits in with the writer's results. There is, however, no possibility of using the writer's graphs to establish the fact that teflon can be assigned a friction value, under the experimental conditions used, equal to one third or

one quarter of that of nylon, perspex, or terylene; nor can the statement be endorsed unconditionally that "the friction is directly proportional to the applied load". It is untrue at high loadings and high speeds.

With the present state of our knowledge of the friction of ice in general, it is premature to assign friction values to the various plastic materials because these values depend not only on temperature but on loading, speed, and the condition of the ice; some believe that even the atmospheric humidity plays a part. Ice simply does not conform to the ordinary laws of friction and the explanation of its anomalous behavior almost certainly depends on the fact that it expands on freeezing. One other point, however, must not be overlooked—the observations are being made on this anomalous solid near its melting point.

The graphs submitted above do nonetheless give an idea of the order in which the various plastics must be arranged for kinetic friction value. It must be stressed, however, that this is merely a suggested order and is not based on a statistical treatment of a large number of measurements.

At $-15°$ C. the suggested order is as follows: 1. bakelite (smallest); 2. teflon; 3. terylene; 4–6. methyl methacrylate, cellulose acetate, polystyrene; 7. nylon; 8. polyethylene (largest).

At $-5°$ C. it is somewhat harder to arrange the materials but the graphs lead one to suggest the following order: 1, 2. teflon, bakelite; 3–7. terylene, methyl methacrylate, polystyrene, cellulose acetate, nylon; 8. polyethylene.

The measurements at $-15°$ C. simply will not allow nylon to be bracketed with terylene; other measurements not reported here endorsed that conclusion.

CONCLUSIONS

(1) At high speeds on ice the departure from Amontons' Law is more pronounced than at low speeds.

(2) At $-15°$ C. high speed reduces the friction more markedly than at $-5°$ C.

(3) Teflon and bakelite have lower kinetic friction values on ice than most other plastics have. Polyethylene has a comparatively high one.

REFERENCES

Bowden, F. P. 1953. Proc. Roy. Soc. (London), A, **217**: 462.
Bowers, R. C., Clinton, W. C., and Zisman, W. A. 1954. Modern Plastics, **31**: 131. Feb.
Niven, C. D. 1954. Can. J. Phys. **32**: 782.

END-FIRE ARRAYS OF MAGNETIC LINE SOURCES MOUNTED ON A CONDUCTING HALF-PLANE[1]

By R. A. Hurd

ABSTRACT

Formulae are developed for the far-field radiation patterns of end-fire arrays of magnetic line sources mounted on the surface of a half-plane. Patterns have been plotted for a number of interesting cases. It is found that the Hansen–Woodyard optimum end-fire condition no longer holds when the array is near the edge of the half-plane. The theory seems to describe reasonably well the behavior of corrugated surface radiators embedded in a finite ground plane, providing the array is removed from the edge by a distance about equal to the array length.

INTRODUCTION

Although there is a considerable body of literature dealing with various aspects of diffraction by a half-plane, the problem of antenna arrays in the presence of a half-plane seems to have received little attention. Moullin (1949, pp. 196–198) has computed some patterns for arrays radiating broadside to the half-plane, while Elliott (1954) has considered approximately the effect of a finite ground plane on the radiation pattern of a corrugated surface.

In this paper we derive expressions for the radiation patterns of arrays of magnetic line sources (e.g. slots) embedded in a perfectly conducting half-plane. The sources are taken to be infinitely long, and are presumed to run parallel to the edge of the plane (in the z direction), making the problem two-dimensional. It is assumed that the sources radiate only into the region *above* the plane, and that the phasing is such that the array would normally end-fire towards the edge of the plate. The effect of the plate is to cause the direction of fire to be tilted away from the line of the array, as indicated in Fig. 1. We shall be interested in finding out how the beam tilt, the beam width, and the side-lobe level behave as functions of the various parameters of the array.

EXPRESSION FOR THE RADIATED FIELDS

Suppose, in the (ρ, ϕ, z) co-ordinate system, we have a plane wave impinging on the plate from a direction ϕ; Fig. 2. The wave is assumed to have only a

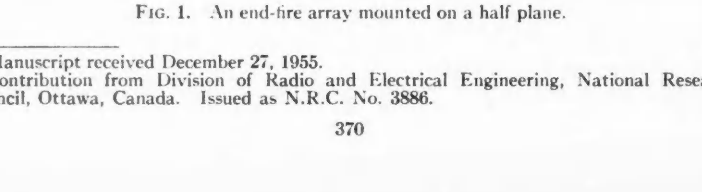

FIG. 1. An end-fire array mounted on a half plane.

[1]Manuscript received December 27, 1955.
Contribution from Division of Radio and Electrical Engineering, National Research Council, Ottawa, Canada. Issued as N.R.C. No. 3886.

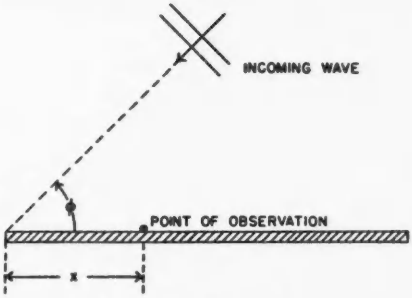

FIG. 2. The co-ordinate system.

z-component of magnetic field. Then from Baker and Copson (1950, pp. 142–144) the field at a point $(x, 0)$ on the screen is

$$H_z(x,0) = \frac{2}{\sqrt{\pi}} \exp(i\pi/4 + ikx\cos\phi) \int_{-\infty}^{\sqrt{2kx}\cdot\cos\phi/2} e^{-ix^2}dx. \tag{1}$$

A time dependence of $e^{i\omega t}$ has been assumed, and $k = \omega/c$.

By the principle of reciprocity Equation (1) gives the radiation pattern of a magnetic line source at $(x, 0)$.

Consider now an array of $N+1$ line sources on the plate a distance d apart. The amplitudes are assumed equal, but the phase of each is taken to be βd relative to the next. The pattern of the array becomes*

$$H_z = \frac{2e^{i\pi/4}}{\sqrt{\pi}} \sum_{n=0}^{N} \exp[i\beta nd + ik(D+nd)\cos\phi] \int_{-\infty}^{\sqrt{[2k(D+nd)]}\cos\phi/2} e^{-ix^2}dx. \tag{2}$$

Here D is the distance from the edge to the first element of the array. Making use of the integral

$$\int_{-\infty}^{0} e^{-ix^2}dx = 1/2\sqrt{\pi}\, e^{-i\pi/4}, \tag{3}$$

Equation (2) becomes

$$H_z = \sum_{n=0}^{N} \{1 \pm (1+i)[C(y) - iS(y)]\} \exp[i\beta nd + ik(D+nd)\cos\phi] \tag{4}$$

where $y = 2k(D+nd)\cos^2\phi/2$, and where $C(y)$ and $S(y)$ are the Fresnel integrals defined by

$$C(y) = \frac{1}{\sqrt{2\pi}} \int_0^y \cos x \frac{dx}{\sqrt{x}},$$

$$S(y) = \frac{1}{\sqrt{2\pi}} \int_0^y \sin x \frac{dx}{\sqrt{x}}.$$

In Equation (4), the (+) sign is to be taken in the "lit" region $0 < \phi < \pi$, the (−) in the shadow region $\pi < \phi < 2\pi$.

*The case of arrays of magnetic or electric line sources making some arbitrary angle with the half-plane could be treated by an easy extension of the present analysis.

Equation (4) is cumbersome for computational purposes, especially when N is large. A considerable improvement results if we consider a continuous array; that is, we let $d \rightarrow 0$, $N \rightarrow \infty$, in such a way that Nd remains constant and equal to L, the array length. The summation is replaced by an integration which can be performed easily. Equation (4) becomes

$$(5)\qquad H_z = \frac{e^{i(\beta-k+\gamma)u}}{i(\beta-k+\gamma)}\{1\pm(1+i)[C(\gamma u)-iS(\gamma u)]\}\Bigg|_{u=D}^{u=D+L} \pm\sqrt{\frac{\gamma}{\beta-k}}\,\frac{(i-1)}{\beta-k+\gamma}[C(\gamma u)+iS(\gamma u)]\Bigg|_{u=(\beta-k)D}^{u=(\beta-k)(D+L)}$$

where $\gamma = 2k\cos^2\phi/2$. Here again the $(+)$ signs pertain to the region $0 \leqslant \phi \leqslant \pi$, the $(-)$ signs to $\pi \leqslant \phi \leqslant 2\pi$.

Henceforth our calculations will be based on Equation (5). Whether or not a continuous array is a good approximation of a discrete one will depend on how large d is. As indicated later, the approximation seems good for d as large as $\lambda/4$ at least.

It is of interest to examine several limiting forms of (5). If we let $\beta \rightarrow k$, we obtain an end-fire array with free space phasing, whose pattern is given by

$$(6)\qquad H_z = \frac{e^{i\gamma u}}{i\gamma}\{1\pm(1+i)[C(\gamma u)-iS(\gamma u)]\}\pm(i-1)\sqrt{\frac{u}{\gamma}}\Bigg|_{u=D}^{u=D+L}.$$

If we let D become very large and assume that ϕ is sufficiently far removed from π so that γD is large, we have $C \rightarrow 1/2$, $S \rightarrow 1/2$, and therefore

$$(7)\qquad H_z = -2i\frac{e^{i(\beta-k+\gamma)u}}{\beta-k+\gamma}\Bigg|_{u=D}^{u=D+L} \quad \text{for } 0 \leqslant \phi < \pi, \text{ and}$$

$$(8)\qquad H_z = O(\gamma D)^{-\frac{1}{2}} \quad \text{for } \pi < \phi \leqslant 2\pi.$$

Equation (7) is just the pattern of an end-fire array embedded in an infinite ground plane.

When $\phi = \pi$, so that $\gamma = 0$, Equation (5) simplifies to

$$(9)\qquad H_z = \frac{e^{i(\beta-k)u}}{i(\beta-k)}\Bigg|_{u=D}^{u=D+L}.$$

THE RADIATION PATTERNS

When γ and D are such that the approximation of Equation (7) does not apply, it is necessary to resort to plotting Equation (5). This has been done in Figs. 3–7 for different values of $(\beta-k)L$ in the range 0 to 2π, with $\alpha = D/(D+L) = 0$. Normalized power is here plotted against the abscissa $\eta = (2kL)^{1/2}\sin\psi/2$, where $\psi = \pi-\phi$.

If we exclude the case $(\beta-k)L = 2\pi$, we observe that, for constant and large L, and increasing $\beta-k$:

(a) the main beam tilt decreases,

(b) the beam width increases,

(c) the side-lobe level increases.

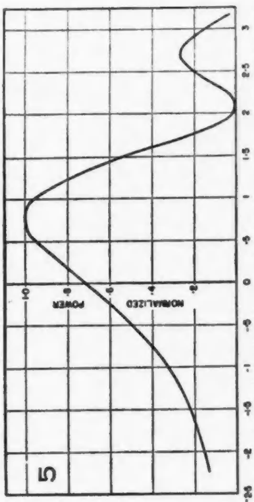

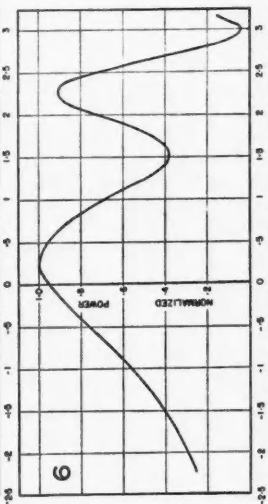

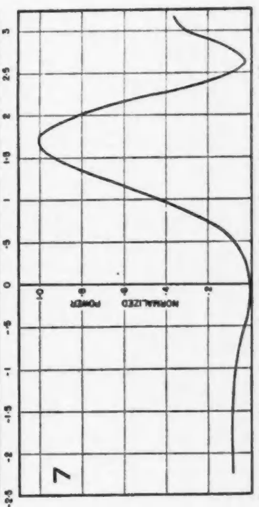

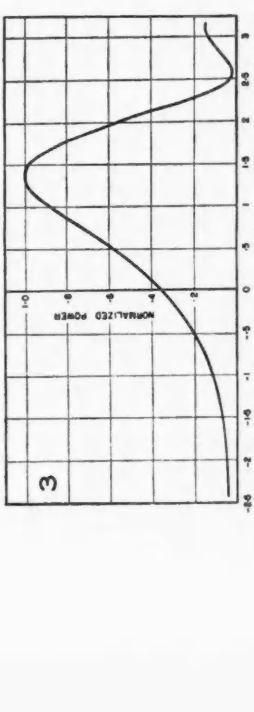

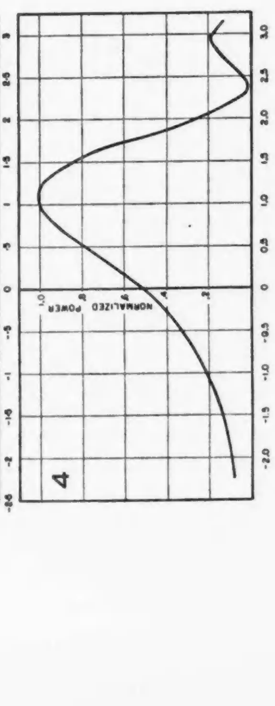

FIG. 3. Power pattern for $\beta = k$, $\alpha = 0$.
FIG. 4. Power pattern for $(\beta - k)L = \pi/2$, $\alpha = 0$.
FIG. 5. Power pattern for $(\beta - k)L = \pi$, $\alpha = 0$.
FIG. 6. Power pattern for $(\beta - k)L = 3\pi/2$, $\alpha = 0$.
FIG. 7. Power pattern for $(\beta - k)L = 2\pi$, $\alpha = 0$.

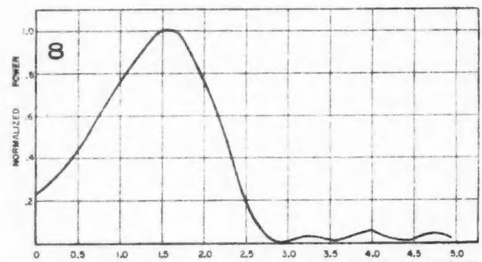

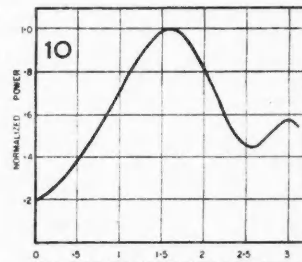

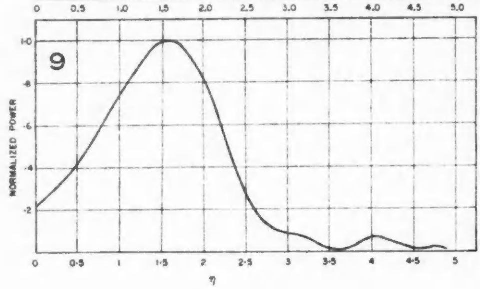

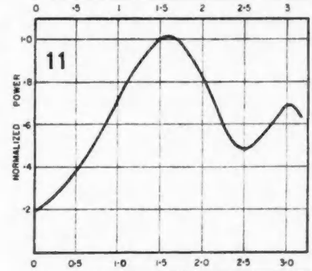

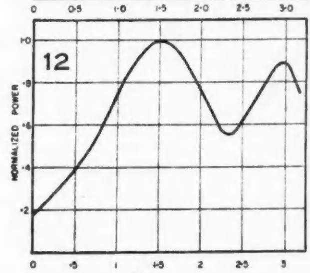

FIG. 8. Power pattern for $\beta = k$, $\alpha = 1/3$.
FIG. 9. Power pattern for $\beta = k$, $\alpha = 1/2$.
FIG. 10. Power pattern for $\beta = k$, $\alpha = 3/4$.
FIG. 11. Power pattern for $\beta = k$, $\alpha = 4/5$.
FIG. 12. Power pattern for $\beta = k$, $\alpha = 1$.

It thus appears that the directivity *decreases* continuously as $\beta - k$ increases. This is in direct contrast to what happens in a normal end-fire array, where the gain is a maximum for $(\beta - k)L = \pi$ (see Hansen and Woodyard 1938).

The pattern corresponding to $(\beta - k)L = 2\pi$ is an interesting one (Fig. 7). Apparently here the "main" lobe has been pushed into the shadow region, as evidenced by the low maximum near $\eta = -2$; and the "first side-lobe" has become the new main beam.

A second set of patterns is shown in Figs. 8–12. Here we take $\beta = k$ and let α range between 1/3 and 1. The abscissa in each case is taken to be $\eta = \sqrt{[2k(D+L)]}\sin\psi/2$. For $D+L$ constant and large we note that the half-power beam width is roughly constant up to $\alpha = 3/4$, at which point the beam width becomes meaningless because of high side-lobes. At $\alpha = 1/3$ the side-lobe level is lowest, being comparable to that of an ordinary end-fire array without ground plane; but the beam width is narrower than that of the enhanced end-fire array of length $D+L$ with no ground plane. For $\alpha = 1$

(Fig. 12), we get the expected pattern of a point source on a half-plane. Fig. 12 also gives the pattern for small ψ of a finite array at a large distance from the edge.

In Figs. 13–16 we plot the interesting case of $(\beta-k)L = \pi$ for various α values; (the curve for $\alpha = 1$ is the same as when $\beta = k$). The abscissae are

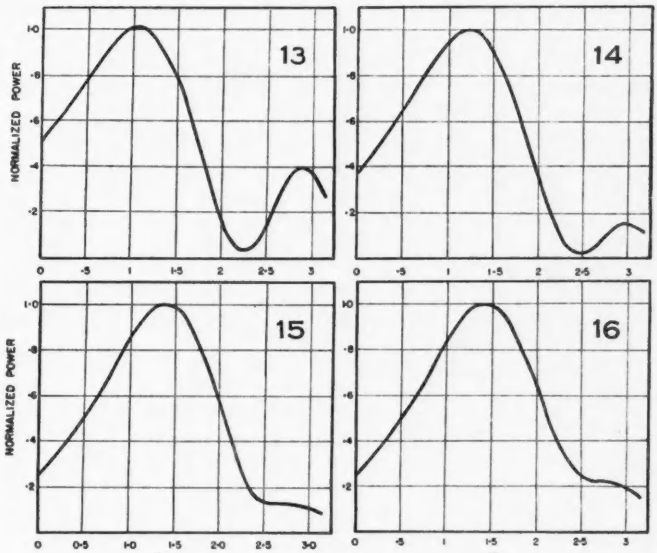

FIG. 13. Power pattern for $(\beta-k)L = \pi$, $\alpha = 1/3$.
FIG. 14. Power pattern for $(\beta-k)L = \pi$, $\alpha = 1/2$.
FIG. 15. Power pattern for $(\beta-k)L = \pi$, $\alpha = 3/4$.
FIG. 16. Power pattern for $(\beta-k)L = \pi$, $\alpha = 4/5$.

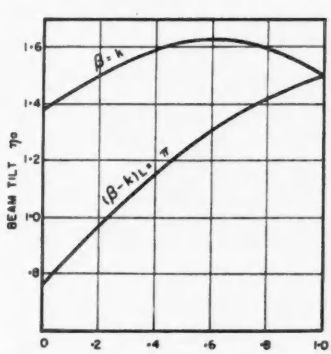

FIG. 17. The beam tilt η_0 as a function of α.

again $\eta = \sqrt{[2k(D+L)]} \sin \psi/2$. Here the beam width and the side-lobe level reach minima for α between 1/2 and 3/4. Thus the directivity is maximal here. In Fig. 17 we show the variation of the beam tilt η_0 with α for the cases $\beta = k$ and $(\beta - k)L = \pi$.

Comparing the patterns for $\beta = k$ with those for $(\beta - k)L = \pi$ it is seen that the directivity of the former is greater for α up to about 1/2. For $\alpha = 3/4$ the $(\beta - k)L = \pi$ pattern has become definitely more directive.

ANALOGY WITH SURFACE WAVE ANTENNAE

It is to be expected that corrugated surface and dielectric slab radiators will perform in a manner analogous to the end-fire arrays here considered. It is of interest then to compare previous theoretical and experimental results on corrugated surface antennae with the present theory.

In an interesting paper, Elliott (1954) has calculated the effect of a finite ground plane on the radiation pattern of a corrugated surface. We compare in Figs. 18 and 19 our results with Elliott's theoretical and experimental results.

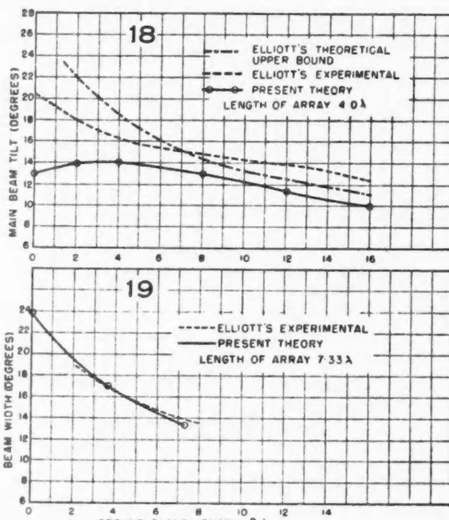

FIG. 18. Comparison of experimental and theoretical results on the beam tilt.
FIG. 19. Comparison of experimental and theoretical results on the beam width.

It is seen that insofar as the beam tilt is concerned, Elliott's theory agrees more nearly with experiment. On the other hand, our values of beam width agree quite well with experiment.*

It appears from Fig. 18 that our theory is not too applicable to corrugated surfaces as far as the beam tilt is concerned when α is less than 1/2. For α greater than 1/2 agreement is reasonable. We have seen that at $\alpha = 1/2$ the directivity is much the same for $\beta = k$ as for $(\beta - k)L = \pi$. It is therefore sug-

*Elliott does not give a theoretical value for the beam width, other than a lower bound.

gested that the end-fire condition $(\beta-k)L = \pi$ may not be optimal for corrugated surfaces with α near 1/2.

An experimental study of this point seems desirable.

COMPARISON WITH DISCRETE ANTENNA

In Fig. 20 we compare the pattern of a discrete array having $d = \lambda/4$, $D = 0, L = 2\lambda$, $(\beta-k)L = \pi$ with the relevant continuous array. The patterns

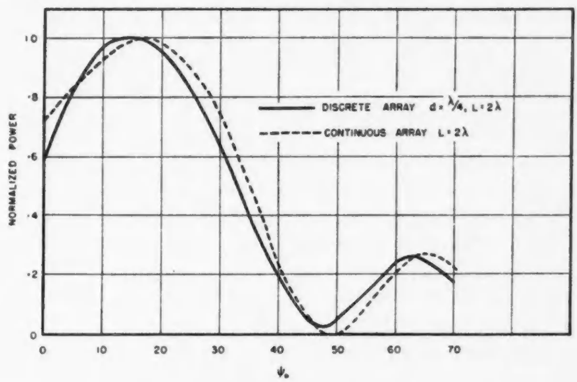

FIG. 20. Comparison of discrete and continuous array.

show generally good agreement, and appear to justify basing our computations on the continuous distribution.

CONCLUSIONS

Exact expressions have been derived for the far fields of an end-fire system of equally spaced magnetic line sources mounted on a half-plane. The continuous array appears to be a reasonable approximation to a discrete array for source spacings of up to $\lambda/4$. Three sets of patterns have been computed for the continuous array; they are:

(i) ground plane length $D = 0$, $(\beta-k)L$ ranging between 0 and 2π,

(ii) $\beta = k$, various values of $\alpha = D/(D+L)$,

(iii) $(\beta-k)L = \pi$, various values of α.

The continuous end-fire array seems to represent fairly well a corrugated surface with finite ground plane provided $\alpha > 1/2$ approximately.

ACKNOWLEDGMENT

The author wishes to thank Mrs. N. M. McCreery and Miss M. L. Taylor for doing most of the computations.

REFERENCES

BAKER, B. B. and COPSON, E. T. 1950. The mathematical theory of Huygens' principle. 2nd ed. Oxford University Press, London.

ELLIOTT, R. S. 1954. Trans. I.R.E. Professional Group on Antennae and Propagation, Vol. AP-2, 2, April.

HANSEN, W. W. and WOODYARD, J. R. 1938. Proc. I.R.E. **26**: 333.

MOULLIN, E. B. 1949. Radio aerials. Oxford University Press, London.

THE RELATIONSHIP BETWEEN THE STATISTICAL AND FIELD THEORETICAL TREATMENTS OF MULTIPLE MESON PRODUCTION[1]

By Yasushi Takahashi[2]

ABSTRACT

The aim of this note is to point out the relation between Fermi's statistical theory of multiple meson production and the field theoretical treatment.

Since Heisenberg emphasized the theoretical importance of multiple meson production as a phenomenon beyond the applicability of quantum field theory, many investigations have been made. Among them, the LOW theory and the statistical discussion by Fermi are well known (Fermi 1950; Lewis 1951; Milburn 1955). These theories are based on assumptions considered to be appropriate for fast and slow collisions, respectively. By fast we mean that the collision time is very much shorter than the reaction time.

As is well known, the LOW theory is valid when the Bloch–Nordsieck approximation is good. On the other hand Fermi's idea is that the energy will be concentrated in a small volume during the collision and statistical equilibrium will be reached so that the probability that a certain number of particles are created is essentially determined by statistical laws. This assumption would be a good approximation if the collision time were long enough compared with the reaction time.

We shall show in this note the relation between these two theories.[3]

According to our previous paper (Umezawa *et al.* 1952), the total probability for the production of n mesons by a nucleon is

$$(1)^4 \quad w_n = \frac{1}{n!}\int_{(\text{con.})}\cdots\int \frac{d\mathbf{k}_1}{(2\pi)^3}\cdots\frac{d\mathbf{k}_n}{(2\pi)^3}\,\Delta N(\mathbf{k}_1)\ldots\Delta N(\mathbf{k}_n)\,.\,|v(\Delta P,\Delta E)|^2,$$

where (con.) signifies that the integration has to be carried out in such a way as to satisfy the conservation laws

$$(2) \qquad \begin{cases} \Delta\mathbf{P} = \sum_{i=1}^{n}\mathbf{k}_i, \\ \Delta E = \sum_{i=1}^{n} K_i. \end{cases}$$

[1]Manuscript received October 28, 1955.

Contribution from the Division of Pure Physics, National Research Council, Ottawa, Canada. Issued as N.R.C. No. 3885.

[2]National Research Laboratories Postdoctorate Fellow; now at Department of Physics, State University of Iowa, Iowa City, Iowa.

[3]The importance of this problem was specially emphasized by Professor Taketani a few years ago.

[4]It is of importance that (1) is derived under the assumption that the $O(k)$ and $v(\Delta P, \Delta E)$ (see below) are commutable with one another, i.e., the production of each meson takes place in a statistically independent way. The notation is as follows:

$$\Delta N(k) = \frac{1}{2}\frac{g^2}{K}\left(\frac{\Delta O(k)}{K-k_0}\right)^2, \qquad \sqrt{(k^2+\mu^2)} = K, \qquad \mu = \text{the meson mass;}$$

$\Delta O(k) = O'(k) - O''(k)$ is the difference of $O(k)$ before and after the nucleon scattering by the potential v. $O(k)$ is a quantity describing the nucleon state in the meson cloud.

If we work with the occupation number representation, (1) can be rewritten as

$$w_n = \frac{1}{n!}\sum_{i_1}\sum_{\substack{i_2 \\ \text{(con.)}}}\cdots\sum_{i_n}\left\{\frac{\Delta N(k_{i1})}{V}\right\}\cdots\left\{\frac{\Delta N(k_{in})}{V}\right\}\cdot|v(\Delta P, \Delta E)|^2$$

$$= \frac{1}{n!}\sum_{\substack{n=n_1+\dots \\ \text{(con.)}}} n!\prod_s \frac{1}{n_s!}\left\{\frac{\Delta N(k_s)}{V}\right\}^{n_s}\cdot|v(\Delta P, \Delta E)|^2$$

$$\equiv \sum_{\substack{n=n_1+\dots \\ \text{(con.)}}} dw_n(n_1, n_2, \dots), \tag{3}$$

where

$$dw_n(n_1, n_2, \dots) = \prod_s \frac{1}{n_s!}\left\{\frac{\Delta N(k_s)}{V}\right\}^{n_s}\cdot|v(\Delta P, \Delta E)|^2 \tag{4}$$

with

$$\begin{cases} n = \sum_s n_s, \\ \Delta\mathbf{P} = \sum_s \mathbf{k}_s n_s, \\ \Delta E = \sum_s K_s n_s. \end{cases} \tag{5}$$

The quantity $dw_n(n_1, n_2, \dots)$ is interpreted to be the probability for the production of n_1 mesons with momentum k_1, n_2 mesons with momentum k_2, and so on.

It should be noted that our observation of multiple meson production phenomena is not that of w_n but that of the most probable $dw_n(n_1, n_2, \dots)$. From this point of view, we shall try to find the most probable distribution under the conservation condition.[5] This is easily done as follows: For the sake of simplicity we will assume $\Delta N(k)$ to be independent of the direction of $\mathbf{k}$. In this case, the momentum conservation law may be omitted. The most probable distribution will be obtained by maximizing dw_n under variation of all the arguments $n_1, n_2, \dots$, subject to the energy conservation law; thus,

$$\frac{\partial}{\partial n_s}\left[\log\prod_s \frac{1}{n_s!}\left\{\frac{\Delta N(k_s)}{V}\right\}^{n_s} + \beta\left\{\Delta E - \sum_s K_s n_s\right\}\right] = 0. \tag{6}$$

This gives

$$n_s = \frac{\Delta N(k_s)}{V}e^{-\beta K_s}, \tag{7}$$

where β will be determined by

$$\Delta E = \sum_s K_s n_s = (2\pi)^{-3}\int K\Delta N(k)\, e^{-\beta K}dk. \tag{8}$$

Then the multiplicity n will be given by

$$n = \sum_s n_s = (2\pi)^{-3}\int \Delta N(k)\, e^{-\beta K}dk. \tag{9}$$

---

[5]Since we are interested in the production of any number of mesons, the conservation of the meson number is not required.

We immediately notice the similarity between our equations (8) and (9) and Fermi's statistical theory. Our ΔN plays the same role as Fermi's Ω. In fact, if we take Ω as ΔN, which is independent of k but proportional to E^{-1} (E is the energy of the incident nucleon), we get from (9) and (8)

$$n = 1.42(w-2)^{3/4}/w^{1/4}, \quad (w \equiv E/M), \tag{10}$$

which is in agreement with Fermi's multiplicity.[6] The above assumption exactly corresponds to Fermi's choice

$$\Omega = \Omega_0 \frac{2M}{E} = \frac{4\pi}{3} \mu^{-3} \frac{2M}{E}. \tag{11}$$

Our $\Delta N(k)$ has wider freedom than Fermi's Ω does.

We may thus conclude that Fermi's statistical treatment of meson production is not far from the field theoretical discussion, in spite of their difference in appearance, and can be considered as a special case where the meson cloud spectrum $\Delta N(k)$ is proportional to E^{-1}.

A detailed account will appear later on.

ACKNOWLEDGMENT

The author wishes to express his thanks to Dr. Allcock for helpful discussions.

REFERENCES

FERMI, E. 1950. Progr. Theoret. Phys. (Japan), **5**: 570.
LEWIS, H. W. 1951. Revs. Mod. Phys. **24**: 241. Complete references will be found in this review article.
MILBURN, R. H. 1955. Revs. Mod. Phys. **27**: 1.
UMEZAWA, H., TAKAHASHI, Y., and KAMEFUCHI, S. 1952. Phys. Rev. **85**: 505.

Note added in proof: Since this paper was submitted, almost the same discussion of the problem by Dr. Ito (to be published in the Progress of Theoretical Physics) was brought to my attention. I would like to thank Dr. Ito for informing me of his results before publication.

[6]Fermi's formula (32) has a minor mistake. It should be $1.34(w-2)^{3/4}/w^{1/4}$.

GAMMA RADIATION FROM THE PROTON BOMBARDMENT OF BORON TEN[1]

By G. B. Chadwick,[2] T. K. Alexander,[3] and J. B. Warren[4]

ABSTRACT

The gamma rays resulting from the bombardment of B^{10} with protons of energies from 0.5 to 2.0 Mev. have been observed with a sodium iodide scintillation counter. Capture radiation, of energy

$$E_\gamma = 8.81 \pm 0.05 + 10/11\ E_p \text{ Mev.},$$

showed a broad resonance at $E_p = 1135 \pm 15$ kev. At this energy, the radiation had an angular distribution of the form $1+(0.50\pm0.05)\cos^2\theta$ and a total cross section $(3.5\pm1.0)10^{-30}$ cm.[2] Several lower energy radiations were also observed and assigned tentatively to cascade transitions in C^{11}.

The cross section for the 430 kev. radiation from the reaction $B^{10}(p, \alpha\gamma)Be^7$ was found to be 0.21 ± 0.05 barn at $E_p = 1.52$ Mev. This radiation was found to be isotropic.

INTRODUCTION

The compound nucleus, C^{11*}, formed in the capture by B^{10} of protons of energy less than 3 Mev. decays mainly by alpha-particle emission. Brown *et al.* (1951) observed two groups of alpha particles corresponding to the formation of the residual nucleus, Be^7, in its ground and first excited states. The ground state group showed two broad resonances, at $E_p = 1.1$ and 1.5 Mev., while the other showed only one resonance at $E_p = 1.5$ Mev. Radiation of energy 9.47 Mev. from the competing reaction $B^{10}(p, \gamma)C^{11}$ was first observed by Walker (1950), who bombarded a thick target enriched in B^{10} with 1.16 Mev. protons and resolved the radiation with a magnetic pair spectrometer. The excitation function of this reaction was subsequently studied by two groups of investigators with conflicting results. Krone and Seagondollar (1953) reported resonances at $E_p = 0.78$, 0.95, and 1.33 Mev., while Day and Huus (1954) reported only one at $E_p = 1.2$ Mev. and possibly another at $E_p =$ 2.4 Mev.

In view of this discrepancy we have investigated the capture radiation from $B^{10}+p$ with a sodium iodide scintillation counter, and have searched for possible cascade transitions. A measurement of the cross section for production of 430 kev. radiation from the reaction $B^{10}(p, \alpha\gamma)Be^7$ was also made for comparison with previous measurements.

EXPERIMENTAL

Targets of magnetically separated B^{10}, stated to be 400 μgm./cm.[2] and 250 μgm./cm.[2] thick, deposited on gold and platinum, were kindly supplied by the Isotopes Division, A.E.R.E., Harwell. These targets were bombarded with resolved proton beams of energies from 0.5 to 2.0 Mev. produced by the

[1]Manuscript received November 24, 1955.
Contribution from the Department of Physics, University of British Columbia, Vancouver, B.C.
[2]Now at Cavendish Laboratory, Cambridge, England.
[3]Now at Chalk River Laboratories, Atomic Energy of Canada, Chalk River, Ontario, Canada.
[4]On leave of absence at National University, Canberra, Australia.

University of British Columbia Van de Graaff generator, and were steam heated to reduce carbon contamination. Proton energies were determined by measuring the accelerating voltage with a generating voltmeter which was calibrated with the well-known resonances of the reaction $F^{19}(p, \alpha\gamma)O^{16}$.

The gamma radiation was detected with a sodium iodide scintillation counter consisting of a 2 in. long by $1\frac{3}{4}$ in. diameter sodium iodide block mounted on an R.C.A. 6342 photomultiplier. The pulse height distribution from the counter was displayed on a 30 channel pulse height analyzer. Gamma-ray energies were determined by calibrating the system with the 2.62 Mev. radiation from Th C″ and the 6.13 Mev. radiation from the reaction $F^{19}(p, \alpha\gamma)O^{16}$. An occasional further calibration was made with the 9.17 Mev. gamma ray from the reaction $C^{13}(p, \gamma)N^{14}$ at E_p = 1.76 Mev. (Woodbury *et al.* 1953).

Preliminary runs showed that large gain shifts occurred in the photomultiplier when the counting rate arising from the 430 kev. radiation from the prolific reaction $B^{10}(p, \alpha\gamma)Be^7$ became too large. Such behavior has been reported previously by Caldwell and Turner (1954). In order to ensure stability, the rate of counting pulses representing over 0.4 Mev. energy release in the phosphor was monitored separately and kept below 3000 per second. This limitation made the time required to obtain a spectrum of the 9 Mev. radiation rather long and necessitated long term stability from the electronic system.

RESULTS

(*a*) *The 9 Mev. Radiation*

Figure 1 shows a typical pulse height distribution from the counter due to the radiation from the reaction $B^{10}(p, \gamma)C^{11}$ taken at 1.0 Mev. proton energy.

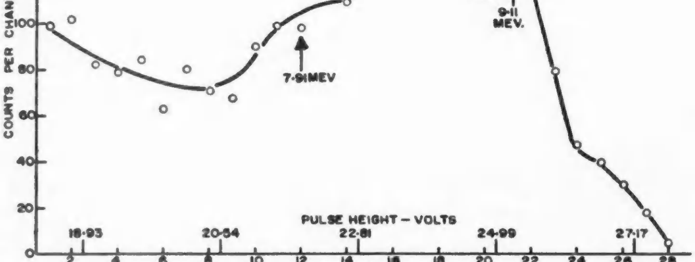

FIG. 1. Pulse height distribution from NaI(Tl) scintillation counter showing the 9.64 Mev. radiation from the reaction $B^{10}(p, \gamma)C^{11}$ at E_p = 1.0 Mev. Counter 10 cm. from target at 90° to incident beam direction.

The presence of $9.64 \pm .07$ Mev. radiation is obvious; the rise in the region of 7.9 Mev. is not attributed to a separate gamma ray, but rather to differential absorption of low energy bremsstrahlung quanta from fast pair electrons produced in the crystal.

Such spectra were obtained for proton energies from 0.5 to 1.6 Mev. in 100 kev. steps and with the counter at 90° to the beam. The gamma-ray energy varied with proton energy in the manner expected for a simple capture process, i.e.

$$E_\gamma = Q+10/11\ E_p,$$

where E_p was taken to be the incident proton energy less one half that lost in the target. The proton energy loss in the target was assumed to be the same as that for an equal mass per sq. cm. of beryllium, for which element the stopping power has been measured by Madsen (1953). Thus, for example, it was assumed that a 400 μgm./cm.^{2} target placed at 45° to the beam would reduce the energy of 1 Mev. protons by about 120 kev.

The mean Q value so determined from 10 measurements was 8.81 Mev. with a statistical deviation of 0.02 Mev. However in view of experimental uncertainties such as target thickness and multiplier drift we would only estimate our Q value error to be within ± 100 kev. The currently accepted mass values and p–n mass difference give $Q = 8.697$ Mev. (Ajzenberg and Lauritsen 1955), which is perhaps a little low but hardly outside the experimental uncertainties.

The excitation function of the 9 Mev. radiation is shown in Fig. 2. In plotting this curve the proton energy has been corrected for target thickness as described before. The yield was measured at 90° to the incident beam and

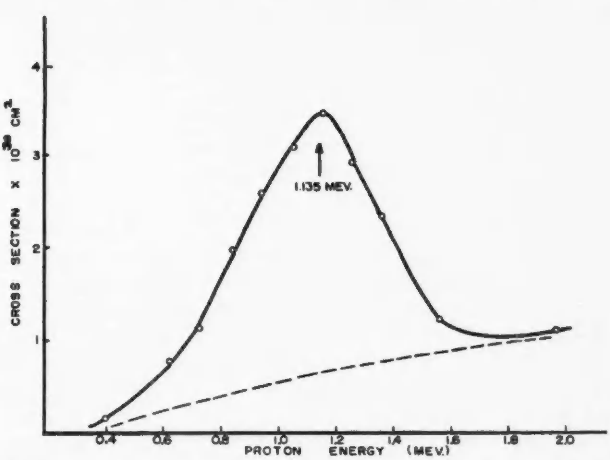

FIG. 2. Excitation function of the 9 Mev. gamma ray from the reaction $B^{10}(p, \gamma)C^{11}$. Proton energy corrected for target thickness, total cross section corrected for the angular distribution $(1+0.5 \cos^2\theta)$.

all counts falling in an energy interval of 2.4 Mev. below the full gamma-ray energy were taken as proportional to the 9 Mev. radiation, and it is believed this interval contained very few arising from 6 Mev. components in the radiation. The background subtracted was mostly from cosmic-ray events, since the runs were of long duration. A small beam-dependent background was noticed from radiation of energy above 10 Mev. which, if due entirely to the reaction $B^{11}(p, \gamma)C^{12}$, showed that there was less than 1 part in 300 of B^{11} in our targets. An angular distribution of the form $(1+0.5\cos^2\theta)$ has been assumed in correcting the 90° yield to total yield.

Because of the general similarity of this excitation function with that found by Brown *et al.* (1951) for the ground state alpha particles from $B^{10}(p, \alpha)Be^7$, the broad resonance at $E_p = 1.14$ Mev. is believed to arise from the same level in C^{11} at an excitation of 9.74 Mev. taking Q for the reaction as 8.70 Mev. After subtracting an assumed smoothly rising contribution from non-resonant capture or from a higher resonance, as shown by the dotted curve in Fig. 2, the full width at half height of the resonance curve is 540 kev. with an estimated uncertainty of ± 40 kev.

The absolute total cross section, σ, at the resonance energy was estimated to be $(3.5\pm1.0)10^{-30}$ cm.^{2} which is a factor of about two smaller than that measured by Day and Huus (1954). This estimate was made by summing all counts corresponding to an energy release of over 7.4 Mev. in the crystal. The gamma-ray interaction cross section data of Davisson and Evans (1952) give the efficiency of the counter as 50%; by postulating a spectral distribution shape similar to that for the 6 Mev. radiation from the $F^{19}(p, \alpha\gamma)O^{16}$ reaction it was estimated that 40% of the 9 Mev. quanta interactions released over 7.4 Mev. energy in the crystal. This counter efficiency figure, together with the solid angle of 0.107 steradians and the target thickness as quoted by the supplier, gives the value of σ quoted above, the main uncertainties arising from counter efficiency and target thickness, which we believe should not cause an error of more than 30% in the cross section.

The angular distribution of the 9 Mev. radiation was measured at the resonance energy with the crystal face 20 cm. from the target in order to keep the 430 kev. gamma-ray flux at a low enough level and to avoid the need of making solid angle corrections. The gamma-ray flux was monitored with a second fixed scintillation counter, which was biased to accept pulses corresponding to an energy release in this counter of between 7 and 10 Mev. To avoid errors due to gain drift the runs at each angle were bracketed by runs at 90°. The resulting angular distribution fits the function $(1+0.5\cos^2\theta)$ quite well as shown in Fig. 3.

The ratio of the yields at 0° and 90° was carefully checked and found to be 1.5 ± 0.05. The distribution showed no large asymmetry about 90° and some of the data gave close equality of the intensity at 45° and 135°, but a small asymmetry about 90° could not be ruled out owing to the limited range of angles permitted by the lead shielding used.

(*b*) *The Intermediate Energy Radiation*

The gamma-ray spectrum from 1.5 to 10 Mev. is shown in Fig. 4, for a proton bombarding energy of 1.1 Mev.

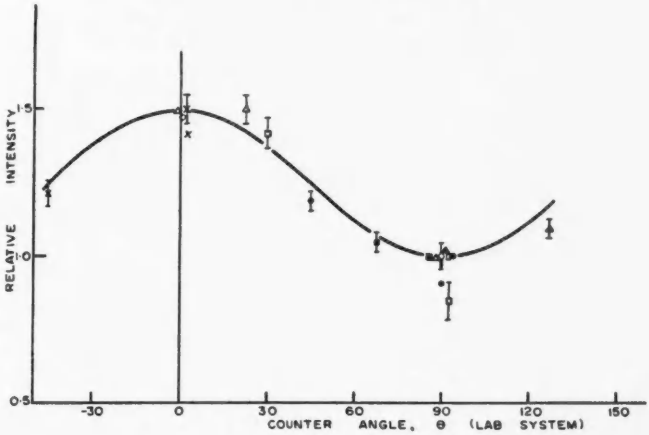

FIG. 3. Angular distribution of the 9 Mev. radiation from $B^{10}(p, \gamma)C^{11}$ at E_p = 1.2 Mev. The different symbols indicate renormalizations to runs at 90°. The full curve is a plot of $(1+0.50 \cos^2\theta)$.

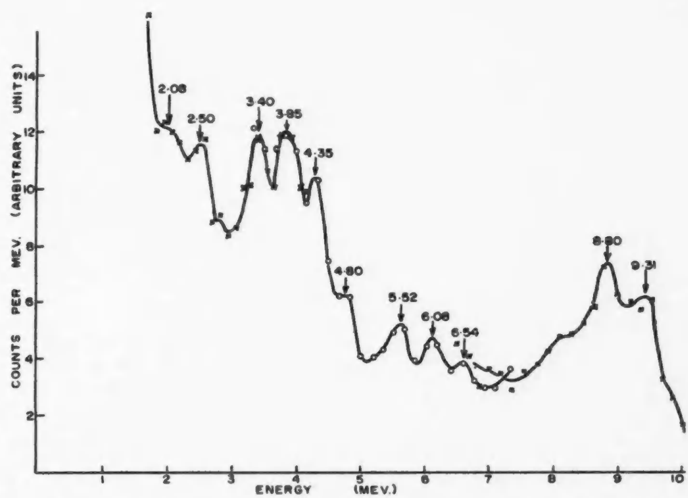

FIG. 4. Intermediate energy radiations from the proton bombardment of B^{10}, background subtracted.

The presence of radiations around 4 Mev. and 6 Mev. is clearly evident. While the spectrum is complex three gamma rays of energies 6.55, 4.80, and 4.35 Mev. appear to be resolved. These could arise from cascade transitions through the levels in C^{11} at 6.35, 4.77, and 4.23 Mev. (Ajzenberg and Lauritsen 1955). The prominence at 2.5 Mev. would indicate radiations at around this energy also. There was evidence too, at lower bombarding energies, for a gamma ray of about 2.9 Mev.

It would be necessary to use coincidence techniques to be sure that these were actually cascade transitions.

(*c*) *The Low Energy Radiation*

The very large flux of 430 kev. radiation from the reaction $B^{10}(p, \alpha)Be^{7*}$ was all too evident in this work. The cross section was measured and found to be 0.21 ± 0.05 barn at $E_p = 1.53$ Mev. This value and the excitation function for this radiation, shown in Fig. 5, were in good accord with the measurements

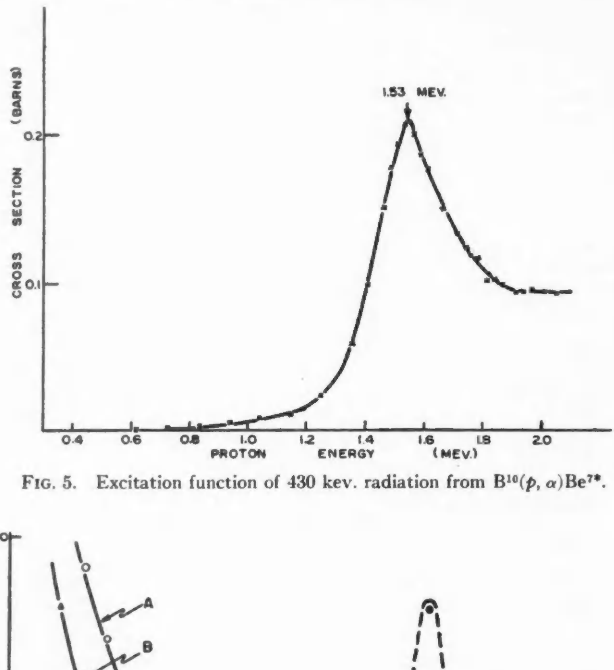

FIG. 5. Excitation function of 430 kev. radiation from $B^{10}(p, \alpha)Be^{7*}$.

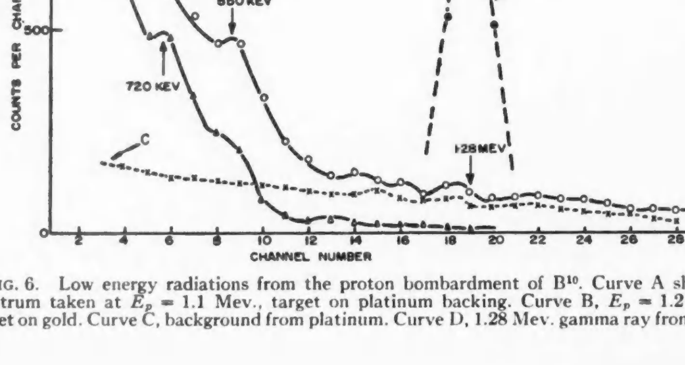

FIG. 6. Low energy radiations from the proton bombardment of B^{10}. Curve A shows a spectrum taken at $E_p = 1.1$ Mev., target on platinum backing. Curve B, $E_p = 1.2$ Mev., target on gold. Curve C, background from platinum. Curve D, 1.28 Mev. gamma ray from Na^{22}.

of Day and Huus (1954). The angular distribution of this 430 kev. radiation was found to be isotropic to within 2% at $E_p = 1.2$ Mev., consistent with the assignment of a spin $\frac{1}{2}$ to the first excited state of Be^7.

Figure 6 shows the spectrum of radiations with energies from 0.6 to 1.5 Mev. At bombarding energies above 1.2 Mev. 720 kev. radiation could be resolved from the background presumably from $B^{10}(p, p'\gamma)B^{10}$. With targets on both gold and platinum backings it was possible to resolve weak radiation of about 850 kev. energy, which might arise from a further cascade in C^{11} or perhaps from some impurity in the target.

DISCUSSION

These results essentially substantiate the findings of Day and Huus (1954) that over the proton bombarding energy range 0.4 to 2 Mev. there is a single broad resonance in the reaction $B^{10}(p, \gamma)C^{11}$ at $E_p = 1.14$ Mev. If the 540 kev. width of this resonance, Γ, neglecting the barrier penetration correction, is assumed to be due essentially to the alpha-particle width, Γ_α, of the corresponding level in C^{11}, the width for re-emission of protons, Γ_p, can be estimated from the cross section of the reaction $B^{10}(p, \alpha)Be^7$. Using the one-level Breit-Wigner formula for the cross section at resonance,

$$\sigma_\alpha = 4\pi\lambda^2 W\,\Gamma_\alpha\Gamma_p/\Gamma^2,$$

where W is the statistical factor. Inserting the value for σ_α obtained by taking the differential cross section found by Brown *et al.* (1951) of 16 mb./steradian and assuming an isotropic distribution for the ground state alpha particles,

$$W\Gamma_p \sim 40 \text{ kev.}$$

Since the angular distribution of the gamma radiation is anisotropic, the total angular momentum, J, of the compound nuclear state $\geqslant \frac{3}{2}$. Hence W, the statistical weight term, $\geqslant \frac{2}{7}$. To estimate Γ_γ, it will be permissible to assume $W = 1$. Then

$$\Gamma_\alpha \sim \Gamma - \Gamma_p \sim 500 \text{ kev.}$$

and

$$\Gamma_\gamma = \Gamma_\alpha\, \sigma_\gamma/\sigma_\alpha \sim 10 \text{ ev.}$$

Weisskopf's formula for the transition probability (Weisskopf 1951) for 9.8 Mev. radiation gives for Γ_γ for E_1 radiation $\sim$470 ev., for M_1 $\sim$20 ev., for E_2 $\sim$0.2 ev., and for M_2 $\sim$0.001 ev., which might suggest that the radiation is M_1.

It is difficult to draw any definite conclusions as to the spin and parity of the excited state of C^{11} corresponding to the observed wide resonance, because of the lack of information regarding the background in Fig. 2. The yield above $E_p = 1.6$ Mev. appears to be either from a higher resonance, as suggested by Day and Huus at 2.4 Mev., or from direct capture. Our data are inadequate to rule out asymmetry about 90° and hence interference.

The ground state of C^{11} is probably a $(\frac{3}{2}-)$ state both on the basis of the assignment to the mirror nucleus B^{11} and on shell model arguments. If, then, the assumption is made that the observed angular distribution is due to a single

state of well-defined angular momentum and if possible interference between various multipolarity gamma rays is neglected, some assignments for the excited state in C^{11} can be rejected. Thus values of $J \geqslant (\frac{7}{2}, + \text{ or } -)$ can probably be discarded on the basis of either the observed radiation width or the failure to observe $\cos^4\theta$ terms in the distribution. $J = (\frac{1}{2}, + \text{ or } -)$ and $J = (\frac{5}{2} + \text{ or } \frac{7}{2} +)$, formed by s-wave protons, would lead to isotropy of the gamma radiation. $J = (\frac{3}{2}, + \text{ or } -)$ can probably be eliminated since these assignments give a distribution of the form $1 + A \cos^2\theta$ with $A \leqslant 0.28$ which is outside our error of measurement. The possibility of $J = (\frac{5}{2}+)$ formed by $l = 2$ protons yields $A \leqslant 0.41$ and, moreover, there is the inherent improbability of d-wave formation when s-wave formation would be possible. The only possibility which has not been eliminated is thus $J = (\frac{5}{2}-)$, formed by p-wave protons and decaying by M_1 radiation, which agrees satisfactorily with the observed pattern, if a contribution of about 10% from the channel spin $\frac{7}{2}$ is taken.*

It must be stressed that this conclusion is based on the drastic assumption of no interference between states of different J values and no radiation multipole interference. An awkward objection to this assignment to the C^{11} state involved is the apparent absence of a resonance in the yield of short-range alpha particles to the first excited state of Be^7 at this energy. Such alphas would, of course, be inhibited by their low available energy.

ACKNOWLEDGMENTS

Two of us (G. B. Chadwick and T. K. Alexander) are grateful to the National Research Council of Canada for scholarships held during the period of this research. We are indebted to the British Columbia Academy of Sciences for an equipment grant to G. B. Chadwick and to Atomic Energy of Canada Ltd. for financial assistance which makes the operation of our Van de Graaff generator possible.

REFERENCES

Ajzenberg, F. and Lauritsen, T. 1955. Revs. Mod. Phys. **24**: 321.
Brown, A. B., Snyder, C. W., Fowler, W. A., and Lauritsen, C. C. 1951. Phys. Rev. **82**: 159.
Caldwell, R. L. and Turner, S. E. 1954. Nucleonics, **12** (No. 12): 47.
Davisson, C. M. and Evans, R. D. 1952. Revs. Mod. Phys. **24**: 63.
Day, R. B. and Huus, T. 1954. Phys. Rev. **95**: 1003.
Krone, R. W. and Seagondollar, L. W. 1953. Phys. Rev. **92**: 935.
Madsen, C. D. 1953. Kgl. Danske Videnskab. Selskab, Mat.-fys. Medd. **27**: 13.
Walker, R. L. 1950. Phys. Rev. **79**: 172 (L).
Weisskopf, V. F. 1951. Phys. Rev. **83**: 1073.
Woodbury, H. H., Day, R. B., and Tollestrup, A. V. 1953. Phys. Rev. **92**: 1199.

*_Note added in proof:_ Cronin, J. W. 1956. Bull. Am. Phys. Soc. I (No. 1), Abstract DA7, suggests 3/2− and 7/2+ for the 1.1 and 1.5 Mev. resonances, respectively, on the basis of α-particle angular distributions. Further work will be required to settle the assignment of the 1.1 Mev. resonance.

AN INVESTIGATION OF THE SODIUM-POTASSIUM EQUILIBRIUM DIAGRAM[1]

BY D. K. C. MACDONALD, W. B. PEARSON, AND LOIS T. TOWLE

ABSTRACT

The study of fundamental properties such as specific heat and electrical resistivity in pure metals has made it very important to know the influence of small amounts of impurity. This has led us to undertake a detailed investigation of the sodium-potassium equilibrium diagram. Previous work had indicated zero solid solubility at each limit (100% Na; 100% K) but the present investigation shows in particular that solubility extends to a few per cent from either limit.

INTRODUCTION

The measurement of such parameters as specific heat, electrical resistivity, can yield a great deal of information about the state of the lattice in a metal. From continuous observations over a wide temperature range on pure alkali metals in particular, we have found (MacDonald 1953, 1955; Dauphinee *et al.* 1955; cf. also Carpenter 1953) that both the specific heat and electrical resistance exhibit an anomalously rapid rise over a temperature range extending some 50° to 100° C. below the melting point. The metals used by us were very pure by physical standards (such as the residual resistivity as $T \rightarrow 0$), and this rise has been interpreted as due to significant concentrations of thermal defects in the lattice as the melting temperature is approached. On this assumption, both parameters permit us to deduce the energy required to create such a defect in the lattice (and these estimates should of course agree within experimental error); while from the calorimetric data specifically the *concentration* of defects at any temperature can be determined, and from the resistive data we can then deduce the scattering cross-section for electrons. Knowledge of the energy required to create the defect and of the scattering cross-section may then enable one to identify with some certainty the specific type of defect (e.g. a vacancy or interstitial atom—cf. e.g. Machlup (1956)). Information about the actual defect concentration may be of value in understanding the melting mechanism, since it is thought that melting may be "triggered" by some critical concentration of lattice defects.

Consequently it is of some importance to be reasonably certain that we are justified in identifying the anomalous rise in specific heat and resistance in this way. Another possible source of such a rise might be the anharmonicity of lattice vibrations which increases as the temperature rises (cf. Born 1933) and this led Dugdale and MacDonald (1954) to study quantitatively in a specific model (a linear chain) the influence of anharmonicity on the thermodynamic parameters. This investigation led us to believe that the rise could not in fact be assigned to this cause.

A further possibility was that the presence of even a rather small concentration of an impurity, insoluble in the solid state but soluble in the liquid,

[1]Manuscript received December 1, 1955.
Contribution from the Division of Pure Physics, National Research Council, Ottawa, Canada. Issued as N.R.C. No. 3911.

might produce such an anomalous rise as the melting point of the ideally pure metal is approached, although the predicted temperature-dependence of specific heat due to this is not of the right form. Nevertheless, in our sodium and potassium,* it was presumed that the significant residual impurity in each case would be the other metal, and since previous determinations of the potassium–sodium equilibrium diagram (van Rossen Hoogendijk 1912; Jänecke 1928; Rinck 1933) had all indicated that there was *no* terminal solid solubility at either limit (100% Na; 100% K), it was felt necessary to re-examine the equilibrium diagram carefully. In fact the published zero solubility of potassium in sodium was already contradicted by the observation (cf. MacDonald and Pearson 1954) that the residual resistance of initially very pure sodium (say $R_{4°K.}/R_{273°K.} \simeq 2\times10^{-4}$) could readily be increased by a factor of several hundred by alloying with a small percentage of potassium indicating very strongly that a significant fraction of the potassium had entered into (random) solid solution.

EXPERIMENTAL METHOD

A rather extended series of measurements of the electrical resistance of potassium–sodium alloys was undertaken and has enabled us to construct an approximate equilibrium diagram for this binary system in considerably more detail than has previously been available. We may mention that a number of our early measurements were undertaken for purposes other than that of determining the equilibrium diagram (e.g. an interest in the resistance of liquid alloys for which as yet no satisfactory theory exists), and the importance of making measurements on alloys essentially in thermal equilibrium—particularly in the vicinity of phase boundaries—and also the influence of supercooling became clear as the investigation proceeded. The method used of measuring resistance as a function of temperature offers considerable advantages in investigating an alkali metal alloy system. This is because of the small amount of alloy required and also because it is only necessary to make measurements on alloys which are strictly in equilibrium when in the vicinity of phase boundaries, and these boundaries can be located if necessary in a rapid preliminary survey. By contrast thermal analysis† involves problems of establishing steady heating or cooling rates and does not generally allow measurements to be made on alloys annealed exactly to equilibrium at a particular temperature.

Alloys were prepared from sodium and potassium of rather high purity, the residual resistance ratio of the primary metals being 2×10^{-4} and $\sim20\times10^{-4}$ respectively. The alloys were prepared *in vacuo* in a glass apparatus (sketched in Fig. 1) which was heated in an oil bath. The molten metals were mixed in the U-tube, A, by vigorous shaking and then forced into the mold, B, and

*These metals were exceedingly pure. For the sodium we are indebted to Messrs. Philips, Eindhoven, Netherlands, and Mitcham, Surrey, England, while the potassium was specially prepared by I.C.I., Ltd., for the Pure Metals Research Committee of the United Kingdom.

†Time–temperature curves taken under steady conditions of heating or cooling of the surrounding heat bath. See, for instance, "Metallurgical Equilibrium Diagrams" (Hume-Rothery, Christian, and Pearson 1952).

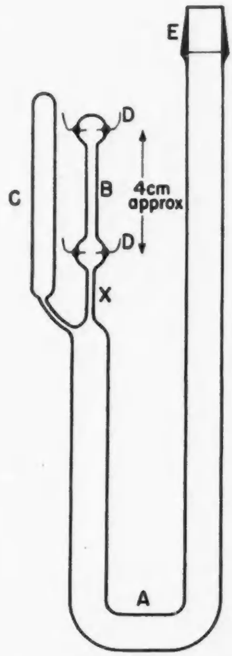

FIG. 1. Schematic drawing of glass apparatus for preparing resistance specimens.

reservoir tube, C, by applying a pressure of one atmosphere of helium after the apparatus was inverted. After cooling, the mold was cut free at X and sealed with Apiezon compound Q covered with Glyptal, which made an air-tight seal that did not exert any appreciable pressure on the metal as it expanded on heating and melting.

The filled molds were placed in a simple thermostat and resistance measurements were made successively with increasing or decreasing temperatures using a galvanometer amplifier (MacDonald 1947). Measurements were made generally only when the alloy attained equilibrium at the holding temperature, particular care being taken about the peritectic and eutectic temperatures in the vicinity of the solid solubility limits. In the cooling cycles, however, supercooling was frequently encountered at the liquidus and isothermal transitions. As no process of seeding was possible the phase boundaries were determined only from measurements made during the heating cycles.

The composition of all alloys examined was determined by chemical analysis. When possible *both* Na and K were separately determined. In dilute alloys, spectroscopic analysis was also used to obtain the concentration of the minor component. The scatter to be noted in the liquidus points of several alloys may be attributed either to the difficulties of sufficiently accurate chemical

analysis or to inhomogeneity along the length of the specimens, despite the vigorous mixing given to the molten metals. Such inhomogeneity may result from the necessity of slowly cooling the molten alloys during preparation in order to maintain a continuous thread of metal in the central capillary of the specimen molds. Thus one alloy in particular which had an analyzed composition of 93.5 at. % K appears from the liquidus temperature and size of eutectic arrest to contain effectively about 90 at. % K.

EXPERIMENTAL RESULTS

The liquidus curves in the equilibrium diagram shown in Fig. 2 agree rather exactly with those obtained by Rinck (1933) by thermal analysis, excepting

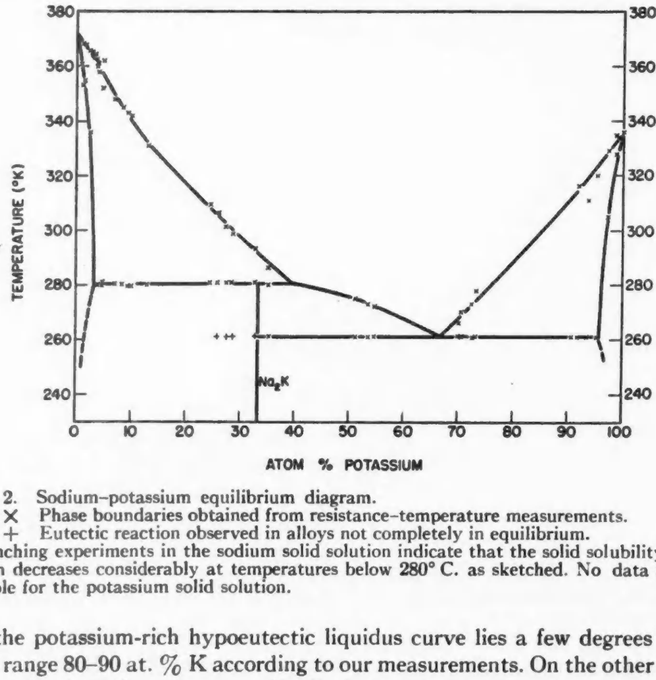

FIG. 2. Sodium–potassium equilibrium diagram.
× Phase boundaries obtained from resistance–temperature measurements.
+ Eutectic reaction observed in alloys not completely in equilibrium.
Quenching experiments in the sodium solid solution indicate that the solid solubility of potassium decreases considerably at temperatures below 280° C. as sketched. No data are yet available for the potassium solid solution.

that the potassium-rich hypoeutectic liquidus curve lies a few degrees lower in the range 80–90 at. % K according to our measurements. On the other hand, we, for the first time, have specifically looked for and found an appreciable range of solid solution formed by both Na and K.

The peritectic temperature is determined as 280.5±1° K. where liquid containing ~40 at. % K reacts with the sodium solid solution containing ~3 at. % K to form Na_2K. At the eutectic temperature of 261±1° K., the compound Na_2K and the potassium solid solution containing ~4.5 at. % Na are formed from the liquid containing ~66.6 at. % K at the eutectic point. The larger solid solubility of Na in K than of K in Na is consistent with the expectation that it will be easier for a smaller atom to enter solid solution in a

solvent whose atoms have a larger diameter than vice versa, particularly when the radius ratios differ by 24% as in the present case.

The terminal solid solubility limits at the peritectic and eutectic temperatures were determined by bracketing with alloys which did,—and did not—, show a discontinuity of resistance as a function of temperature at the invariant point. Thus in Na-rich alloys the alloy at 3.1 at. % K showed no jump in resistance while those at 3.7 and 4.5 at. % K gave a small but definite discontinuous increase in resistance at 280° K. on heating. It was found important to ensure that equilibrium was attained in the alloy at each measuring temperature in the vicinity of the isothermal transition as incorrect results could otherwise be obtained apparently indicating a smaller solid solubility than was actually the case. The position of the solid solubility limit was also checked approximately by examining the size of the resistance discontinuity, suitably normalized, as a function of the alloy composition. Owing to the steepness of the solidus curves, bordering the Na and K solid solutions, no accurate estimation of the solidus temperature was attempted except in the most dilute alloys.

The composition of the intermediate phase, proposed as Na_2K in earlier work, was confirmed subsequently by the crystal structure determination of Laves and Wallbaum (1942), who showed that it had a hexagonal C14 type of structure. The structure, therefore, belongs to the group of Laves phases which have a composition A_2B and owe their stability to the ease with which space can be filled with atoms whose radius ratio r_B/r_A is 1.225, which is indeed close to the value of $r_K/r_{Na} = 1.24$ as determined from lattice-spacing measurements. The indication that the eutectic horizontal extended to alloys with lower potassium content than 33.3% (i.e. beyond the compound Na_2K) as found by van Rossen Hoogendijk (1912), by Rinck (1933), and by ourselves is due to lack of equilibrium and incomplete peritectic reaction. van Rossen Hoogendijk showed that the thermal arrests at 261° K. in this composition range below 33% K disappeared after suitable annealing of the specimens. In the present work a discontinuity of resistance could still be found at 261° K. in alloys of 26%, 28.5%, and 32.8% (but not in alloy 24.7% (atom K)) even after they were annealed at 3° to 5° C. below the peritectic temperature for more than eight hours. However, these discontinuities were small and showed no regular variation with the composition of the alloy. We are satisfied that they were the result of incomplete peritectic reaction during the annealing treatment given to the alloys. The present investigation does not therefore dispute the accepted composition of the intermediate phase.

ACKNOWLEDGMENT

We should like to thank Mr. B. Evans for his care in making the numerous soft-glass specimen molds used in this work and Mr. W. Stockdale for carrying out the spectroscopic and chemical analyses of these alloys.

REFERENCES

BORN, M. 1933. *In* Handbuch der Physik, Vol. 24(2). *Edited by* H. Geiger and Karl Scheel. Verlag von Julius Springer, Berlin. p. 675.
CARPENTER, L. G. 1953. J. Chem. Phys. **21**: 2244.

DAUPHINEE, T. M., PRESTON-THOMAS, H., and MARTIN, D. L. 1955. Proc. Roy. Soc. A. **233**: 214.
DUGDALE, J. S. and MACDONALD, D. K. C. 1954. Phys. Rev. **96**: 57. See also ROY, S. K. and MACDONALD, D. K. C. 1955. Phys. Rev. **97**: 673.
HUME-ROTHERY, W., CHRISTIAN, J. W., and PEARSON, W. B. 1952. Metallurgical equilibrium diagrams. Institute of Physics, London.
JÄNECKE, E. 1928. Z. Metallkunde, **20**: 115.
LAVES, F. and WALLBAUM, H. J. 1942. Z. anorg. u. allgem. Chem. **250**: 110.
MACDONALD, D. K. C. 1947. J. Sci. Instr. **24**: 232.
——— 1953. J. Chem. Phys. **21**: 177, 2097.
——— 1955. Report of Bristol Conference on Defects in Crystalline Solids. Physical Society, London. p. 383.
MACDONALD, D. K. C. and PEARSON, W. B. 1954. Proc. Roy. Soc. A, **221**: 534.
MACHLUP, S.* 1956. J. Chem. Phys. **24**: 169.
RINCK, E. 1933. Compt. rend. **197**: 49.
VAN ROSSEN HOOGENDIJK VAN BLEISWIJK, G. L. C. M. 1912. Z. anorg. Chem. **74**: 152.

*We are grateful to Dr. Machlup for letting us see his manuscript before publication.

ELECTRICAL BREAKDOWN IN ARGON AT ULTRAHIGH FREQUENCIES[1]

By A. D. MacDonald and J. H. Matthews[2]

ABSTRACT

Measured values of breakdown electric fields in pure argon gas are presented. Measurements were made in two resonant cavities at a frequency of 2800 Mc./sec. and for pressures varying from 4×10^{-2} to 200 mm. of mercury. The present results are in agreement with those of Krasik, Alpert, and McCoubrey.

In recent years breakdown electric fields have been measured for a number of gases at frequencies in the neighborhood of 3000 Mc./sec. (Herlin and Brown 1948; MacDonald and Brown 1949*a*, *b*). These microwave measurements are particularly useful in giving us information about the fundamental collision processes in the gas. There are two reasons for this. First, secondary effects at the walls of the container are small. Second, with reasonable gas pressure variations the phenomena vary from those in which the electron collision frequency is much greater than the field frequency to those in which it is much less.

This paper presents measured values of breakdown fields for pure argon. Krasik, Alpert, and McCoubrey (1949) made some measurements of breakdown and maintaining fields at 2950 Mc./sec. in argon, but the present work covers a wider range of variation of the experimental parameters. The experimental procedures are similar to those described previously (MacDonald and Brown 1949*a*, *b*; MacDonald and Betts 1952). A block diagram of the apparatus is shown in Fig. 1. Power generated by a c-w. magnetron operating at 2800 Mc./sec. is coupled to a resonant cavity by a coaxial transmission line.

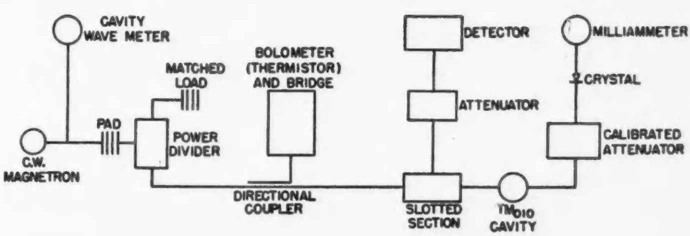

Fig. 1. Block diagram of the microwave apparatus.

A known fraction of the power is measured by a thermistor. The power absorbed by the cavity, the cavity *Q*, and the known field configuration are used in the usual manner to determine the electric field (Brown and Rose 1952; Rose and Brown 1952). The cavities in which breakdown takes place are made

[1]Manuscript received January 3, 1956.
Contribution of the Department of Physics, Dalhousie University, Halifax, Nova Scotia. Supported by the Defence Research Board of Canada (Grant 9512-09).
[2]Holder of a National Research Council Studentship.

of oxygen-free high-conductivity copper and connected through kovar to an all-glass vacuum system. The vacuum system maintains a pressure of less than 5×10^{-7} mm. of mercury with the pumps shut off for a period sufficiently long to make a series of measurements. All argon used had an impurity content of less than one part in 10^4. Mass spectroscopic analysis by the manufacturer indicated that several of the samples used had considerably less than one part in 10^5 impurity. The amount of the impurities present had no measurable effect on the breakdown fields. The impurities present were nitrogen, some easily removable hydrocarbons, and traces of hydrogen. Ionizations resulting from collisions of atoms in low-lying metastable states with impurity atoms, which greatly affect breakdown fields in helium and neon, are not important. The reason is that the metastable levels in argon are at approximately 11.5 volts and are therefore lower than the ionization potentials of the impurities present.

The measurements were made in cylindrical cavities having heights of 0.159 cm. and 0.476 cm., and characteristic diffusion lengths of 0.0505 cm. and 0.151 cm. The experimental data are presented in Fig. 2, which also in-

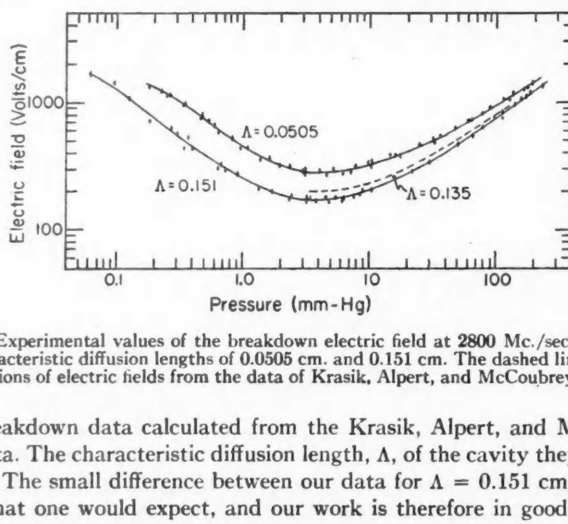

FIG. 2. Experimental values of the breakdown electric field at 2800 Mc./sec. for cavities having characteristic diffusion lengths of 0.0505 cm. and 0.151 cm. The dashed line represents our calculations of electric fields from the data of Krasik, Alpert, and McCoubrey.

cludes breakdown data calculated from the Krasik, Alpert, and McCoubrey (1949) data. The characteristic diffusion length, Λ, of the cavity they used was 0.135 cm. The small difference between our data for Λ = 0.151 cm. and their data is what one would expect, and our work is therefore in good agreement with theirs. It will be noted in Fig. 2 that at pressures of the order of 0.1 mm. of mercury there is a change in the slope of the curves. At these pressures the electron mean free path becomes comparable with the cavity dimensions, effects at the container walls become important, and the discharge is no longer diffusion controlled as it is at the higher pressures.

The curves in Fig. 2 represent the average of several sets of data and the maximum error in the electric field is less than 5% and in the pressures less than 2%.

In previous studies of breakdown in helium, hydrogen, and neon (MacDonald and Brown 1949*a*, *b*; MacDonald and Betts 1952), the measured break-

down fields have been compared with those predicted on the basis of kinetic theory calculations using distribution functions derived from the Boltzmann equation. Such a derivation requires the solution of a differential equation, which includes among its parameters an analytical expression for the cross section for collisions between electrons and atoms of the gas under consideration. For argon this cross section is a very complex function of electron energy and a suitable approximation which permits solution of the differential equation has not yet been made.

REFERENCES

BROWN, S. C. and ROSE, D. J. 1952. J. Appl. Phys. **23**: 711.
HERLIN, M. A. and BROWN, S. C. 1948. Phys. Rev. **74**: 291.
KRASIK, S., ALPERT, D., and MCCOUBREY, A. O. 1949. Phys. Rev. **76**: 722.
MACDONALD, A. D. and BETTS, D. D. 1952. Can. J. Phys. **30**: 565.
MACDONALD, A. D. and BROWN, S. C. 1949*a*. Phys. Rev. **75**: 411.
——— 1949*b*. Phys. Rev. **76**: 1634.
ROSE, D. J. and BROWN, S. C. 1952. J. Appl. Phys. **23**: 719.

REFLECTION AND TRANSMISSION AT A SLOTTED DIELECTRIC INTERFACE[1]

By R. E. Collin

ABSTRACT

A theoretical analysis of a slotted dielectric interface is given for the case of a plane wave incident at an angle θ_i and polarized with the electric vector parallel to the slots. A variational solution yielding upper and lower bounds to the parameters of the equivalent circuit for the interface is given. A numerical example for a wave incident at an angle of 30° on a slotted dielectric with a relative dielectric constant of 2.56 at a wavelength of 3.14 cm. shows that the phase shifts introduced into the reflected and transmitted waves are of the order of 1°. Also the impedance transformation across the interface is just that due to the change in wave impedance. Such a slotted dielectric may be used to match a microwave lens to free space. A theoretical calculation shows that the reflection coefficient does not exceed 5% for angles of incidence up to 30° in the wavelength range 3–3.28 cm. for a slotted section used to match a dielectric of relative dielectric constant 2.56 to free space. Without a matching section the reflection coefficient is 23% or more.

1. INTRODUCTION

When a uniform T.E.M. wave is incident at an angle θ_i on a plane dielectric sheet a fraction of the incident radiation is reflected and the rest is transmitted into the dielectric sheet and propagates at an angle θ_r. For a perpendicular polarized wave the reflection coefficient is

$$\frac{\sec\theta_r - \sqrt{\kappa}\sec\theta_i}{\sec\theta_r + \sqrt{\kappa}\sec\theta_i}$$

where κ is the relative dielectric constant of the material. The reflected wave can be eliminated by means of an intermediate dielectric sheet with an effective thickness of one-quarter wavelength and a wave impedance equal to the geometric mean of those of the two media to be matched. The difficulty in producing such a matching layer is due to the lack of suitable materials with the required dielectric constants. An equivalent matching layer can be made by slotting the dielectric interface. The thickness of the slots is chosen to obtain the required wave impedance and the depth is determined so that the section is effectively a quarter wave long. In order to design such a matching section it is necessary to know the parameters of the equivalent transmission line circuit for the interface. One particular form of slotted interface with a perpendicular polarized wave incident at an arbitrary angle θ_i will be considered here. The slots are assumed parallel to the incident electric vector. The particular case of normal incidence has been analyzed before (Collin 1953; Collin and Brown 1955*b*), and the main purpose of this article is to extend the analysis to the case of oblique incidence.

Such slotted surfaces are of considerable value in matching the surfaces of dielectric microwave lenses to free space.

[1]Manuscript received November 4, 1955.

Contribution from Canadian Armament Research and Development Establishment, Valcartier, Que.

2. FORMULATION OF PROBLEM

The type of slotted interface to be analyzed is illustrated in Fig. 1. Each dielectric tongue is of thickness t and is separated by an air space of thickness a. The spacing of the slots is s and is uniform for all x. A T.E.M. wave with the electric vector along the y-axis is incident at an angle θ_i on the interface from

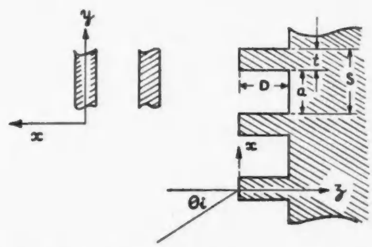

FIG. 1. Slotted dielectric matching section.

the region $z < 0$. The incident wave has components E_y, H_x, and H_z and no other field components are excited by the structure since it is uniform along the y direction. Consequently the total field can be derived from the one scalar component E_y by means of the following equations:

$$j\omega\mu H_z = -\frac{\partial E_y}{\partial x}, \qquad j\omega\mu H_x = \frac{\partial E_y}{\partial z}. \tag{1}$$

The scalar function E_y satisfies the following wave equation:

$$\frac{\partial^2 E_y}{\partial x^2}+\frac{\partial^2 E_y}{\partial z^2}+\kappa(x)\, k_0^2 E_y = 0, \tag{2}$$

where $k_0^2 = \omega^2\mu\epsilon = 4\pi^2/\lambda_0^2$

and
$$\begin{aligned} \kappa(x) &= \kappa \quad \text{for} \quad |x| \leqslant \tfrac{1}{2}t \pm ns,\ n = 0, 1, 2, \ldots;\ 0 \leqslant z \leqslant D, \\ &= \kappa \quad \text{for} \quad z \geqslant D, \\ &= 1 \quad \text{otherwise;} \end{aligned}$$

m.k.s. units are used and the time factor $e^{j\omega t}$ is suppressed. The free space wavelength is λ_0. The boundary conditions to be imposed on E_y are continuity of E_y and its normal derivative at all air–dielectric interfaces.

The incident electric field will be taken as

$$s^{-\frac{1}{2}} \exp[-jk_0(x \sin \theta_i + z \cos \theta_i)] .$$

When this wave strikes the interface a reflected wave

$$Rs^{-\frac{1}{2}} \exp[-jk_0(x \sin \theta_i - z \cos \theta_i)]$$

plus higher order diffraction modes will be excited in the region $z < 0$. The amplitude of the reflected wave is $|R|$ where R is the complex reflection coefficient. It will be convenient to consider this uniform incident T.E.M. wave propagating at an angle θ_i to the interface normal as a non-uniform wave propagating along the z-axis since this leads to a simple transmission line equivalent circuit for the structure.

In the slotted region waves propagating or attenuated along the z-axis will be excited so that E_y will be in the form of a summation over normal modes, i.e.

$$\sum F_m(x)(b_m^+ e^{-\gamma_m z} + b_m^- e^{\gamma_m z}).$$

Substituting into the wave equation yields the following equation for the normal mode function F_m:

$$\frac{d^2F_m}{dx^2} + (\gamma_m^2 + \kappa(x)k_0^2)F_m = 0. \tag{3}$$

Because of the periodicity of $\kappa(x)$ a solution of the form†

$$F_m = e^{-j\beta x}\,\phi_m(x)$$

exists such that ϕ_m is a periodic function of x of period s (Morse and Feshbach 1953). Since the incident field varies with x as

$$\exp(-jk_0x \sin\theta_i)$$

it is necessary for all field components to have this same progressive change in phase with x and thus

$$\beta = k_0 \sin\theta_i. \tag{4}$$

3. SOLUTION FOR $F_m(x)$

Let the two independent solutions to the wave equation (3) in $-\frac{1}{2}s \leqslant x \leqslant \frac{1}{2}s$ be ψ_m^e and ψ_m^o having even and odd symmetry about $x = 0$ respectively. (Superscripts e and o are used to distinguish between the functions having even and odd symmetry.) Since $\psi_m^{e,o}$ are solutions to the wave equation, both $\psi_m^{e,o}$ and $d\psi_m^{e,o}/dx$ are continuous at $x = \pm\frac{1}{2}t$. The functions $\psi_m^{e,o}$ will have an eigenvalue l_m in the region

$$|x| \leqslant \tfrac{1}{2}t \pm ns, \quad n = 0, 1, 2, \ldots,$$

and k_m in the free space regions. The eigenvalues l_m and k_m satisfy the conditions

$$\gamma_m^2 = l_m^2 - \kappa k_0^2 = k_m^2 - k_0^2. \tag{5}$$

The solution for all x is F_m and will be a linear combination of ψ_m^e and ψ_m^o, thus

$$F_m = A_m\psi_m^e + B_m\psi_m^o. \tag{6}$$

For propagation along the x-axis it is necessary that

$$\begin{aligned} F_m(\tfrac{1}{2}s) &= e^{-j\beta s}F_m(-\tfrac{1}{2}s), \\ F_m'(\tfrac{1}{2}s) &= e^{-j\beta s}F_m'(-\tfrac{1}{2}s), \end{aligned} \tag{7}$$

where the prime indicates d/dx. Substituting for F_m and F_m' from Eq. (6) and making use of the symmetry properties of $\psi_m^{e,o}$ allows one to write the following two equations which must hold for the particular value $x = \frac{1}{2}s$:

$$\begin{aligned} A_m(1-e^{-j\beta s})\psi_m^e + B_m(1+e^{-j\beta s})\psi_m^o &= 0, \\ A_m(1+e^{-j\beta s})\psi_m'^e + B_m(1-e^{-j\beta s})\psi_m'^o &= 0. \end{aligned} \tag{8}$$

†This is a direct application of Floquet's theorem. The problem here is similar to the quantum-mechanical one of flow of electrons in a periodic square wave potential field.

For a solution to exist the determinant must vanish. This condition yields the following eigenvalue equation:

$$\tan^2\beta(\tfrac{1}{2}s) = -\left.\frac{\psi_m'^e\,\psi_m^o}{\psi_m^e\,\psi_m'^o}\right|_{x=\frac{1}{2}s}. \tag{9}$$

The eigenvalues l_m, k_m, and γ_m are determined by this equation when β is given. However this leads to complicated algebra and a simpler method of deriving the eigenvalues by means of matrices is given in Appendix I.

The coefficient B_m is given by

$$B_m = -A_m j \tan\beta(\tfrac{1}{2}s)\left.\frac{\psi_m^e}{\psi_m^o}\right|_{x=\frac{1}{2}s} = -j\alpha_m A_m. \tag{10}$$

The coefficient A_m will be chosen so that

$$\int_{-\frac{1}{2}s}^{\frac{1}{2}s} F_m F_m^* = 1, \tag{11}$$

where the star denotes the complex conjugate value. Expressions for A_m are given in Appendix II. It is readily shown that the functions F_m are orthogonal to F_n^* with $m \neq n$. The functions ϕ_m are given by

$$\phi_m = e^{j\beta x} F_m. \tag{12}$$

Now $\phi_m(x+s) = e^{j\beta(x+s)} F_m(x+s) = e^{j\beta x} F_m(x) = \phi_m(x)$ from Eq. (7). Thus ϕ_m is periodic as it should be. Since $\phi_m\phi_n^* = F_mF_n^*$ the functions ϕ_m are orthogonal to ϕ_n for $m \neq n$ also.

It is now necessary to derive explicit forms for $\psi_m^{e,o}$. In $-\frac{1}{2}t \leqslant x \leqslant \frac{1}{2}t$, let

$$\psi_m^e = \cos l_m x, \qquad \psi_m^o = \sin l_m x.$$

In $\frac{1}{2}t \leqslant x \leqslant \frac{1}{2}s$, let

$$\psi_m^e = a_m^e \cos k_m(x-\theta_m^e), \qquad \psi_m^o = a_m^o \sin k_m(x-\theta_m^o)\,.$$

Then in $-\frac{1}{2}s \leqslant x \leqslant -\frac{1}{2}t$,

$$\psi_m^e = a_m^e \cos k_m(x+\theta_m^e), \qquad \psi_m^o = a_m^o \sin k_m(x+\theta_m^o)\,.$$

The phase angles $\theta_m^{e,o}$ and coefficients $a_m^{e,o}$ are as yet undetermined. At $x = \pm\frac{1}{2}t$, $\psi_m^{e,o}$ and $\psi_m'^{e,o}$ must be continuous, thus

$$\cos l_m(\tfrac{1}{2}t) = a_m^e \cos k_m(\tfrac{1}{2}t-\theta_m^e),$$

$$l_m \sin l_m(\tfrac{1}{2}t) = k_m a_m^e \sin k_m(\tfrac{1}{2}t-\theta_m^e),$$

and similarly for ψ_m^o and $\psi_m'^o$. The coefficient a_m^e is given by

$$a_m^e = \cos l_m(\tfrac{1}{2}t) \sec k_m(\tfrac{1}{2}t-\theta_m^e) \tag{13}$$

and the phase angle θ_m^e is given by the transcendental equation

$$l_m \tan l_m(\tfrac{1}{2}t) = k_m \tan k_m(\tfrac{1}{2}t-\theta_m^e)\,. \tag{14}$$

Similarly it is found that

$$a_m^o = \sin l_m(\tfrac{1}{2}t) \csc k_m(\tfrac{1}{2}t-\theta_m^o), \tag{15}$$

$$l_m \cot l_m(\tfrac{1}{2}t) = k_m \cot k_m(\tfrac{1}{2}t-\theta_m^o)\,. \tag{16}$$

Eqs. (13) to (16) give solutions for $a_m^{e,o}$ and $\theta_m^{e,o}$ when l_m and k_m are known. The equation derived for l_m and k_m in Appendix I is

$$\cos \beta s = \cos l_m t \cos k_m a - \frac{k_m^2 + l_m^2}{2k_m l_m} \sin l_m t \sin k_m a. \tag{17}$$

Eq. (17) together with the condition $k_m^2 = l_m^2 - (\kappa - 1)k_0^2$ derivable from Eq. (5) yields the allowed values of l_m and k_m for given values of t, a, and β.

The functions F_m are now completely specified and the electric field in the slotted section may be taken as

$$\sum_{m=1}^{\infty} F_m (b_m^+ e^{-\gamma_m z} + b_m^- e^{\gamma_m z}) = e^{-j\beta x} \sum_{m=1}^{\infty} \phi_m (b_m^+ e^{-\gamma_m z} + b_m^- e^{\gamma_m z}). \tag{18}$$

The magnetic field components follow by differentiation as indicated by Eqs. (1). The coefficients b_m will be determined by the continuity conditions on E_y and H_x at $z = 0$.

4. SOLUTION FOR THE FIELDS IN REGION $z < 0$

In the region $z < 0$ there is an incident wave

$$s^{-\frac{1}{2}} \exp[-jk_0(x \sin \theta_i + z \cos \theta_i)]$$

and a reflected wave

$$Rs^{-\frac{1}{2}} \exp[-jk_0(x \sin \theta_i - z \cos \theta_i)]$$

plus higher order modes excited. The higher order diffraction field will be a superposition of plane waves given by (Berz 1951)

$$\sum_{-\infty}^{\infty}{}' c_n\, s^{-\frac{1}{2}} \exp[-jk_0(x \sin \theta_n - z \cos \theta_n)], \tag{19}$$

where the prime indicates the exclusion of the term $n = 0$. Because of the periodicity of the structure and the fact that the field must show a progressive phase change along the x-axis it is necessary that

$$k_0 \sin \theta_n = k_0 \sin \theta_i + \frac{2n\pi}{s}, \quad n = \pm 1, \pm 2, \ldots,$$

or

$$\sin \theta_n = \sin \theta_i + \frac{n\lambda_0}{s}, \quad n = \pm 1, \pm 2, \ldots. \tag{20}$$

The corresponding value of $\cos \theta_n$ is

$$\cos \theta_n = \sqrt{(1 - \sin^2 \theta_n)} = -j\Gamma_n k_0^{-1}. \tag{21}$$

When $\sin^2\theta_n > 1$ the sign of Γ_n is chosen to give decaying waves along the negative z-axis. In order that none of these higher order waves shall propagate in the negative z direction it is necessary for $\sin^2\theta_n$ to be greater than unity for all $n \neq 0$. From Eq. (20) this imposes the following condition on the maximum spacing that can be used:

$$s < \frac{\lambda_0}{1 + |\sin \theta_i|} \tag{22}$$

for all values of λ_0 and θ_i of interest. When such a slotted interface is used as a matching section, λ_0 in Eq. (21) must be replaced by $\lambda_0/\sqrt{\kappa}$ to ensure that none of the higher order waves will propagate in the solid dielectric region.

This condition also ensures that only one mode will propagate in the slotted section, i.e. all γ_m are real except γ_1. The total electric field in the region $z < 0$ is therefore

$$(23)\quad s^{-\frac{1}{2}}e^{-j\beta x}\Big[\exp(-jk_0 z\cos\theta_i)+R\exp(jk_0\cos\theta_i) + \sum_{-\infty}^{\infty}{}' c_n\exp[-j(2n\pi/s)x]e^{\Gamma_n z}\Big].$$

At $z = 0$, E_y and H_x or equivalently E_y and $\partial E_y/\partial z$ must be continuous. Thus from Eqs. (18) and (23)

$$(24)\qquad 1+R+\sum_{-\infty}^{\infty}{}' c_n\exp[-j(2n\pi/s)x] = \sqrt{s}\sum_{m=1}^{\infty}(b_m^+ + b_m^-)\phi_m,$$

$$(25)\qquad (1-R)\Gamma_0-\sum_{-\infty}^{\infty}{}' c_n\Gamma_n\exp[-j(2n\pi/s)x] = \sqrt{s}\sum_{m=1}^{\infty}(b_m^+ - b_m^-)\gamma_m\phi_m,$$

where $\Gamma_0 = jk_0\cos\theta_i$. The solution to these two equations determines the amplitude and phase of the reflected and transmitted waves. A rigorous solution would be difficult to obtain so a variational procedure that will give upper and lower bounds on the equivalent circuit parameters for the interface will be used instead.

5. VARIATIONAL SOLUTION

The variational procedure adopted here is a modification of that introduced by Schwinger (unpublished). It is fully described by Collin and Brown (1955*a*) in a paper on the junction effect between an empty and inhomogeneously filled waveguide. The method is the analytic equivalent of the Weissfloch (1942) experimental technique for finding the equivalent circuit of a waveguide discontinuity. The slotted dielectric interface is represented by two transmission lines of electrical length u and v connected by an ideal transformer of turns ratio $n:1$ as illustrated in Fig. 2. The characteristic impedances of the lines

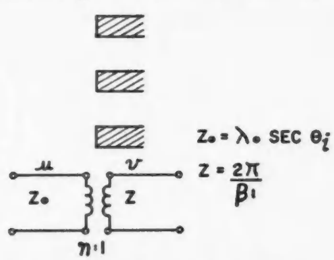

FIG. 2. Equivalent circuit for slotted dielectric interface.

will be taken equal to the wavelength along the z-axis in the free space region and slotted section. With reference to Fig. 2 a field minimum is located a distance d in front of the interface when a short-circuiting plane is placed a distance l from the interface in the slotted section where

$$Z_0\tan(\beta_0 d+u) = -n^2 Z\tan(\beta_1 l+v).$$

The parameters u, v, and n completely specify the effect of the interface on the propagating mode and are determined by an analysis of the curve $\beta_0 d+\beta_1 l$ vs. $\beta_1 l$ where

$$\beta_0 = k_0 \cos\theta_i, \qquad \beta_1 = |\gamma_1|,$$

l = position of short-circuit from the interface in the slotted section, d = position of an electric field minimum in the region $z < 0$, measured from the interface. A unique value for the parameters u, v, and n is only obtained provided l and d are chosen large enough so that all the evanescent modes have decayed to a negligible value at the short-circuit and field minimum positions.

The variational expressions giving $\beta_0 d$ as a function of $\beta_1 l$ are derived in a similar manner as for the waveguide case referred to. For the present problem these expressions are

$$\begin{aligned}
-\frac{1}{s}\beta_0 \cot\beta_0 d \int_{-\frac{1}{2}s}^{\frac{1}{2}s} G\,dx \int_{-\frac{1}{2}s}^{\frac{1}{2}s} G^* dx
&= \frac{1}{s}\sum_{-\infty}^{\infty}{}' \Gamma_n \int_{-\frac{1}{2}s}^{\frac{1}{2}s} G\exp[j(2n\pi/s)x]dx \int_{-\frac{1}{2}s}^{\frac{1}{2}s} G^*\exp[-j(2n\pi/s)x]dx \\
&\quad +\beta_1 \cot\beta_1 l \int_{-\frac{1}{2}s}^{\frac{1}{2}s} G\phi_1^* dx \int_{-\frac{1}{2}s}^{\frac{1}{2}s} G^*\phi_1 dx \\
&\quad +\sum_{m=2}^{\infty} \gamma_m \coth\gamma_m l \int_{-\frac{1}{2}s}^{\frac{1}{2}s} G\phi_m^* dx \int_{-\frac{1}{2}s}^{\frac{1}{2}s} G^*\phi_m dx,
\end{aligned} \tag{26}$$

$$\begin{aligned}
\frac{-\tan\beta_0 d}{s\beta_0} \int_{-\frac{1}{2}s}^{\frac{1}{2}s} H dx \int_{-\frac{1}{2}s}^{\frac{1}{2}s} H^* dx
&= \frac{1}{s}\sum_{-\infty}^{\infty}{}' \Gamma_n^{-1} \int_{-\frac{1}{2}s}^{\frac{1}{2}s} H\exp[j(2n\pi/s)x]dx \int_{-\frac{1}{2}s}^{\frac{1}{2}s} H^*\exp[-j(2n\pi/s)x]dx \\
&\quad +\beta_1^{-1}\tan\beta_1 l \int_{-\frac{1}{2}s}^{\frac{1}{2}s} H\phi_1^* dx \int_{-\frac{1}{2}s}^{\frac{1}{2}s} H^*\phi_1 dx \\
&\quad +\sum_{m=2}^{\infty} (\gamma_m \coth\gamma_m l)^{-1} \int_{-\frac{1}{2}s}^{\frac{1}{2}s} H\phi_m^* dx \int_{-\frac{1}{2}s}^{\frac{1}{2}s} H^*\phi_m dx,
\end{aligned} \tag{27}$$

where $e^{-j\beta z}G(x)$ is the electric field in the aperture plane $z = 0$ when the slotted section is terminated by a short circuit at $z = l$ and $e^{-j\beta z}H(x)/j\omega\mu$ is the x component of the magnetic field in the plane $z = 0$ under the same conditions. Eqs. (26) and (27) are positive definite quadratic forms and therefore yield upper and lower bounds on cot $\beta_0 d$ respectively. In practice the functions G and H are approximated by a finite series. For instance, let

$$G = \sum_{-N}^{N} \frac{c_n}{\sqrt{s}} \exp[-j(2n\pi/s)x]; \tag{28}$$

then

$$-c_0^2\beta_0 \cot\beta_0 d = \mathfrak{z}\sum_{-N}^{N}{}' \Gamma_n c_n^2 + \left(\sum_{-N}^{N} c_n P_{n1}\right)^2 \beta_1 \cot\beta_1 l + \sum_{m=2}^{\infty} \gamma_m \left(\sum_{-N}^{N} c_n P_{nm}\right)^2, \tag{29}$$

where l has been assumed large enough so that coth $\gamma_m l$ may be replaced by unity for all $m > 1$, and where

$$P_{nm} = \frac{1}{\sqrt{s}}\int_{-\frac{1}{2}s}^{\frac{1}{2}s} \phi_m \exp[j(2n\pi/s)x]dx = \frac{1}{\sqrt{s}}\int_{-\frac{1}{2}s}^{\frac{1}{2}s} \phi_m^* \exp[-j(2n\pi/s)x]dx.$$

The general formula for P_{nm} is given in Appendix II. Since the slotted section is terminated in a short circuit all the coefficients c_n may be taken as real. When the slotted section is terminated in a matched load the coefficients c_n would, in general, be complex. Furthermore the variational expressions for the input admittance and impedance would involve the aperture field for a wave incident at an angle $-\theta_i$ in place of the conjugate fields. The coefficients c_n in Eq. (29) are determined by solving the set of equations obtained by setting all the partial derivatives with respect to c_n for $|n| > 0$ equal to zero. There is no loss in generality by taking c_0 equal to unity. The summation over m is not terminated but in practice the cross coupling factors P_{nm} approach zero rapidly for large m when $m \neq n$. For $m = n$, P_{nm} approaches unity for large m.

Equation (27) may be handled in a similar manner.

6. NUMERICAL EXAMPLE

The equivalent circuit parameters for a slotted interface having the following dimensions:

$$s = 1 \text{ cm.},$$
$$t = 0.35 \text{ cm.},$$
$$\kappa = 2.56,$$

were evaluated for a free space wavelength of 3.14 cm. and an angle of incidence of 30°. For this example the value of β_1 is 2.32 and $\beta_0 = 1.73$. Sufficient accuracy was obtained by using a constant term only for G and H. A plot of $\beta_1 l+\beta_0 d$ vs. $\beta_1 l$ is given in Fig. 3 from which it is seen that the maximum error

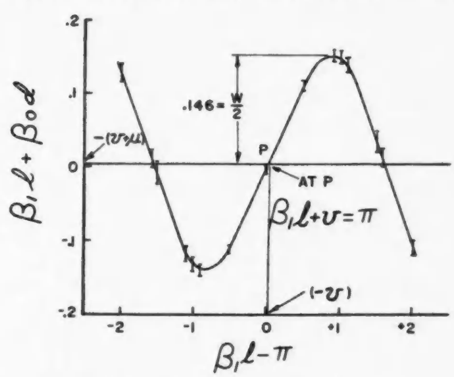

FIG. 3. Theoretical curve of $\beta_0 d+\beta_1 l$ vs. $\beta_1 l$.

in $\beta_0 d$ does not exceed ± 0.015 radians and hence a position d of a field minimum is correct to within ± 0.009 cm. The turns ratio n of the ideal transformer is given by

$$n = \sqrt{\frac{\beta_1}{\beta_0}} \cot \frac{\pi+w}{4} = 1.00 \pm .005,$$

where w is the total peak to peak width of the curve. From the curve the electrical lengths of the two transmission lines, u and v, are estimated to be $0.85° \pm .4°$ and $-1.15° \pm .4°$ respectively. It is seen that there is a negligible phase shift introduced into the reflected and transmitted waves. Also the impedance transformation at the junction may be taken as that due to the change in wave impedance in going from free space into the slotted section. The reason for this behavior can be readily appreciated by referring to Fig. 4

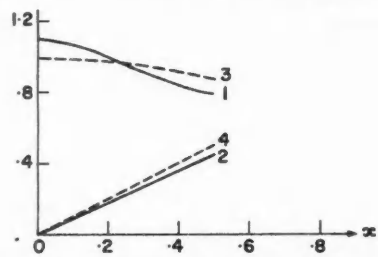

FIG. 4. Comparison of functions $F_1(x)$ and $e^{-j\beta x}$.
1—Real part of $F_1(x)$, 2—Imaginary part of $F_1(x)$,
3—Real part of $e^{-j\beta x}$, 4—Imaginary part of $e^{-j\beta x}$.

where the real and imaginary parts of F_1 and $e^{-j\beta x}$ are plotted. It is seen that F_1 differs from $e^{-j\beta x}$ by less than $\pm 12\%$ and hence the amplitudes of the higher order modes excited are small.

Since such a slotted dielectric behaves like a homogeneous dielectric with an effective dielectric constant κ_e equal to $(\beta_1^2/k_0^2)+\sin^2\theta_i$ at the wavelength λ_0 and angle of incidence θ_i, the design of a slotted dielectric matching layer is relatively straightforward. The requirements are that the spacing s must be less than

$$\frac{\lambda_0}{\sqrt{\kappa}(1+|\sin\theta_i|)}$$

and the thickness be such that

$$\kappa_e - \sin^2\theta_i = [(1-\sin^2\theta_i)(\kappa - \sin^2\theta_i)]^{\frac{1}{2}}.$$

The depth of the slots D is chosen as

$$\frac{\lambda_0}{4\sqrt{\kappa_e - \sin^2\theta_i}}$$

or one quarter wavelength. These equations are the same as for a homogeneous dielectric of dielectric constant κ_e. For the following parameters:

$$s = 1 \text{ cm.}, \qquad t = 0.35 \text{ cm.},$$
$$D = 0.635 \text{ cm.}, \qquad \lambda_0 = 3.14 \text{ cm.},$$
$$\kappa = 2.56,$$

a wave incident at an angle of 15° is perfectly matched to a dielectric of relative dielectric constant 2.56. The magnitude of the reflection coefficient for angles of incidence of 0°, 15°, and 30° in the wavelength range of 3.00 to 3.28 cm. is

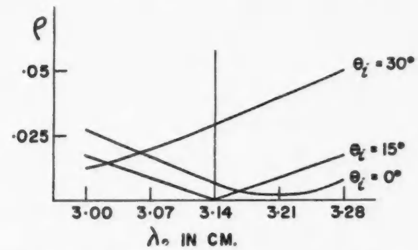

Fig. 5. Modulus of reflection coefficient for a slotted dielectric matching section.

plotted in Fig. 5. The reflection coefficient does not exceed 0.05 as compared to 0.23, 0.24, 0.275 for the above angles of incidence when no matching section is used.

7. CONCLUSIONS

A variational solution for the parameters of the equivalent circuit of a slotted dielectric interface for a wave incident at an angle to the interface normal and polarized with the electric vector parallel to the slots has been given. For the usual values of dielectric constants and angles of incidence that would be encountered in practice the phase shifts introduced into the reflected and transmitted waves are very small being of the order of 1°. A quarter wave matching section may be constructed from such a slotted dielectric and will match a plane wave to the solid dielectric medium over a wide frequency band and a considerable range of angles of incidence with negligible reflection. The slotted dielectric has some similarity with the parallel plate media. One outstanding difference is the possibility of choosing a spacing s such that there will only be one reflected wave. For parallel plate media the spacing must be greater than a half wavelength so that for angles of incidence above a certain critical angle two reflected waves appear (Berz 1951).

For a wave incident with the magnetic vector parallel to the slots the wave impedance and also the wavelength in the slotted section is different so that a match will not be obtained. The same is true for a homogeneous dielectric when $\theta_i \neq 0$ with the exception that the wavelength does not change with a change in the polarization. In order to match both polarizations simultaneously an additional degree of freedom in the design must be introduced. This can be done by cutting an additional set of slots perpendicular to the first set. The theoretical analysis of such a structure would be difficult. Some experimental work on such a matching section has however been done (Jones and Cohn 1955).

REFERENCES

Berz, F. 1951. Proc. Inst. Elect. Engrs. (London), Pt. III, **98**: 47.
Collin, R. E. 1953. Ph.D. Thesis, Univ. of London.
——— 1955. Proc. I.R.E. **43**: 179.

Collin, R. E. and Brown, J. 1955*a*. Inst. Elect. Engrs. (London), Monograph No. **145R**, Aug.
——— 1955*b*. Inst. Elect. Engrs. (London), Monograph No. **149R**, Sept.
Jones, E. M. and Cohn, S. B. 1955. J. Appl. Phys. **26**: 452.
Morse, P. M. and Feshbach, H. 1953. Methods of theoretical physics. McGraw-Hill Book Company, Inc., New York.
Schwinger, J. Unpublished. Mass. Inst. Technol. Lecture Notes (*edited by* D. S. Saxon).
Weissfloch, A. 1942. Hochfrequenztech. u. Elektroakustik. **60**: 67.

APPENDIX I

With reference to Fig. 6 the electric field for the m'th mode will be a linear combination of two waves propagating in the positive and negative x directions. Let the amplitude of the forward and backward travelling waves be a_1 and b_1

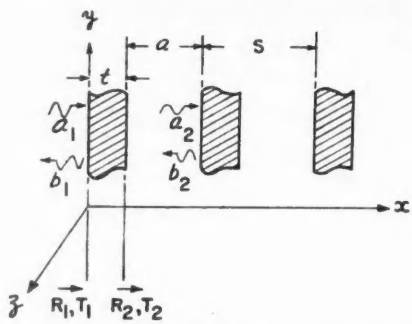

Fig. 6. Periodic slotted dielectric medium.

respectively at $x = 0$ and a_2 and b_2 respectively at $x = s$. The electric field of the forward travelling wave is proportional to $e^{-jl_m x}$ in the dielectric sections and $e^{-jk_m x}$ in the free space sections. The z component of the magnetic field is proportional to $l_m e^{-jl_m x}$ and $k_m e^{-jk_m x}$ respectively. For the negative travelling wave the signs in the exponential terms are changed to positive. The wave admittances may be taken proportional to l_m in the dielectric sections and k_m in the free space sections. The reflection coefficient R_1 and transmission coefficient T_1 looking to the right at $x = 0$ are given by the following expressions:

$$R_1 = \frac{k_m - l_m}{k_m + l_m}, \qquad (30)$$

$$T_1 = 1 + R_1.$$

At $x = t$ the corresponding quantities are

$$R_2 = -R_1, \qquad (31)$$

$$T_2 = 1 - R_1.$$

It may be shown (Collin 1955) that the amplitudes a_1, b_1 are related to a_2, b_2 by the following matrix equation:

$$\begin{bmatrix} a_1 \\ b_1 \end{bmatrix} = \frac{e^{j(l_m t + k_m a)}}{T_1 T_2} \begin{bmatrix} 1 & R_1 e^{-j2l_m t} \\ R_1 & e^{-j2l_m t} \end{bmatrix} \begin{bmatrix} 1 & -R_1 e^{-j2k_m a} \\ -R_1 & e^{-j2k_m a} \end{bmatrix} \begin{bmatrix} a_2 \\ b_2 \end{bmatrix} \qquad (32)$$

$$= \begin{bmatrix} A_{11} & A_{12} \\ A_{21} & A_{22} \end{bmatrix} \begin{bmatrix} a_2 \\ b_2 \end{bmatrix}.$$

In order to have a mode propagating down the periodic structure in the positive x direction it is necessary that $a_2 = e^{-j\beta s}a_1$ and $b_2 = e^{-j\beta s}b_1$. Therefore

$$\begin{bmatrix} a_1 \\ b_1 \end{bmatrix} = \begin{bmatrix} A_{11} & A_{12} \\ A_{21} & A_{22} \end{bmatrix} \begin{bmatrix} e^{-j\beta s}a_1 \\ e^{-j\beta s}b_1 \end{bmatrix}, \tag{33}$$

which has a solution if the determinant of the resulting two simultaneous equations vanishes. The vanishing of the determinant gives

$$A_{11}A_{22}-A_{12}A_{21}+e^{2j\beta s}-e^{j\beta s}(A_{11}+A_{22}) = 0. \tag{34}$$

When the appropriate values for the matrix elements A_{ij} are substituted from Eq. (32) into Eq. (34) and the resulting equation simplified the following eigenvalue equation is obtained:

$$\cos \beta s = \cos l_m t \cos k_m a - \frac{l_m{}^2+k_m{}^2}{2l_m k_m} \sin l_m t \sin k_m a. \tag{35}$$

This equation together with the relation $k_m{}^2 = l_m{}^2-(\kappa-1)k_0{}^2$ permits a solution for l_m and k_m to be obtained when β is given. When m becomes large l_m and k_m approach equality and the term $(l_m{}^2+k_m{}^2)/2l_m k_m$ approaches unity. The eigenvalue equation thus becomes

$$\cos \beta s = \cos(l_m t+k_m a) \approx \cos l_m s$$

and hence $l_m = (2m\pi/s)\pm\beta$. Under these conditions $\theta_m{}^{e,o}$ approach zero, $a_m{}^{e,o}$ approach unity, and B_m approaches jA_m for m even and $-jA_m$ for m odd. Thus the functions ϕ_m for m even approach $\exp[j(2m\pi/s)x]$ and for m odd $\exp[-j(2m\pi/s)x]$. When $\beta = 0$, Eq. (35) reduces to

$$[l_m \tan l_m(\tfrac{1}{2}t)+k_m \tan k_m(\tfrac{1}{2}a)][l_m \cot l_m(\tfrac{1}{2}t)+k_m \cot k_m(\tfrac{1}{2}a)] = 0. \tag{36}$$

The vanishing of the first bracket gives the eigenvalues for normal mode functions which have even symmetry about the points $x = \frac{1}{2}t$, $\frac{1}{2}(s+t)$, while the vanishing of the second bracket gives the eigenvalues for the normal mode functions which have odd symmetry about the points $x = \frac{1}{2}t$, $\frac{1}{2}(s+t)$. The

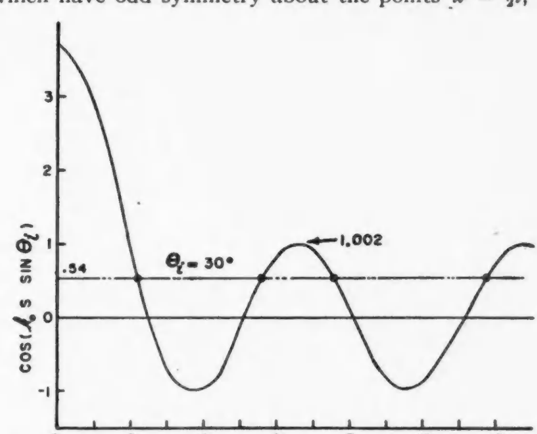

FIG. 7. Curve for determining the eigenvalues l_m as a function of angle of incidence, $t = 0.35$ cm., $s = 1$ cm., $k_0 = 2$, $\kappa = 2.56$.

latter modes are not excited in the case of normal incidence when $\beta = 0$. When $\beta \neq 0$ the modes are not separated into two discrete groups.

Fig. 7 gives a plot of the right-hand side of Eq. (35) as a function of l_m for $s = 1$ cm., $t = 0.35$ cm., $\kappa = 2.56$, and $k_0 = 2$. The eigenvalues l_m are readily determined from the points of interception of this curve with the straight line $\cos(k_0 s \sin\theta_i)$ when the angle of incidence θ_i is given. From the figure it is seen that the right-hand side of Eq. (35) approaches $\cos l_m s$ rapidly.

The eigenvalue equation for a wave polarized with the electric vector in the xz-plane may be derived in a similar manner. It is as follows:

$$\cos\beta s = \cos l_m t \cos k_m a - \frac{\kappa^2 k_m{}^2 + l_m{}^2}{2\kappa k_m l_m} \sin l_m t \sin k_m a. \tag{37}$$

This equation does not have a simultaneous solution with Eq. (35) so the wavelength in the slotted section will be different for the two polarizations. When $\beta = 0$ the normal modes again split into two sets having even and odd symmetry properties and with the following eigenvalue equations respectively:

$$\begin{aligned} l_m \tan l_m(\tfrac{1}{2}t) + \kappa k_m \tan k_m(\tfrac{1}{2}a) &= 0, \\ l_m \cot l_m(\tfrac{1}{2}t) + \kappa k_m \cot k_m(\tfrac{1}{2}a) &= 0. \end{aligned} \tag{38}$$

APPENDIX II

The coefficients A_m are chosen so that the normal mode functions F_m are normalized. Thus

$$\int_{-\frac{1}{2}s}^{\frac{1}{2}s} F_m F_m^* dx = A_m^2 \int_{-\frac{1}{2}s}^{\frac{1}{2}s} [(\psi_m{}^e)^2 + \alpha_m^2 (\psi_m{}^o)^2] dx = 1. \tag{39}$$

Substituting for $\psi_m{}^e$ and $\psi_m{}^o$ and integrating gives the following expression for A_m:

$$\begin{aligned} A_m^{-2} &= \frac{t}{2}(1+\alpha_m^2) + \frac{a}{2}[(a_m{}^e)^2 + \alpha_m^2 (a_m{}^o)^2] \\ &\quad + \frac{1-\alpha_m^2}{2l_m} \sin l_m t + \frac{(a_m{}^e)^2}{2k_m} [\sin 2k_m(\tfrac{1}{2}s - \theta_m{}^e) - \sin 2k_m(\tfrac{1}{2}t - \theta_m{}^e)] \\ &\quad - \frac{(a_m{}^o)^2}{2k_m} [\sin 2k_m(\tfrac{1}{2}s - \theta_m{}^o) - \sin 2k_m(\tfrac{1}{2}t - \theta_m{}^o)]. \end{aligned} \tag{40}$$

The cross coupling factors P_{nm} are defined by the following integral

$$\begin{aligned} P_{nm} &= \int_{-\frac{1}{2}s}^{\frac{1}{2}s} \frac{\phi_m}{\sqrt{s}} \exp[j(2n\pi/s)x] dx \\ &= \frac{2A_m}{\sqrt{s}} \int_0^{\frac{1}{2}s} \left[\psi_m{}^e \cos\left(\beta + \frac{2n\pi}{s}\right)x + \alpha_m \psi_m{}^o \sin\left(\beta + \frac{2n\pi}{s}\right)x \right] dx. \end{aligned} \tag{41}$$

Carrying out the integrations gives the following expression for P_{nm}:

$$\begin{aligned}
\frac{P_{nm}\sqrt{s}}{A_m} &= \frac{1-\alpha_m}{r_{mn}} \sin r_{mn}(\tfrac{1}{2}t) + \frac{1+\alpha_m}{h_{mn}} \sin h_{mn}(\tfrac{1}{2}t) \\
&\quad + a_m^{\,e}\left[\frac{\sin[f_{mn}(\frac{1}{2}s) - k_m\theta_m^{\,e}] - \sin[f_{mn}(\frac{1}{2}t) - k_m\theta_m^{\,e}]}{f_{mn}}\right. \\
&\qquad \left. + \frac{\sin[g_{mn}(\frac{1}{2}s) - k_m\theta_m^{\,e}] - \sin[g_{mn}(\frac{1}{2}t) - k_m\theta_m^{\,e}]}{g_{mn}}\right] \\
&\quad + \alpha_m a_m^{\,o}\left[\frac{\sin[g_{mn}(\frac{1}{2}s) - k_m\theta_m^{\,o}] - \sin[g_{mn}(\frac{1}{2}t) - k_m\theta_m^{\,o}]}{g_{mn}}\right. \\
&\qquad \left. - \frac{\sin[f_{mn}(\frac{1}{2}s) - k_m\theta_m^{\,o}] - \sin[f_{mn}(\frac{1}{2}t) - k_m\theta_m^{\,o}]}{f_{mn}}\right],
\end{aligned} \tag{42}$$

where

$$\begin{aligned}
r_{mn} &= l_m + \beta + 2n\pi/s, \\
h_{mn} &= l_m - \beta - 2n\pi/s, \\
f_{mn} &= k_m + \beta + 2n\pi/s, \\
g_{mn} &= k_m - \beta - 2n\pi/s.
\end{aligned}$$

THE AXIAL-FLOW ERROR IN THE THERMAL-CONDUCTIVITY PROBE[1]

By J. H. Blackwell[2]

ABSTRACT

In connection with the development of the thermal-conductivity probe the author has used a new boundary condition of Jaeger to find an expression for an upper limit to the axial-flow error in these devices. Unlike in previous attempts at this problem the short-circuiting effect of the probe material is taken into account.

INTRODUCTION

The idealization of "radial flow" is frequently employed in the solution of transient heat flow problems with axial symmetry in an infinite medium but convenient criteria have not often been available for determining the minimum length of the source or sink of heat for this idealization to be valid.

A recent paper by Jaeger (1955) makes possible solutions of this problem for the important practical cases where the heat source is a thin wire or thin-walled hollow cylinder of good conductor.

It is the purpose of the present note to show how Jaeger's radial boundary condition may be used to find, in convenient form, an upper limit to the axial-flow error in thermal-conductivity probes (Blackwell 1954; Hooper and Lepper 1950).

DESCRIPTION OF THE PROBLEM

A thermal-conductivity probe is normally a circular cylinder of good thermal conductor. It is either solid with a small radius or hollow with a thin wall so that radial temperature differences in the probe material are negligible to first order. It is provided with a heater and some means of measuring temperature at the center of its length.

In practical applications the probe is either buried in the external medium whose thermal constants are being measured (granular material) or inserted in a long hole (solid material). In the design of these devices it is obviously important to determine in advance the minimum length of the probe for simple radial flow theory to be valid.

It is possible to set up idealized radial–axial heat flow problems which must have greater or smaller axial flow effects than occur with a practical probe. Case II of a previous paper by the author (1953) provides an example of the latter and it is the present purpose to solve a corresponding example of the former.

The problem considered is that of an infinitely long cylinder of good conductor, whose cross-section satisfies the conditions given above for a practical

[1]Manuscript received November 30, 1955.
Contribution from the Department of Geophysics, Research School of Physical Sciences, Australian National University, Canberra, Australia.
[2]Visiting Research Fellow; on leave from University of Western Ontario.

probe, and which is immersed in an external medium of infinite extent. Heat is supplied to a finite length of this cylinder only, corresponding to the length of the probe.

Then, provided that a real probe is immersed sufficiently well that external boundary effects are negligible and that other mechanisms of heat transfer than conduction may be disregarded, the real axial heat loss must be less than that of the idealized problem. With the possible exception of the presence of convection in certain geophysical applications, the restrictions stated have little experimental significance.

ANALYSIS

We wish to solve the following problem and compare solutions with the corresponding one for radial flow:

$$(1)\qquad \frac{\partial^2\theta}{\partial\rho^2}+\frac{1}{\rho}\frac{\partial\theta}{\partial\rho}+\frac{\partial^2\theta}{\partial z^2}=\frac{1}{\kappa}\frac{\partial\theta}{\partial t},\qquad a<\rho<\infty,\quad -\infty<z<\infty,\quad t>0,$$

subject to

$$(2)\qquad \begin{aligned} \theta &= 0, &\qquad t &= 0,\, a<\rho<\infty,\, -\infty<z<\infty,\\ \theta_1 &= 0, & t &= 0,\end{aligned}$$

$$(3)\qquad \begin{aligned} -K\frac{\partial\theta}{\partial\rho} &= \frac{\delta K_1}{2\pi a}\left[\frac{A}{K_1}\{U(z+L)-U(z-L)\}+\frac{\partial^2\theta_1}{\partial z^2}-\frac{1}{\kappa_1}\frac{\partial\theta_1}{\partial t}\right]\\ &= H(\theta_1-\theta), \qquad\qquad \rho=a,\; t>0,\end{aligned}$$

where

ρ, z, t	are the radial and axial co-ordinates and the time,
$\theta(\rho, z, t), K, \kappa$	are the temperature, conductivity, and diffusivity of the external medium,
$\theta_1(z, t), K_1, \kappa_1$	are the corresponding quantities for the probe,
a	is the probe radius,
L	is the probe half-length,
δ	is the probe cross-section,
A	is the heat supplied to the probe/unit volume/unit time,
H	is the "outer conductivity" at $\rho = a$ (a measure of the contact resistance between probe and medium),
$U(x)$	is the unit step-function.

Equation (3) is Jaeger's boundary condition (equation (21) of his paper) modified for the presence of contact resistance and to include the axial conditions of the present problem.

By standard methods, we find the Laplace transform of the temperature in the cylinder:

$$(4)\qquad \Theta_1=\frac{2Aa^2}{pK_1}\left(\frac{\kappa_1}{\kappa}\right)\frac{1}{2\pi}\int_{-\infty}^{\infty}\frac{\sin L\omega\, e^{iz\omega}\{K_0(\beta a)+(K/aH)\beta a\, K_1(\beta a)\}\, d\omega}{\omega[(\beta^2a^2+b)\{K_0(\beta a)+(K/aH)\beta a\, K_1(\beta a)\}+B\beta a K_1(\beta a)]}$$

where p is the transform variable,

$\beta = (q^2 + \omega^2)^{\frac{1}{2}}$,

$q = (p/\kappa)^{\frac{1}{2}}$,

$b = \omega^2 a^2(\kappa_1/\kappa - 1)$,

$B = 2\pi a^2 K\kappa_1/\delta K_1\kappa$.

The axial-flow error obviously increases with time and in the case of pure radial-flow (Blackwell 1954) the conductivity K is inversely proportional to $\partial\theta_1/\partial(\ln t)$ for $T_r = \kappa t/a^2 \gg 1$. It is therefore permissible and also convenient to discuss the axial flow error in terms of an approximate value of $\partial\theta_1/\partial(\ln t)]_{z=0}$ valid for large T_r. If in our analysis, we take into account the further requirement that L/a is large, we arrive at a simple relationship between $\partial\theta_1/\partial(\ln t)$ in the radial and radial–axial cases.

By standard methods of the Laplace Transformation and assuming orders of integration may be reversed, we obtain from equation (4),

$$\frac{\partial\theta_1}{\partial t}\Big]_{z=0} = \frac{2Aa^2}{K_1}\left(\frac{\kappa_1}{\kappa}\right)\frac{1}{2\pi}\int_{-\infty}^{\infty}\frac{\sin L\omega}{\omega}\exp(-\omega^2\kappa t)\,F(\omega)\,d\omega, \tag{5}$$

where

$$F(\omega) = \frac{1}{2\pi i}\int_{Br_2}\frac{\{K_0(qa)+(K/aH)qaK_1(qa)\}\,e^{tp}dp}{(q^2a^2+b)\{K_0(qa)+(K/aH)qaK_1(qa)\}+BqaK_1(qa)} \tag{6}$$

and Br_2 is the contour $ABCDE$ of Fig. 1.

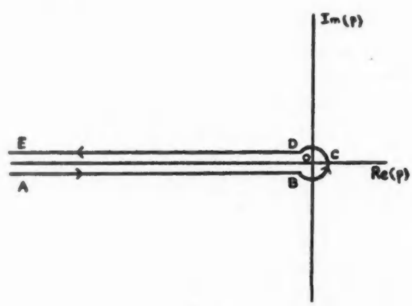

FIG. 1.

Following Goldstein's method we then expand the integrand of $F(\omega)$ in ascending powers of qa; term-by-term integration should then result in an expansion suitable for large T_r (Blackwell 1954; Goldstein 1932). In the present instance we retain dominant terms only and get

$$F(\omega) = \frac{1}{2\pi i}\int_{Br_2}\frac{\{\ln(\frac{1}{2}qa)+\gamma-(K/aH)\}\,e^{tp}dp}{-B+b\{\ln(\frac{1}{2}qa)+\gamma-(K/aH)\}} \tag{7}$$

where γ is Euler's constant $= 0.5772\ldots$.

Since the major contribution to the integral of equation (5) comes from

values of ω such that $|\omega L| \ll \pi$, we can treat $\omega^2 a^2$ and hence b/B as small quantities, and expand the integrand of (7) again, obtaining

$$(8)\quad F(\omega) \approx \left(-\frac{1}{B}\right)\frac{1}{2\pi i}\int_{Br_2}\left[\ln(\tfrac{1}{2}qa)+\gamma-\frac{K}{aH}+\left(\frac{b}{B}\right)\left\{\ln(\tfrac{1}{2}qa)+\gamma-\frac{K}{aH}\right\}^2 + \left(\frac{b}{B}\right)^2\left\{\ln(\tfrac{1}{2}qa)+\gamma-\frac{K}{aH}\right\}^3+\ldots\right]e^{tp}dp.$$

The term integrals of equation (8) are either well-known or easily derivable (Blackwell 1954; Jeffreys and Jeffreys 1946) and we find

$$(9)\quad F(\omega) \approx \frac{1}{2Bt}\left[1-\left(\frac{b}{B}\right)\left[\ln 4T_r-\gamma+\frac{2K}{aH}\right] + \frac{1}{4}\left(\frac{b}{B}\right)^2\left[-\frac{\pi^2}{2}+3\left\{\ln 4T_r-\gamma+\frac{2K}{aH}\right\}^2\right]+\ldots\right].$$

Introduce the dimensionless parameters

$$\epsilon = K_1/K,$$

$$\eta = K_1\kappa/K\kappa_1 \text{ (ratio of thermal capacities/unit volume),}$$

and $$\sigma = \frac{2d}{a}\left(1+\frac{d}{2a}\right) \approx \frac{2d}{a} \qquad \text{for hollow probes,}$$

$$= 1 \qquad \text{for ``needle'' probes.}$$

Then

$$\delta = \pi a^2\sigma,$$

$$B = 2/\sigma\eta,$$

$$b/B = \tfrac{1}{2}\omega^2 a^2(\epsilon-\eta),$$

and substituting from (9) into (5),

$$(10)\quad \left.\frac{\partial\theta_1}{\partial t}\right]_{z=0} \approx \frac{Aa^2}{K}\left(\frac{\sigma}{4t}\right)\left[\frac{1}{\pi}\int_{-\infty}^{\infty}\frac{\sin L\omega}{\omega}\exp(-\omega^2\kappa t)\,d\omega - \left(\ln 4T_r-\gamma+\frac{2K}{aH}\right)\frac{a^2\sigma(\epsilon-\eta)}{2\pi}\int_{-\infty}^{\infty}\omega\sin L\omega\exp(-\omega^2\kappa t)\,d\omega + \left\{-\frac{\pi^2}{2}+3\left(\ln 4T_r-\gamma+\frac{2K}{aH}\right)^2\right\}\frac{a^4\sigma^2(\epsilon-\eta)^2}{16\pi}\int_{-\infty}^{\infty}\omega^3\sin L\omega\exp(-\omega^2\kappa t)\,d\omega\right].$$

Hence

$$(11)\quad \left.\frac{\partial\theta_1}{\partial(\ln t)}\right]_{z=0} = \left(\frac{Q}{4\pi K}\right)R$$

where

$$(12)\quad R = \operatorname{erf}x-2\pi^{-\frac{1}{2}}CSx^3e^{-x^2}+\pi^{-\frac{1}{2}}C^2\{-\tfrac{1}{2}\pi^2+3S^2\}x^4(\tfrac{1}{2}+\tfrac{1}{2}x-x^2)e^{-x^2};$$

$$x = L/2\sqrt{\kappa t}, \qquad C = \sigma a^2(\epsilon-\eta)/L^2,$$

$$S = \ln 4T_r-\gamma+2K/aH.$$

The factor R gives the ratio between the respective values of $\partial\theta_1/\partial(\ln t)$ and hence the required limit to the axial-flow error. The first term of R is

independent of the probe parameters and may be thought of as due to axial flow in the external medium alone; for a given value of t it approaches unity as $L \to \infty$. The remaining terms in the bracket correct the first for the presence of probe and contact resistance and approach zero as $L \to \infty$. For design purposes, we need only retain the second term, the third giving an estimate of the error made in assuming $b/B \ll 1$. As expected the second term varies directly with the ratio of conductivities and the probe cross-section.

As $\delta = \pi a^2\sigma \to 0$, $R \to \operatorname{erf} x$, a result which happens to be true exactly (Blackwell 1953). This value of R provides the lower limit to the axial-flow error referred to earlier.

The parameters C and x used above both contain L. It is convenient for design purposes to introduce a further parameter

$$\lambda = L/a, \quad \text{the length–diameter ratio.}$$

Rewriting the first two terms of equation (12)

$$R \approx \operatorname{erf}[\lambda(4T_r)^{-\frac{1}{2}}] - 2\sigma\pi^{-\frac{1}{2}}\lambda(\epsilon-\eta)(4T_r)^{-3/2}\, S \exp[-\lambda^2/4T_r]. \tag{13}$$

Inserting the asymptotic expression for the error function we obtain the relative error due to axial flow

$$\Delta R = 1 - R = \pi^{-\frac{1}{2}} \exp[-\lambda^2/4T_r]\, [(4T_r)^{\frac{1}{2}}/\lambda + 2\sigma\lambda(\epsilon-\eta)(4T_r)^{-3/2}S]\,. \tag{14}$$

The error in ΔR introduced by this further approximation is $\lesssim 0.0004$ for $\lambda(4T_r)^{-\frac{1}{2}} \gtrsim 2$.

NUMERICAL EXAMPLE

The maximum value of T_r used in an experiment is set by consideration of the basic radial-flow theory and is unlikely ever to exceed 25. If we take this value for T_r, and $2K/aH = 2$ (a rather large contact-resistance for many practical applications), equation (14) becomes

$$(\Delta R)_{\max} = \exp[-0.01\lambda^2]\, [5.64/\lambda + 0.680\times 10^{-2}\sigma\lambda(\epsilon-\eta)]\,. \tag{15}$$

Equation (15) is an appropriate form in which to use the criterion.

Take the case of a hollow brass probe of, say, $1\frac{1}{4}$ in. O.D. $\times$ $\frac{1}{8}$ in. wall for use in a geophysical application where we know $K \sim 0.005$ c.g.s., $\kappa \sim 0.01$ c.g.s. How long should the probe be?

We have $\epsilon = 50.0$, $\eta = 1.50$, $\sigma = 0.40$, and hence

$$(\Delta R)_{\max} = [5.64/\lambda + 0.132\lambda] \exp[-0.01\lambda^2]\,. \tag{16}$$

The expression (16) is now evaluated for trial values of λ:

λ	$5.64/\lambda$	0.132λ	$\exp[-0.01\lambda^2]$	$(\Delta R)_{\max}$
20	0.282	2.64	0.0183	0.053
25	0.226	3.30	0.00192	0.007
30	0.188	3.96	0.000123	0.00051

We observe that $\lambda = 25$ gives a maximum error slightly under 1% while for $\lambda = 30$, the error is negligible for any normal thermal experiment.

On the other hand, consider a solid probe of the same outside diameter. The parameter σ is now unity and for

$$\lambda = 25, \quad (\Delta R)_{max} = 0.017;$$

$$\lambda = 30, \quad (\Delta R)_{max} = 0.0012.$$

It will be noted that the relative errors have been more than doubled.

ACKNOWLEDGMENTS

The author wishes to express his gratitude to Prof. J. C. Jaeger for helpful comments throughout. He would also like to thank the referee for suggesting the final approximation contained in equation (14) above.

REFERENCES

Blackwell, J. H. 1953. Can. J. Phys. **31**: 472.
——— 1954. J. Appl. Phys. **25**(No. 2): 137.
Goldstein, S. 1932. Proc. London Math. Soc. **34**: 51.
Hooper, F. C. and Lepper, F. R. 1950. J. Am. Soc. Heating Ventilating Engrs. **22**: 129.
Jaeger, J. C. 1955. Quart. J. Mech. Appl. Math. **8**(Pt. 1): 101.
Jeffreys, H. and Jeffreys, B. 1946. Mathematical physics. Cambridge University Press, London. p. 373.

INTEGRALS OF INTEREST IN METALLIC CONDUCTIVITY*

By D. K. C. MacDonald and Lois T. Towle

The electrical resistivity, ρ, of an idealized metal may be expressed in the form:

$$(1)\qquad \frac{\rho}{\rho_\infty} = \frac{4}{T_\infty}\cdot\frac{T^5}{\theta^4}\int_0^{\theta/T}\frac{z^5dz}{(e^z-1)(1-e^{-z})}$$

$$\equiv \frac{4}{T_\infty}\cdot\frac{T^5}{\theta^4}\,.\,J_5(\theta/T),$$

a formula due originally to Bloch (1929, 1930). ρ_∞ is the resistivity at some sufficiently high temperature T_∞ ($>\theta$), and θ is the characteristic (Debye) temperature of the metal.†

The corresponding expression for the electronic thermal resistivity, W, is considerably more complex (cf. Wilson 1953, p. 285) and is in poor agreement with the experimental data (cf. e.g. Wilson *loc. cit.*, pp. 288–290). A crude physical argument suggests that corresponding to equation (1) we might expect the thermal resistivity to be given approximately by:

$$(2)\qquad \frac{W}{W_\infty} = 2\frac{T^2}{\theta^2}\int_0^{\theta/T}\frac{z^3dz}{(e^z-1)(1-e^{-z})}$$

$$\equiv 2\frac{T^2}{\theta^2}\,.\,J_3(\theta/T)$$

and indeed White, Woods, and MacDonald (1956) have found that this expression fits the experimental results surprisingly well.

Sondheimer (1950) has tabulated the integrals $J_r(x)$ with r = 5, 7, 9, 11, 13, 15, 17 for x ranging from 0.8 to ∞, and Grüneisen (1933) earlier gave a very full table of $(4/x^4)J_5(x)$, this form being chosen to have the limit unity as x tends to zero. It appears possible that values of $J_2(x)$ and $J_6(x)$ may be useful in the future as well as $J_3(x)$ which occurs in (2) above, and we have therefore tabulated here these integrals for x from 0.1 to ∞ ($J_1(x)$ does not converge at the lower limit). For completeness we have also included $J_4(x)$ which arises in the Debye formula for the specific heat C_v of a solid:

$$(3)\qquad C_v = 9R\left(\frac{T}{\theta}\right)^3\int_0^{\theta/T}\frac{z^4dz}{(e^z-1)(1-e^{-z})}$$

$$\equiv 9R\left(\frac{T}{\theta}\right)^3.\,J_4\left(\frac{\theta}{T}\right).$$

*Issued as N.R.C. No. 3895.

†We do not here enter into any discussion of the appropriate choice for θ.

TABLE OF $J_r(x) = \int_0^x \frac{z^r dz}{(e^z-1)(1-e^{-z})}$

x	$J_2(x)$	$J_3(x)$	$J_4(x)$	$J_6(x)$
0.1	0.09997	0.0050	0.0003	0.000002
0.25	0.2496	0.0312	0.0052	0.00019
0.5	0.4966	0.1237	0.04115	0.00616
1.0	0.9730	0.4798	0.3172	0.1885
1.2	1.1540	0.6788	0.5365	0.4573
1.5	1.4122	1.0269	1.0079	1.3319
2	1.8017	1.706	2.2016	5.0858
3	2.4111	3.211	5.9632	29.69
4	2.8067	4.579	10.7293	88.59
5	3.0392	5.614	15.3671	182.22
6	3.1657	6.3033	19.1210	295.40
8	3.2624	6.9581	23.5874	507.00
10	3.2844	7.1505	25.2812	639.21
13	3.2895	7.2061	25.9273	713.85
20	3.2899	7.2123	25.9639	732.31
∞	3.2899	7.2124	25.9757	732.49

NOTE: $\lim_{x\to 0} J_r(x) = x^{r-1}/(r-1)$;

$\lim_{x\to\infty} J_r(x) = r! \sum_{s=1}^{\infty} \frac{1}{s^r} \equiv r!\,\zeta(r)$, where $\zeta(r)$ is the Riemann zeta-function.

Hence $J_2(\infty) = \pi^2/3$,
$J_4(\infty) = 4\pi^4/15$,
$J_6(\infty) = 16\pi^6/21$.

BLOCH, F. 1929. Z. Physik, **52**: 555.
——— 1930. Z. Physik, **59**: 208.
GRÜNEISEN, E. 1933. Ann. Physik, **16**: 530.
SONDHEIMER, E. H. 1950. Proc. Roy. Soc. A, **203**: 75.
WHITE, G. K., WOODS, S. B., and MACDONALD, D. K. C. 1956. Proc. Roy. Soc. A. In press.
WILSON, A. H. 1953. The theory of metals. 2nd ed. Cambridge University Press, London.

RECEIVED DECEMBER 21, 1955.
DIVISION OF PURE PHYSICS,
NATIONAL RESEARCH COUNCIL,
OTTAWA, CANADA.

ON THE THERMOELECTRIC POWER OF DILUTE METALLIC ALLOYS*

BY A. B. BHATIA† AND D. K. C. MACDONALD

The thermoelectric power S of a metal is given by (e.g. Mott and Jones 1936)

$$S = -\frac{\pi^2 k^2 T}{3e}\left\{\frac{\partial \log \rho(E)}{\partial E}\right\}_{E=\zeta} \tag{1}$$
$$\equiv -\frac{\pi^2 k^2 T}{3e\zeta}\left\{\frac{\partial \log \rho(E)}{\partial \log E}\right\}_{E=\zeta},$$

where $\rho(E)$ is the electrical resistivity corresponding to some value E of the Fermi energy, ζ is the actual Fermi energy, and the other symbols in (1) have

*Issued as N.R.C. No. 3909.
†National Research Laboratories Postdoctorate Fellow; now at Physics Department, University of Alberta, Edmonton, Alberta.

their usual significance. If then we assume Matthiessen's rule to be valid we may write:

$$\rho = \rho_T + \rho_0, \tag{2}$$

where ρ_T is the resistivity of a metal in the absence of impurities, due to the thermal agitation of the metal ions, and ρ_0 is the resistivity due to chemical impurities and physical imperfections. Using (2) in (1), we then have:

$$S = -\frac{\pi^2 k^2 T}{3e\zeta}\left[\frac{\rho_T}{\rho}\cdot\frac{\partial \log \rho_T}{\partial \log E}+\frac{\rho_0}{\rho}\cdot\frac{\partial \log \rho_0}{\partial \log E}\right]_{E=\zeta}. \tag{3}$$

Further discussion in this note will be confined to the quantity $\partial\log\rho_0/\partial\log E$ which for brevity we call C.

If we assume quasi-free electrons ($E \propto |\mathbf{k}|^2$), then

$$C = -1+\left(\frac{\partial \log A}{\partial \log E}\right)_{E=\zeta}, \tag{4}$$

where A is the effective scattering cross-section per impurity center. In the case of an impurity atom of valence $Z+1$ dissolved in a monovalent metal, Mott (1936) calculated the potential approximately* due to this atom using the Thomas–Fermi method, and obtained:

$$V(r) = (Ze/r)\exp(-r/r_0), \tag{5}$$

where r_0 is a screening radius which in this treatment is independent of Z. Using the Born approximation, Mott then found:

$$A = \frac{\pi Z^2 e^4}{2E^2}\left\{\log(1+E/E_1)-\frac{E/E_1}{1+E/E_1}\right\}, \tag{6a}$$

where $E = m_{\text{eff}}v^2/2$, $E_1 = \hbar^2/8m_{\text{eff}}r_0^2$, m_{eff} being the effective electron mass. If now we treat E_1 as a constant for the metal we obtain for C the curve of Fig. 1 as a function of ζ/E_1. It will be seen that C lies between -1 and -3

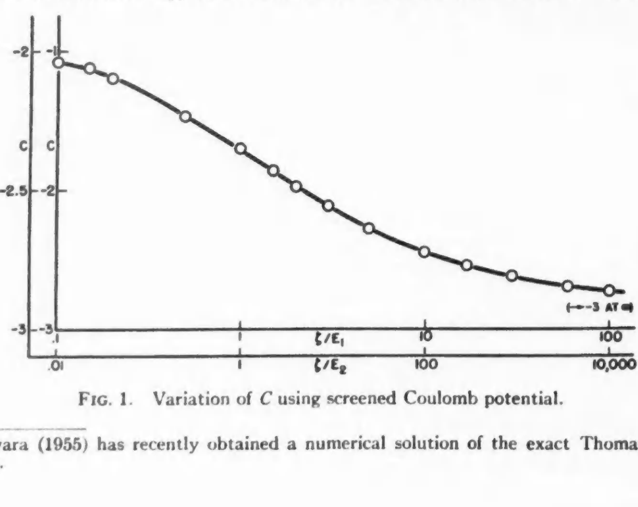

FIG. 1. Variation of C using screened Coulomb potential.

*Fujiwara (1955) has recently obtained a numerical solution of the exact Thomas–Fermi equation.

(cf. MacDonald and Pearson 1953, and also Domenicali and Otter 1954). Alternatively we may substitute for r_0 the theoretical value dependent on electron-concentration derived by Mott, and we have (still assuming quasi-free electrons):

$$(6b)\qquad A = \frac{\pi Z^2 e^4}{2E^2}\left\{\log(1+E/E_2)^{\frac{1}{2}} - \frac{(E/E_2)^{\frac{1}{2}}}{1+(E/E_2)^{\frac{1}{2}}}\right\},$$

where $E_2 = m_{\text{eff}}e^4/2\pi^2\hbar^2$, $\simeq 1.35$ ev. if $m_{\text{eff}} \simeq m$. The variation of C in this case is also shown in Fig. 1 as a function of ζ/E_2, and C now lies between -2 and -3.

However, measurements in this laboratory (e.g. MacDonald and Pearson 1953, 1954, 1955) of the thermoelectric power at low temperatures of certain low concentration alloys (e.g. tin and iron in copper) indicate a much wider range of values of C (sometimes $|C|$ may even exceed 100) than obtained from Mott's formula. If we assume the validity* of equations (1) to (3) and of the assumption of quasi-free electrons, the explanation for this discrepancy must be sought in the calculations of $V(r)$ and of the scattering cross-section A.

Since the screened Coulomb potential (5) for an impurity ion is only a rather crude approximation which in particular takes no account of the specific ion structure, we thought it worth while to consider also the potential $V = V_1 + V_2$ where:

$$(7)\qquad V_1 = (A/r)\exp(-r/r_0);\; V_2 = B \text{ for } 0 \leqslant r \leqslant r_1,\; B = -(3A/r_1)(r_0/r_1)^2,$$
$$= 0 \text{ for } r > r_1.$$

The calculation of scattering cross-section is straightforward on the *Born approximation*, and the range of variation of C is greatest if we set $r_0/r_1 = 1/3$. C is plotted against kr_1 in Fig. 2 (where k is the electron wave-number) and we see that C now lies between $+3$ and -3. If we assume r to be about the radius of the Wigner–Seitz atomic sphere, the value of kr_1 at the Fermi surface will be about 1.5 and hence $C \simeq +1$. Thus although the possible range of C has been increased, we are still as far as ever from obtaining values of C comparable with those observed experimentally.

We should also mention that Friedel (1955)† has shown that when the potential V of the impurity center is such that there exists a virtual state(s) of some non-zero angular momentum close to the Fermi energy, such a state(s) can cause the appearance of a maximum and minimum in the $\rho(E)$ vs. E curve. Somewhat higher values of $|C|$ would now be possible and Friedel has shown, assuming a square-well form of potential, that the existence of such a virtual state is not incompatible with a reasonable choice of parameters for the well. It still seems improbable, however, that we can increase C by some two orders

*It appears that any considerable modification of the E–$\mathbf{k}$ relation from that assumed can be ruled out as an adequate explanation: (i) since this would effect a large change in the thermoelectric power of the *pure* parent metal also (cf. e.g. MacDonald and Roy, Phil. Mag. **44**: 1364, 1953), and (ii) because experimentally the values of $|C|$ depend markedly on the specific *solute* atom.

†We are most grateful to Dr. Friedel for sending us a copy of his manuscript before publication.

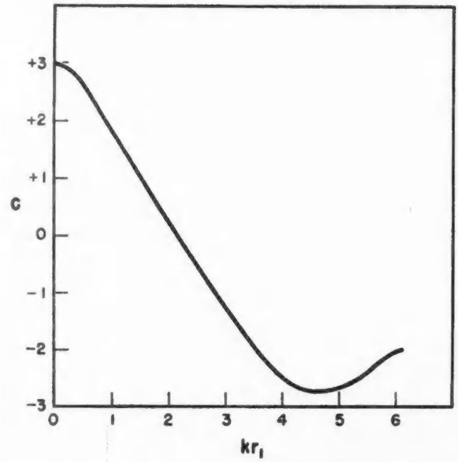

FIG. 2. Variation of C using compound potential specified in text.

of magnitude. An exact calculation to determine the upper bound of $|C|$ for a square well potential is in progress.

We should emphasize in conclusion that any explanation based on equation (2) assuming a linear variation of ρ_0 with impurity concentration can only be incomplete, particularly at low temperatures. This is particularly so because of the striking "saturation" effects observed (e.g. MacDonald and Pearson, *loc. cit.*) in certain very dilute alloys which appear undoubtedly to be intimately connected with the occurrence of an anomalous minimum of electrical resistance in these alloys at low temperatures (cf. also MacDonald 1953, 1955). We therefore believe that a theory should continue to be sought for a *specifically low-temperature* component of electron scattering which could give rise to the anomalous resistance-minimum and large thermoelectric power in dilute alloys.*

We are grateful to Dr. W. B. Pearson, D.F.C., for discussions.

DOMENICALI, C. A. and OTTER, F. A. 1954. Phys. Rev. **95**: 1134.
FRIEDEL, J. 1955. Ann. phys. In press.
FUJIWARA, H. 1955. J. Phys. Soc. Japan, **10**: 339, 727.
KORRINGA, J. and GERRITSEN, A. N. 1953. Physica, **19**: 457.
MACDONALD, D. K. C. 1953. Physica, **19**: 841.
——— 1955. Rapp. 10ᵉ Congr. Solvay, Brussels (held in 1954). (Pub. R. Stoops, Bruxelles.)
MACDONALD, D. K. C. and PEARSON, W. B. 1953. Proc. Roy. Soc., A, **219**: 373.
——— 1954. Phil. Mag. **45**: 491.
——— 1955. Acta Metallurgica, **3**: 392, 403.
MOTT, N. F. 1936. Proc. Cambridge Phil. Soc. **32**: 281.
MOTT, N. F. and JONES, H. 1936. Theory of properties of metals and alloys. The Clarendon Press, Oxford.
PEARSON, W. B. 1955. Phil. Mag. **46**: 911.

RECEIVED NOVEMBER 7, 1955.
DIVISION OF PURE PHYSICS,
NATIONAL RESEARCH COUNCIL,
OTTAWA, CANADA.

*We should like to mention here the work of Korringa and Gerritsen (1953). Let us remark also that recent work by Pearson (1955) has enabled the anomalous component of resistance to be isolated experimentally and this shows indeed a rapid decay with increasing temperature.

CANADIAN JOURNAL OF PHYSICS

Notes to Contributors

Manuscripts

(i) ***General.*** Manuscripts, in English or French, should be typewritten, double spaced, on paper $8\frac{1}{2} \times 11$ in. **The original and one copy are to be submitted.** Tables and captions for the figures should be placed at the end of the manuscript. Every sheet of the manuscript should be numbered.

Style, arrangement, spelling, and abbreviations should conform to the usage of this journal. Names of all simple compounds, rather than their formulas, should be used in the text. Greek letters or unusual signs should be written plainly or explained by marginal notes. Superscripts and subscripts must be legible and carefully placed.

Manuscripts and illustrations should be carefully checked before they are submitted. Authors will be charged for unnecessary deviations from the usual format and for changes made in the proof that are considered excessive or unnecessary.

(ii) ***Abstract.*** An abstract of not more than about 200 words, indicating the scope of the work and the principal findings, is required, except in Notes.

(iii) ***References.*** References should be listed **alphabetically by authors' names,** unnumbered, and typed after the text. The form of the citations should be that used in issues of this journal published in 1956; in references to papers in periodicals, titles should not be given and only initial page numbers are required. The names of periodicals should be abbreviated in the form given in the most recent *List of Periodicals Abstracted by Chemical Abstracts*. All citations should be checked with the original articles and each one referred to in the text by the authors' names and the year.

(iv) ***Tables.*** Tables should be numbered in roman numerals and each table referred to in the text. Titles should always be given but should be brief; column headings should be brief and descriptive matter in the tables confined to a minimum. Vertical rules should be used only when they are essential. Numerous small tables should be avoided.

Illustrations

(i) ***General.*** All figures (including each figure of the plates) should be numbered consecutively from 1 up, in arabic numerals, and each figure referred to in the text. The author's name, title of the paper, and figure number should be written in the lower left corner of the sheets on which the illustrations appear. Captions should not be written on the illustrations (see Manuscripts (i)).

(ii) ***Line Drawings.*** Drawings should be carefully made with India ink on white drawing paper, blue tracing linen, or co-ordinate paper ruled in blue only; any co-ordinate lines that are to appear in the reproduction should be ruled in black ink. Paper ruled in green, yellow, or red should not be used unless it is desired to have all the co-ordinate lines show. All lines should be of sufficient thickness to reproduce well. Decimal points, periods, and stippled dots should be solid black circles large enough to be reduced if necessary. Letters and numerals should be neatly made, preferably with a stencil (**do NOT use typewriting**) and be of such size that the smallest lettering will be not less than 1 mm. high when reproduced in a cut 3 in. wide.

Many drawings are made too large; originals should not be more than 2 or 3 times the size of the desired reproduction. In large drawings or groups of drawings the ratio of height to width should conform to that of a journal page but the height should be adjusted to make allowance for the caption.

The original drawings and one set of clear copies (e.g. small photographs) are to be submitted.

(iii) ***Photographs.*** Prints should be made on glossy paper, with strong contrasts. They should be trimmed so that essential features only are shown and mounted carefully, with rubber cement, on white cardboard with no space or only a **very** small space (less than 1 mm.) between them. In mounting, full use of the space available should be made (to reduce the number of cuts required) and the ratio of height to width should correspond to that of a journal page ($4\frac{3}{4} \times 7\frac{1}{2}$ in.); however, allowance must be made for the captions. Photographs or groups of photographs should not be more than 2 or 3 times the size of the desired reproduction.

Photographs are to be submitted in duplicate; if they are to be reproduced in groups one set should be mounted, the duplicate set unmounted.

Reprints

A total of 50 reprints of each paper, without covers, are supplied free. Additional reprints, with or without covers, may be purchased.

Charges for reprints are based on the number of printed pages, which may be calculated approximately by multiplying by 0.6 the number of manuscript pages (double-spaced typewritten sheets, $8\frac{1}{2} \times 11$ in.) and including the space occupied by illustrations. An additional charge is made for illustrations that appear as coated inserts. The cost per page is given on the reprint requisition which accompanies the galley.

Any reprints required in addition to those requested on the author's reprint requisition form must be ordered officially as soon as the paper has been accepted for publication.

Contents

Printed in Canada by University of Toronto Press